CHAPTER

PROPERTIES OF CASTINGS

9

Having made our casting, it may appear visually perfect, but the warm hopes encouraged by its comforting appearance can quickly be dashed when its properties are checked.

Very often, the tensile properties reveal that the casting may be strong, passing the requirement for strength specified by the customer, but its ductility is below the specified requirement. This is common. Alternatively, everything appears to be fine, but the casting leaks. This is also common.

The customer can be impressively intransigent when it comes to demanding his specified properties. After all, when accepting the order from the customer, the foundry had agreed to provide the specified properties.

This section reviews some of the potential problems.

9.1 TEST BARS

Test bars are used to test the tensile properties of the cast metal. They are used in various ways:

1. To test a melt before or at the same time as the pouring of the casting (even though the test bar will probably require heat treatment, and so often be tested days after the pouring of the casting);
2. To test the casting as a cast-on feature of the casting, accompanying the casting through heat treatment, and finally cut off and tested, sometimes in the presence of the customer's inspector;
3. To test the casting as a specimen excised (i.e. cut out) from the casting as part of a destructive test of the casting.

The cast-on test bars and excised bars both will be tolerably representative of the material of the casting and tend not to cause any serious problems of interpretation, even though exact simulation of conditions throughout the main body of casting are clearly not achieved and are probably not achievable. These bars are generally accepted as being sufficiently representative.

The main problems with test bars are with the separately cast bars. This section focuses on these.

Invariably, at the present day, separately cast test bars are poorly designed, so they give poor representations of the properties of the castings. These unrepresentative low properties make the task of the foundry, already hard, even harder. To reduce their problems with obtaining reasonably representative bars, foundries will give the job of pouring to one particular person who is known to have a good pouring 'technique' and who can therefore achieve properties that are believed to be representative. Stories abound of those foundries who should pour test bars for each melt from day to day, but who have poured a week's supply on Monday morning because they happened to know it was a good melt and their expert pourer was available at the time. Such stories probably show my age; I have not heard of such practices in recent years.

The design of all current test bars pre-dates the concepts of surface turbulence, air entrainment and critical velocity and pre-dates experimental verification of their filling action by such techniques as video X-ray and computer simulation. Thus at the time of writing it is regrettable that all our world standards of test bar designs are unsatisfactory. Some are seriously poor. None can faithfully reproduce the actual quality of the melt; all impair the melt during the filling of the mould, explaining the scatter in properties that are usually observed. The scatter can be important, possibly causing a perfectly good batch of castings to be scrapped if properties appear (misleadingly) to be low.

Complete Casting Handbook. http://dx.doi.org/10.1016/B978-0-444-63509-9.00009-1

Because all current national and international test bar moulds known to the author appear to be designed to maximise defects, there seems to be no point in describing any of them. I am taking the initiative to describe the features of one test bar mould below that has been properly developed and is known to give representative results.

The 10 Test Bar Mould

The concept is shown in Figure 9.1. The design has been proven by video X-ray to be free from air entrainment.

This mould casting 10 bars at a time was specifically designed for research. The design was optimised by Dispinar and Campbell (2005) using Al-7Si-Mg alloy poured into resin-bonded sand moulds viewed by X-ray radiographic video. All 10 bars fill beautifully, so that their tensile properties have been found to be indistinguishable and to exhibit minimal scatter. This makes the mould ideal for carrying out studies on the optimisation of heat treatment for instance, in which from only 10 moulds, 100 test bars are quickly produced, all with practically identical as-cast properties. Other studies requiring large numbers of bars for statistical purposes are also quickly generated from relatively few moulds.

However, of course, even this design does not deliver a test bar free from damage. This is because the act of pouring metal into the pouring basin is somewhat damaging, and the initial stages of the priming of the down-sprue will be likely to be messy and additionally damaging. The damage in the down-sprue might be reduced by redesigning the assembly so that the bars were horizontal, thus much smaller fall heights would be suffered, giving much lower filling velocities and

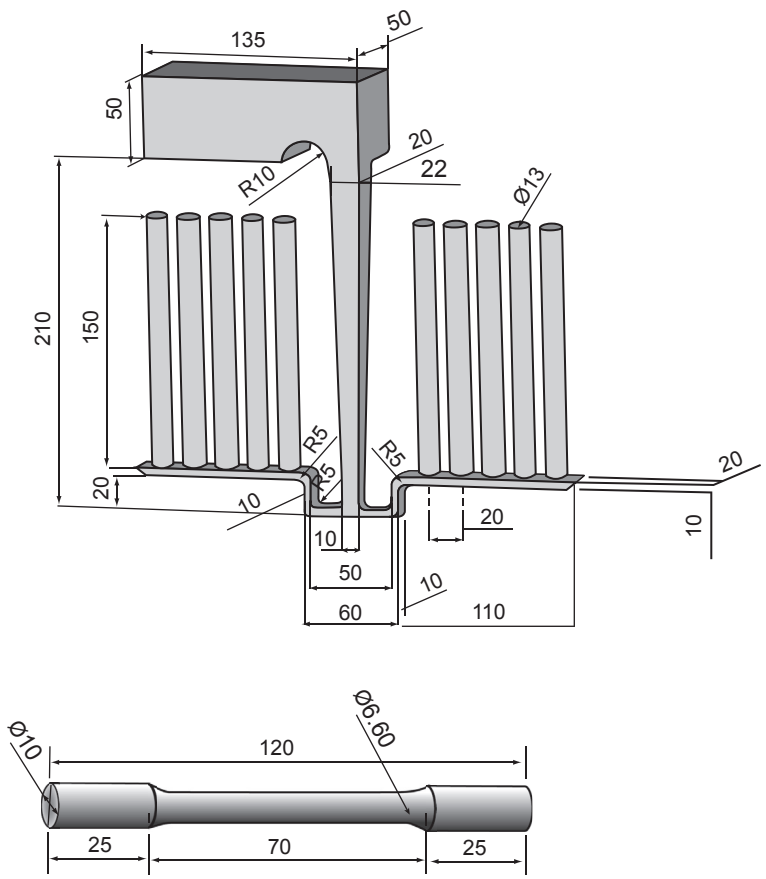

FIGURE 9.1

The Birmingham, United Kingdom, 10 test bar casting and test piece (Dispinar and Campbell, 2005).

thus reduced damage to the metal. It would be useful to compare the results of vertical and horizontal moulded systems. Ultimately, the pouring basin could be eliminated by contact pouring, and the down-sprue damage could be totally eliminated if the mould were filled from a counter-gravity filling system. The adoption of counter-gravity filling systems is to be strongly encouraged; only then would it be possible to achieve the filling of a test bar with metal that would be truly representative of the melt and the casting.

The mould works quite well for the Al-7Si-Mg alloys in a static pour mode (i.e. the mould is simply poured under gravity and left to cool.) This design fulfils my rule 1 for feeding 'Do not feed'. It seems to work adequately for most alloys, and especially light alloys in which solid feeding is relatively efficient, and where the alloys are of a reasonably good quality—i.e. a small population of small bifilms that are relatively resistant to opening under the reduction of pressure suffered without a feeder.

Early trials targeted at the production of a shaped test bar were abandoned because of the difficulty to ensure that the grip length furthest from the feeder was sound. The provision of a feeder to ensure soundness was probably possible but was not straightforward without introducing other dangers of parallel filling systems and possible overspill between the different filling routes. The penalty that the bars all required to be machined was accepted. The development of a well-shaped test bar capable of being pulled without machining would be welcome.

The offset stepped basin and tapered sprue is designed to ensure that minimal air enters the mould (which appears to be one of the most serious criticisms of current designs). The minimum depth in the basin used for the calculation of the filling system is 25 mm; thus, the sprue is likely to start filling before the basin is filled to its minimum operational height unless a stopper is used in the sprue entrance. Preferably a stopper is employed and only raised when the basin has been filled above the minimum level line. The basin is continued to be topped up after the removal of the stopper.

The mould works well as a sand mould. It would also be appropriate as a permanent metal mould, although the rather narrow channels would require to be increased in size to allow for the thickness of a mould coat.

Naturally, the design could be adapted for the casting of perhaps only two test bars at a time, making it more universally useful. Furthermore, the development at Birmingham showed, in line with expectations, that the design worked well for all types of metals from light alloys via cast irons to steels.

However, for some alloys that are more difficult to feed, and probably as a prudent design where metal quality might be less than optimum, the bars would benefit from the enlargement of the horizontal runners from 20×10 mm to 20×20 mm, plus the provision of a feeder of at least 20×20 mm standing on each arm of the runner (a test bar on each side may need to be sacrificed to make room for the feeder). The feeder on each arm can then pressurise the runner and in turn maintain pressure in the 13 mm diameter castings during freezing. An additional feature that is easily provided to aid feeding from an enhanced temperature gradient is the provision of a cooling fin at the top of each test bar. This is laid on the parting line, 2 mm thick with dimensions approximately 20×30 mm and possibly open at the top of the mould to eliminate any back pressure (metal rarely fills all of the fin).

Alternatively, for alloys that are difficult to feed, a second variant of the 10 test bar mould is designed to be rolled over through 180° immediately after casting. In this case, the runner bar is increased in section to 25×25 mm to act as a feeder after the mould has been inverted. This is somewhat better for alloys which require much feeding, and, of course, reproduces more faithfully the conditions of those processes that use a roll-over mechanism such as the Cosworth operation. Most of the fatigue research from the Birmingham, UK, department has been performed with this casting technique.

The roll-over technique requires the use of a small pivoted cradle and hand crank (it is impressively primitive to look at!) for clamping the mould halves together and inverting the complete mould immediately after casting.

A practical inconvenience experienced with roll-over was that the sprue emptied and poured over the floor. Originally we had suffered this, thinking that the ensuing mess was simply to be tolerated, and assuming that the casting would be unharmed because of the swan neck link to the runner/feeder bar which would have prevented this vital feed metal from the runner bar being lost. However, this was not always true. The metal would sometimes siphon around the swan neck and empty from the runner/feeder which would then collapse inside its oxide skin like a punctured balloon.

Thus a refinement of technique which we found necessary to introduce was to take the sprue cut from the previous casting and use this to plug and freeze the sprue of the current casting immediately before the roll-over. This was a slight inconvenience, but saved the mess on the floor and retained the runner/feeder filled so that feeding could occur efficiently.

Once again, such practical inconveniences would be avoided by the adoption of a side-filled counter-gravity filling system with an integral roll-over facility. Counter-gravity is such a sensible, civilised and economic technology!

K-mould test (Evaluation of melt cleanness)

The K-mould test (Figure 9.2) is used not for the evaluation of mechanical properties but for the evaluation of the cleanness of molten aluminium. It was invented in Japan in 1973 by Kitaoka but not widely published until 2001. A description is given by Wannasin and colleagues (2007). The test is sensitive principally to large oxide bifilms and is valuable for assessing the quality of incoming metal to the foundry and in optimising melt treatments to raise melt quality.

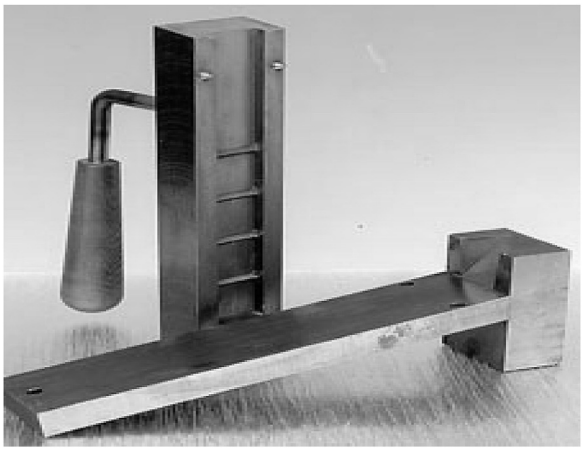

FIGURE 9.2

K-bar test mould.

Courtesy N-Tec (2009).

The test is used in different ways by users. For instance, one user defines a K-value (the number expressing the cleanness) in terms of the total number of oxide films observed on the fracture surfaces. Another user defines K as the number of fracture surfaces (made by breaking at the five V-grooves along the length of the bar) that contain oxides. If all five contain oxides, then the rating is '5'. Most users, understandably, tend to ignore oxide defects smaller than some critical size, usually about 1 mm.

The fundamental feature of the K-bar test is that the fracture is forced to occur at the V-groove; thus, the material is sampled at that point whether there is a defect present or not. Thus the test checks random samples of the material. This differs from a test like the tensile test or a bend test in which failure occurs at the largest defect, giving a pessimistic indication of the general quality of the material.

It will be interesting in the future if material is made without a substantial population of bifilms. The familiar brittle fractures at the five V-notches should then become impossible. The material will simply bend, refusing to fracture.

9.2 THE STATISTICS OF FAILURE

Unfortunately, the properties of materials are not accurately reproducible. For castings in particular, scatter of tensile and fatigue properties has been a traditional concern for all casting users.

This is recognised by many of the world's standards for the testing of castings. If a tensile test bar fails below the strength value required by the specification, the specified procedure is to record the low properties with a record of any visible anomaly on the fracture surface and then break two additional test bars from the same production batch to show that the low property break was due to an inclusion or other anomaly and did not reflect the yield, elongation and ultimate measurements of the metal.

Effectively, the failed result is discarded. The discarding of low values is a practice that has crept in to both foundries and laboratories. Somehow the low results are viewed as a mistake. We turn a blind eye to them. This approach is, of course,

less than honest. Furthermore, it deprives us of valuable information on the real properties of the products we are making. It is a real result, illustrating how the properties reduce as a result of the presence of defects. Because all of the test bar results, 'good' or 'bad', are influenced by the population of defects, the 'outliers' are a good indication of the real spread of results.

When dealing with scattered property results, the common approach is simply to take an average. Occasionally, a standard deviation might also be calculated. The attempt to assess scatter by the use of a standard deviation, usually denoted sigma, σ or s, is of course much better than nothing, but does make the implicit assumption that the distribution of results is Gaussian, or normal. The familiar bell-shaped distribution is shown in Figure 9.3. The value $\pm\ \sigma$ encloses approximately 68% of the scattered results. The value $\pm 2\sigma$ includes 95% and $\pm 2.5\sigma$ includes 99%. Higher multiples of sigma, for instance 3σ (99.73%) and 4σ (99.994%), are less commonly used.

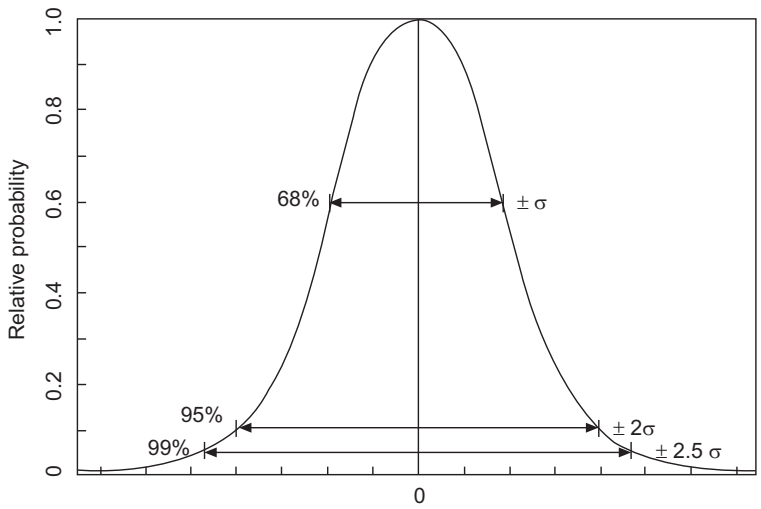

FIGURE 9.3

Gaussian distribution of strengths, showing assessment of scatter using different multiples of the standard mean deviation σ.

If instead we retain all results, good and bad, and plot them to reveal their distribution, we can obtain a histogram such as that in Figure 9.4(a). The shape of the distribution curve is usually not the symmetrical Gaussian form but is skewed, as are many strength distributions (usually negatively skewed) and elongation and fatigue life distributions (usually positively skewed). A close approximation to the shape of the curve was derived theoretically by Weibull (1951). The curve (Figure 9.4(a)) can be plotted as the familiar cumulative distribution (Figure 9.4(b)) and by further mathematical manipulation the curved ends of this plot can be straightened in what is known as a Weibull probability plot (Figure 9.4(c)). In other words, a Weibull probability plot is simply another way of presenting data and checking whether the data follow the Weibull distribution.

In general, the failure properties of metals are accurately described by Weibull (pronounced 'Vybl' where 'y' is as in 'why') distribution. There are good fundamental reasons for this. Weibull derived his distribution in 1951 based on the 'weakest link' concept developed by Pierce in 1926.

In materials research, Weibull analysis was originally used almost exclusively for ceramics and glasses. Although Weibull used tensile strength data from castings as a case study in his historic paper, it was after the work by Green and Campbell (1993, 1994); this approach was applied much more commonly to castings.

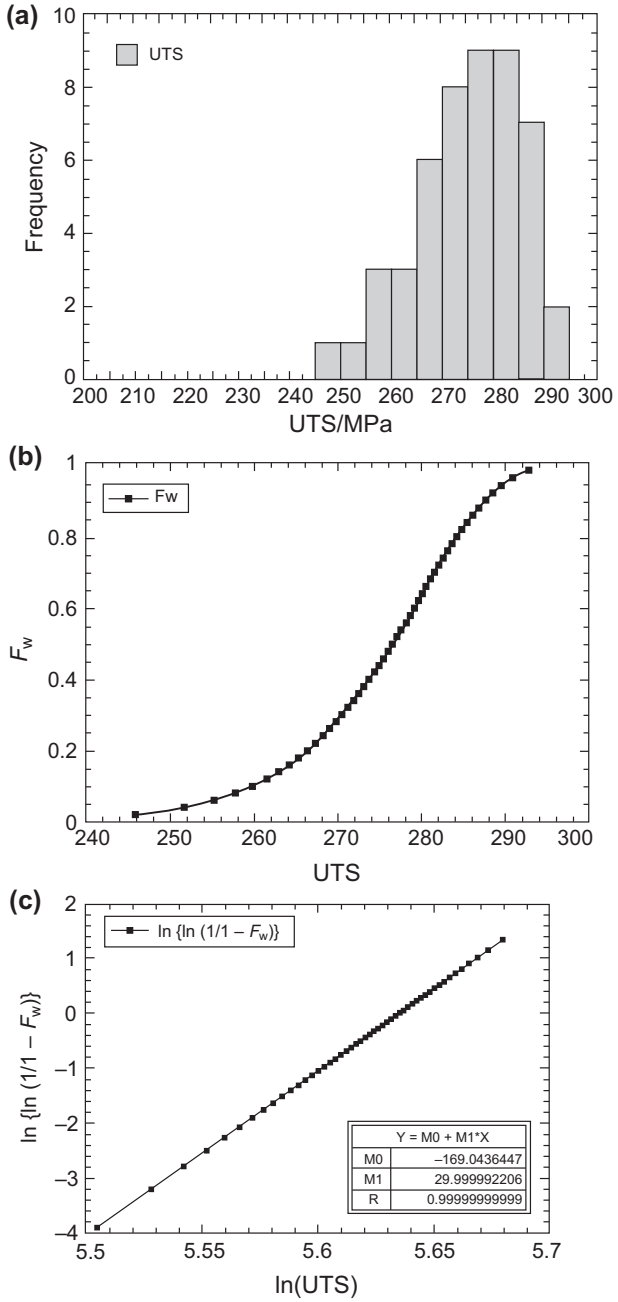

FIGURE 9.4

(a) Typical skewed distribution of tensile strengths as might be obtained from a cast Al-Si alloy *(synthetic data by Green, 1995)*. (b) Distribution identical to that in (a), but replotted as a cumulative distribution (Green, 1995). (c) Plot of the data in (b) showing the simple straight line form of the two-parameter Weibull cumulative distribution (Weibull modulus $m = 30$ and position parameter $\sigma = 280$ MPa) (Green, 1995).

9.2.1 BACKGROUND OF USING WEIBULL ANALYSIS

I am grateful to Professor Murat Tiryakioglu for his major contribution to this section. The Weibull cumulative distribution function is given by the expression

$$F_w = 1 - \exp\left\{-\left(\frac{x - x_T}{x_0}\right)^m\right\} \tag{9.1}$$

where F_w is the cumulative fraction of *failures* up to a given value of x, say strength or fatigue cycles, x_0 is a position (or scale) parameter, x_T is a lower strength threshold below which no specimen fails and m is the shape parameter, referred to as the Weibull modulus. The average and standard deviation of the three-parameter Weibull distribution are given by

$$\overline{x} = x_T + x_0\Gamma\left(1 + \frac{1}{m}\right)$$

and

$$s_x = x_0\sqrt{\Gamma\left(1 + \frac{2}{m}\right) - \left(\Gamma\left(1 + \frac{1}{m}\right)\right)^2}$$

where Γ represents the gamma function. The skewness of the Weibull distribution is a function of only the Weibull modulus. When the Weibull modulus is less than 3.6, then the distribution is positively skewed. For $m > 3.6$, the distribution is negatively skewed.

The threshold is that value below which no failures are expected; even though thousands of tensile tests might be performed, for a finite threshold no test would fail at a lower stress. The presence of a threshold is comforting. However, it can only be derived using the three-parameter Weibull analysis. If it is assumed that there is no threshold (i.e. it is assumed that strength can fall to zero on occasions), then the threshold can be neglected, allowing a simpler analysis using two-parameter Weibull. We shall present examples of both these analyses later.

The previous expression is frequently used with the lower strength x_T set to zero, giving the so-called two-parameter Weibull approximation. Equation (9.1) becomes

$$F_w = 1 - \exp\left\{-\left(\frac{x}{x_0}\right)^m\right\} \tag{9.2}$$

In general, the three-parameter relation should be used, or at least explored, before making the assumption that a lower threshold of value x_T does not exist. Forcing the Weibull fit to assume no threshold can give a misleading interpretation of the data. For instance, Figure 9.7 showing top-poured material versus bottom-gated material shows the same data interpreted (1) as a two-parameter straight line plot or (2) a three-parameter curve. Clearly the three-parameter result is a more faithful representation of the data. Furthermore, the shape parameter (m) and position parameter (scale parameter) x_0 are quite different, so that extreme caution needs to be exercised when attempting to compare the parameters; it is essential to know whether the parameter refer to two- or three-parameter interpretations. An additional fundamental difference between the two plots is that the two-parameter interpretation predicts that strengths can scatter to zero, whereas the three-parameter fit confirms that the results extrapolate to a minimum threshold value, below which no results will be expected. The threshold value is, of course, of enormous importance.

An example of a distribution of Weibullian failures described by Eqn (9.2) is shown in Figure 9.4(a). Unlike the normal distribution there is no reflective symmetry about the mean. To obtain the two-parameter Weibull modulus and position parameter from such a plot requires mathematical curve fitting. Alternatively, these can be found by reducing the cumulative distribution (Figure 9.4(b)) to a straight line plot (Figure 9.4(c)).

After rearranging and taking natural logarithms twice gives

$$\ln\{\ln(1/(1 - F_w))\} = m\ln(x) - m\ln(x_0) \tag{9.3}$$

This can now be presented as a straight line by plotting $\ln(-\ln(1 - F_w))$ as a function of $\ln(x)$ giving the slope m and intercept $-m\ln(x_0)$, from which can be deduced the scale parameter σ. The slope m and the position parameter σ are the

two parameters to emerge from this approach, giving the name 'two-parameter Weibull' to this approach. The data of Figure 9.4(b) are replotted in Figure 9.4(c) with a straight line fitted to the data by simple regression analysis.

The slope of the Weibull plot in the two-parameter analysis is a measure of the average to standard deviation (signal-to-noise) ratio and is known as the Weibull modulus, m.

In two-parameter Weibull distributions, the ratio of average to standard deviation is written as

$$\frac{\bar{x}}{s_x} = \frac{\Gamma\left(1+\frac{1}{m}\right)}{\sqrt{\Gamma\left(1+\frac{2}{m}\right) - \left(\Gamma\left(1+\frac{1}{m}\right)\right)^2}}$$

where $\bar{x}$ is average fracture stress, s_x is the standard deviation and Γ represents the gamma function. When the previous equation is plotted, we obtain the following figure, which yields a surprisingly linear relationship (Tiryakioğlu, 2009)

$$m = 1.279\frac{\bar{x}}{s_x} - 0.5$$

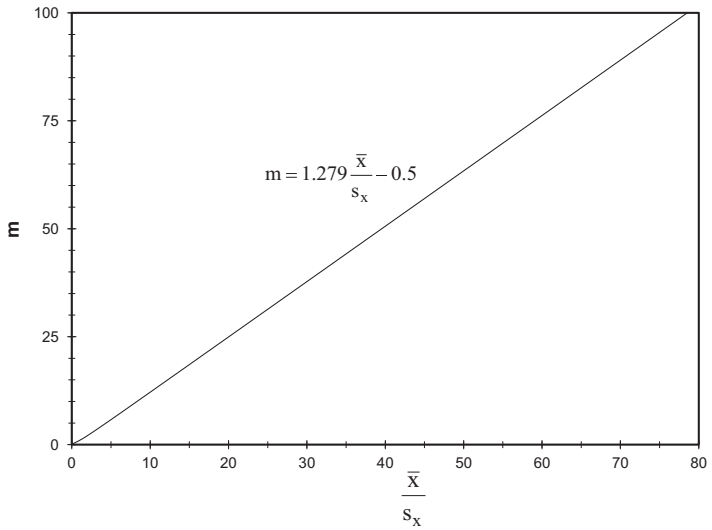

The other important parameters that are derived from a Weibull approach are the position parameter (a measure of the average strength) and the minimum threshold value.

The Weibull analysis can, in principle, estimate the probable value of strength of the weakest casting in a sample of 100 typical castings, or perhaps the weakest one in 10,000. However, of course, when using extrapolations from limited data, the accuracy of the extrapolation needs to be carefully assessed. In addition, as with all extrapolations, uniformity of conditions when extending into the unknown is never certain so that extreme caution, if not outright scepticism, is required. The reader is advised to use the percentile estimation methods described by Hudak and Tiryakioğlu (2009).

In much work using two-parameter Weibull, it has been found that for pressure die castings *m* is often between 1 and 10, whereas for many gravity-filled castings, it is between 10 and 30. For good quality aerospace castings, a value between 50 and 100 is more usual. Values of 150–250 are probably somewhere near a maximum limit defined by the limits of accuracy of strength measurements (i.e. even if all strength results were perfectly identical, the expected modulus of infinity could not be demonstrated because the tensile testing machine would record slightly different strengths because of errors in the machine). It should be noted that all these Weibull parameters are based on the two-parameter interpretation of the Weibull analysis. The more widely applicable three-parameter analysis is dealt with later in this chapter.

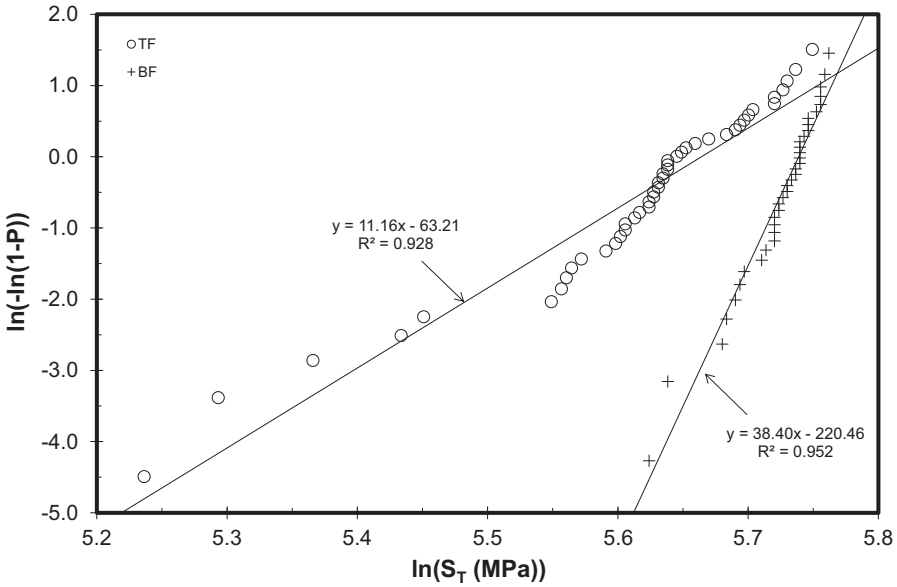

FIGURE 9.5

Two-parameter Weibull plot of strength results for Al-7Si-0.4Mg alloy (i) top filled and (ii) bottom-gated with filter. (Green and Campbell (1994) replotted by Tiryakioglu, Hudak and Okten, 2009).

Figure 9.5 shows data for a single alloy cast in a two ways, displaying the difference in reproducibility between the two filling processes. The data are from sand castings poured variously 'badly' and 'well', giving a Weibull modulus varying between about 10 and 40. These kind of data are some of the simplest demonstrations of the importance of filling techniques on the reliability of cast products. It is also, of course, a clear demonstration of the action of entrainment defects.

9.2.2 PROCEDURE FOR TWO-PARAMETER WEIBULL ANALYSIS

It is implicit in the Weibull distribution that the failure strength of a material is determined by the distribution of defects resulting from its manufacture. The Weibull distribution can be of great use because it is possible to extrapolate back to the very low probability of failure (high reliability) region, and to select a design stress to give a desired failure rate. The following procedure can be used when the volume effect is small. Tiryakioglu and Hudak (2011) give an exemplary guide to the use of the two-parameter approach.

1. Rank the data in ascending order of strength (fatigue life etc.) and assign corresponding ascending failure rank j.
2. Make the extrapolation from a sample of specimens to the population they are drawn from. This is required because the first specimen to fail in the sample tested has a probability of survival of 100% at a stress below its failure stress. However, there is a finite probability that if more specimens were tested, one of them would fail at a lower stress. The most probable unbiased estimate of the probability of survival of the jth specimen in the ranked data is given by Tiryakioglu and Hudak (2008) as

$$F_j = \frac{j - a}{N + b}$$

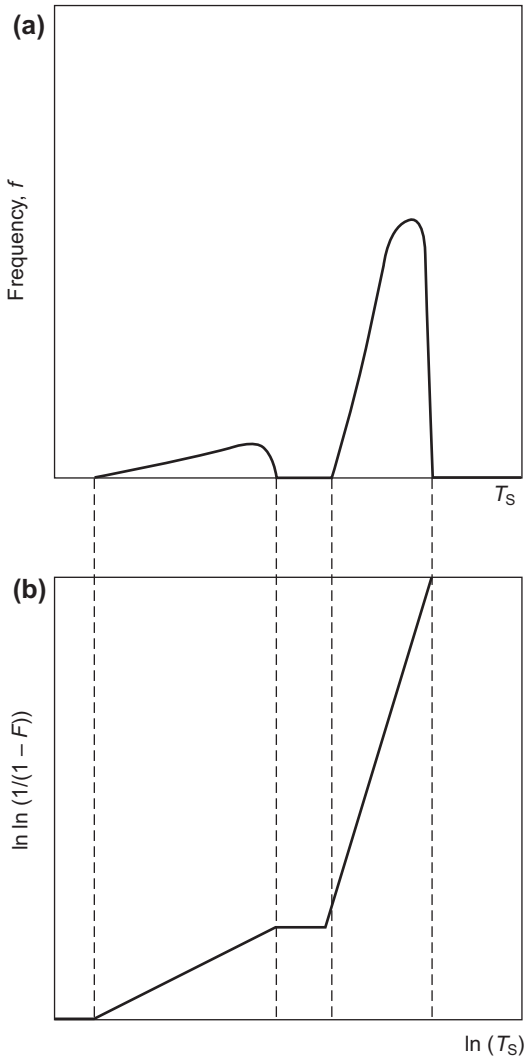

FIGURE 9.6

(a) Bimodal distribution and (b) its corresponding plot in terms of two separate two-parameter Weibull distributions.

where N is the total number of specimens tested and the parameters a and b are listed in Table 9.1.

3. Calculate $\ln\{\ln 1/(1-F)\}$ for each F_j.
4. Calculate $\ln(x)$ for each x.
5. Plot $\ln\{\ln 1/(1-F)\}$ as a function of $\ln x$ and regress through this a best-fit straight line. The Weibull modulus is the slope m of the line.

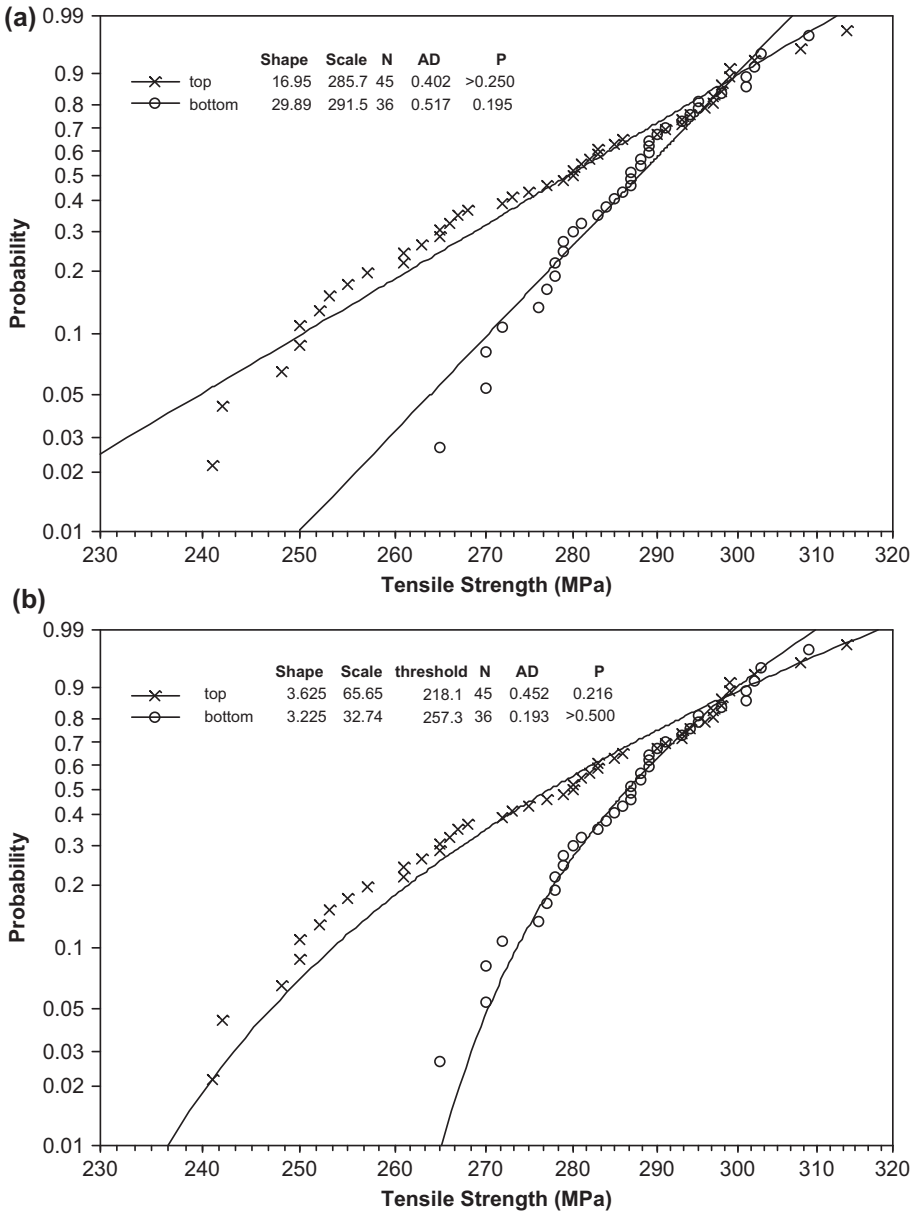

FIGURE 9.7

(a) A pair of strength distributions from top-poured versus bottom-gated castings, ill-fitted by a two-parameter Weibull analysis; (b) a three-parameter Weibull plot illustrating that both distributions have thresholds (lower limit values below which no results are expected).

Courtesy Tiryakioglu (2009).

Table 9.1 Unbiased Probability Estimators (Tiryakioglu and Hudak, 2008)

N	a	b
5	0.173	0.500
6	0.243	0.390
7	0.280	0.310
8	0.309	0.251
9	0.322	0.210
10	0.348	0.190
11	0.367	0.160
12	0.371	0.130
13	0.382	0.110
14	0.388	0.100
15	0.394	0.080
17	0.407	0.050
20	0.417	0.030
22	0.430	0.000
25	0.443	0.000
27	0.448	0.000
30	0.455	0.000
32	0.460	0.000
35	0.465	0.000
40	0.472	0.000
45	0.481	0.000
50	0.486	0.000
55	0.499	0.000
60	0.503	0.000
65	0.509	0.000
70	0.518	0.000
75	0.522	0.000
80	0.516	0.000
90	0.518	0.000
100	0.519	0.000

6. Conduct a goodness-of-fit test by using the coefficient of determination, R^2 of the best fit line. For this test, first calculate the critical value, $R^2_{0.05}$ (Tiryakioğlu et al., 2009)

$$R^2_{0.05} = 1.0637 - \frac{0.4174}{n^{0.3}}$$

If the R^2 of the linear regression from the Weibull probability plot is less than the $R^2_{0.05}$ value, then it can be concluded that the data do not come from a Weibull distribution. If $R^2 \geq R^2_{0.05}$, then the distribution of the mechanical testing data is indeed Weibull.

7. Calculate position parameter x_0

Tiryakioğlu and Hudak (2011) recommend several other steps in the two-parameter Weibull analysis, such as determining confidence intervals for the shape and scale parameters. If a percentile needs to be estimated, such as the design strength, determine the percentile and the confidence level, e.g. 99% confident that 95% of castings have a higher tensile strength. For estimation of Weibull percentiles, the reader is referred to the paper by Hudak and Tiryakioğlu (2009).

9.2.3 THREE-PARAMETER WEIBULL ANALYSIS

Although the two-parameter Weibull approach has been widely used for the analysis of scatter in the mechanical test results of castings, there are plenty of instances where this approach is clearly not valid. If the two-parameter Weibull plot is not a straight line, the distribution is clearly not described by two-parameter Weibull assumptions. The real distribution might be one of several, but the most useful rapid check is to ascertain whether the original assumption making the minimum strength limit x_T equal to zero is correct. If in fact there is a minimum limit to strengths, Eqn (9.3) becomes

$$\ln\{-\ln(1-F)\} = m\ln(x - x_T) - m\ln x_0 \tag{9.4}$$

The Weibull plot then becomes a plot of the left hand side of Eqn (9.4) as the vertical axis, versus $\ln(x - x_T)$ along the horizontal axis. Alternatively, when $\ln(x)$ is used as the x-axis, the distribution is three-parameter type if the data suggest a curve, rather than a line. The data then have to be fitted to give optimised values for the three parameters—m, x_0 and x_T—giving the appropriate appellation 'three-parameter Weibull' analysis.

Those casting processes and conditions that can deliver a distribution that is terminated by a minimum threshold are of enormous importance. It is not easy to predict at this early stage what feature of the casting process would lead to this key advantage. We may find the threshold is reproducible if the processing is carried out with attention to some key detail, such as, for instance, settling time before casting, or turbulence during the pour. A sharp cutoff to the distribution scatter may be an independent factor related to melt quality and turbulence, rather than some metallurgical factor such as cooling rate, chemistry or heat treatment etc.

Conversely, finding that the data indicate that x_T is actually zero, or even negative (i.e. the distribution of strengths or ductilities extrapolate to zero), is a salutary piece of information, which, if correct, warns of enormous danger for safety critical components, some of which will be expected to have zero strength or zero toughness.

Figure 9.8(a) shows strength distributions of two sets of castings. The castings with lower average strength follow a three-parameter Weibull distribution as confirmed by its p value for the Anderson-Darling goodness of fit test being in excess of 0.05. Their threshold strength is 281 MPa. Thus, although the average strength is low, heat treatment, the castings exhibit a minimum strength below which no failures are expected. In contrast, the higher strength castings are members of a population at risk of some with zero strength.

9.2.4 bi-WEIBULL DISTRIBUTIONS

Figure 9.6 shows the case of a bimodal distribution i.e. two separate modes or distributions. Such multiple distributions are relatively common, and an indication of such an effect is to be seen in the poorest data shown in Figure 9.5. The various slopes are usually found to correspond to different distributions of defects. Several slopes can sometimes be distinguished corresponding to pores, new bifilms, old bifilms and sound material. Populations of different varieties of bifilms are to be expected in castings as described in Section 2.2. In addition, Tiryakioglu has drawn attention to the fact that tensile and fatigue life data should be interpreted differently. For tensile data, Weibull mixtures are the result of distinctly different defects, usually '*old*' and '*new*' bifilms. For fatigue data, *surface* or *interior* initiation of cracks limit fatigue (Tiryakioglu, 2015).

For instance, a bimodal distribution of tensile strength results in many castings is to be expected. The melt will already contain a background population of bifilms, usually sub-millimetre size but in large number density, but if the melt enters the mould cavity turbulently the bifilms created at that late stage of filling are usually of large size, at least in the centimetre size range, giving quite different failure modes. A typical example is seen in Figure 2.44.

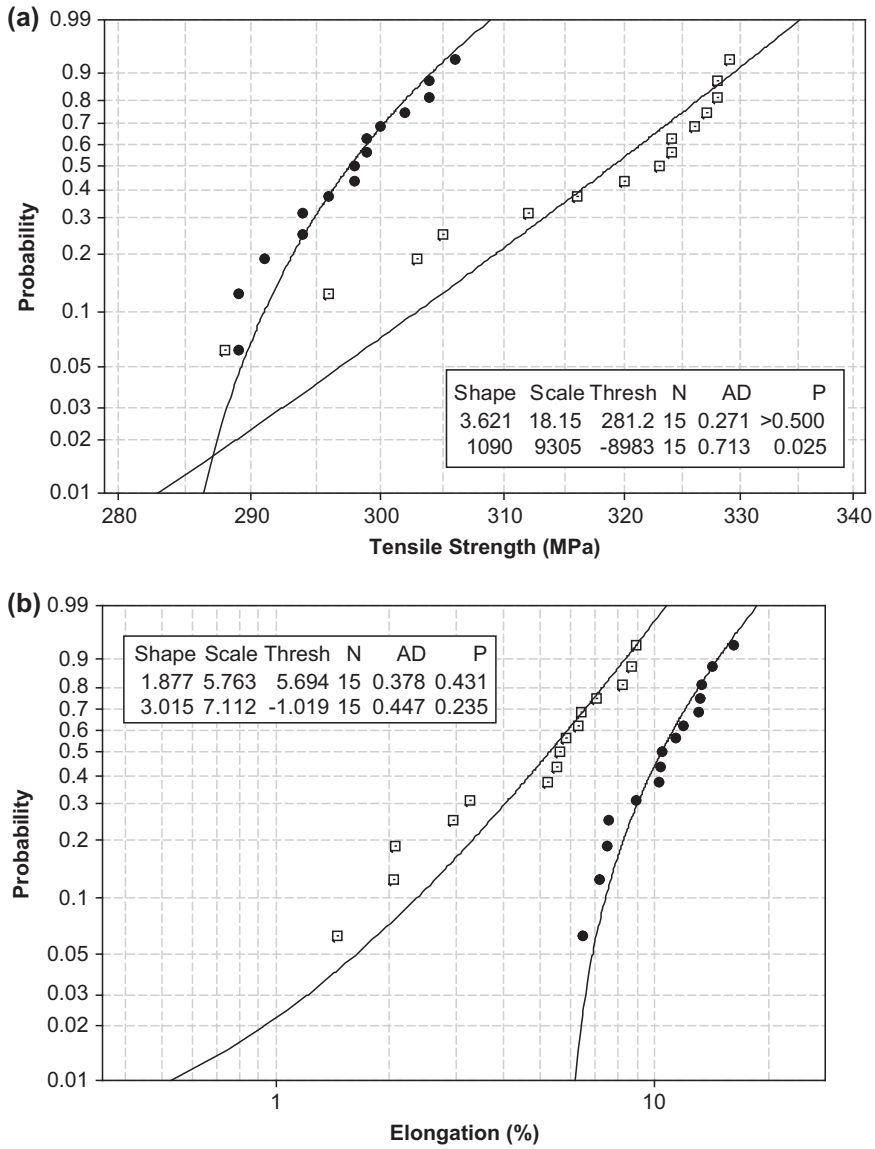

FIGURE 9.8

(a) A comparison of the strength distribution of two sets of castings by three-parameter Weibull. Those with the lower average strength had a minimum threshold of 281 MPa, whereas those with the higher average strength had a strength distribution that extrapolated to zero (actually indicating negative in the curve-fitted result). (b) Elongation results conveyed the message that one set of results, this time higher, were more reliable than those which extrapolated to zero.

Courtesy Alotech Limited and M Tiryakioglu (2009).

In fatigue life data, Weibull mixtures are due to two failure mechanisms being active: failure from cracks initiating from surface defects and interior defects. Surface defects are predominant and interior defects lead to fatigue failure only when there are no cracks initiated by surface defects.

An attempt has been made to fit the castings with higher average strength in Figure 9.8(a) to a three-parameter Weibull plot without success, as indicated by the very low p value. The poor fit suggests a negative (i.e. zero in practical terms) threshold. However, the data strongly suggest that the data may follow a bi-Weibull distribution, as indicated by the two separate regions of the curve. A bi-Weibull distribution is characterised by two different slopes for each part of the Weibull curve; this indicates the presence of two separate failure mechanisms, implying two different defect distributions or two different failure mechanisms.

Figure 9.8(b) shows the ductility results for the same two sets of castings. Both datasets follow three-parameter Weibull distribution as indicated by p values above 0.05. One set has a threshold value of 5.7%, confirming that no castings from this population are expected to fail at an elongation below 5.7%. For the other castings, the threshold elongation value is negative. (The negative result is a mathematical impossibility but effectively equivalent to a result of zero.) Hence some castings from this source can be expected to fail without any elongation. Even here, although the p value indicates a reliable result, the appearance of the data in Figure 9.8(b) may indicate that a bi-Weibull distribution would be an even better description of the data. If so, even for this relatively poor data, a minimum threshold might be found to apply.

The bi-Weibull approach is too complex to present here. The interested reader is recommended to the guidelines set out by Tiryakioglu and me (2010). However, the power and flexibility of this technique to describe the complexity of property distributions in castings is illustrated by Figure 9.9. Sets of samples subjected to various hot isostatic pressing (HIP) routines were subjected to tensile tests. The distributions of the results illustrate that at least two defect populations appeared to be present in all the samples. In some results from this work, there is even a suggestion that three populations were present, but more data would have been required to confirm this.

9.2.5 LIMITS OF ACCURACY

Reliance on the precision of the Weibull moduli derived from a limited number of tests has to be viewed with some caution. For instance, Tiryakioglu and Hudak (2008) have shown (Table 9.1) that for a simulated result of 30 tensile tests that should have a true modulus $m = 26.5$, the actual experimental results to within 95% confidence limits (looking up ± 0.025 in the Table 9.2 giving the fractional errors) will vary from 0.667 to 1.405 times the true result, equivalent to $m = 17.7$ to 37.2. This is a soberingly widespread, warning that the value of m is often less accurately estimated than we might like.

The use of about 30 samples has often been regarded as sufficient to obtain a valid Weibull plot. However, Tiryakioglu's cautionary analysis would indicate that an extrapolation of strength data to a failure rate of one in a 100 will give a corresponding expansion of the uncertainty in the extrapolated result. Despite these legitimate concerns, the result does not further deteriorate too drastically. For instance, for our population of 30 tensile results with true $m = 26.5$, the 0.01 and 0.99 columns of Table 9.1 give factors of 0.611 and 1.493, corresponding to a possible range of $m = 16.2$ to 39.6.

However, further extrapolation to a rate of, for instance, one in a 1000 seems likely to expand the uncertainty of the result to the point of it being worthless. To retrieve some precision many more tests, perhaps a hundred or more, will be needed depending on what accuracy is required.

9.2.6 EXTREME VALUE DISTRIBUTIONS

There is often keen interest in the extrapolation of results of a limited number of tests to assess the failure rate of a casting at a probability, for instance, of one in 10,000 or one in 10 million. The design of safety-critical components on automobiles and aircraft falls into this category. Interestingly, there are techniques for dealing with such improbable extrapolations.

Beretta and Murakami (2001) developed a technique for the quantification of the probability of finding inclusion defects in very clean steels. This awesome task can be likened to the search for the occasional needle in the haystack,

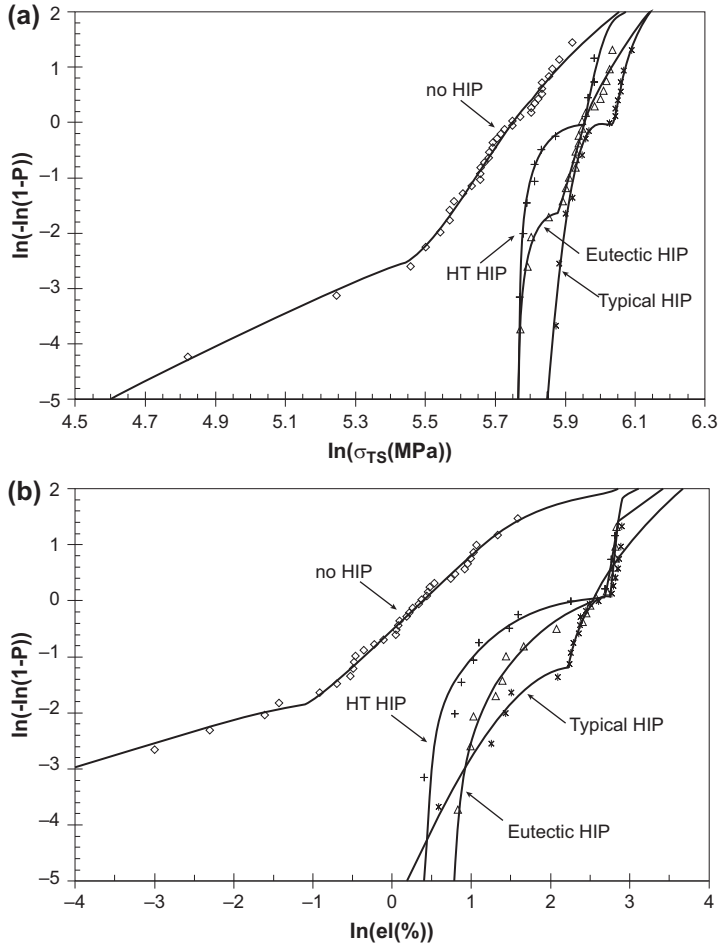

FIGURE 9.9

Three-parameter bi-Weibull plots of (a) strength and (b) elongation for non-HIPped and castings with three different HIPping techniques showing at least two distributions of defects in each set. (Staley et al., 2007).

followed by the necessity of predicting precisely how many needles may be in other random haystacks. Their simple solution is the counting only of the maximum defects in any studied area of the sample, and analysing these data with a largest-extreme-value distribution. They selected the Gumbel distribution (named after its inventor) for their study. They successfully used the technique for the study of pores and cracks.

Tiryakioglu (2008, 2009) has developed the science of extreme value distributions for application to the properties of castings. In particular, in an exercise (2008) to find the best description of the size of fatigue-initiating defects in cast Al alloys, he assesses a wide variety of different distributions including Weibull, lognormal, Frechet, General Pareto, Gumbel and General Extreme Value (GEV). He concludes that Gumbel and GEV descriptions are accurate and appropriate. At this time, these descriptions of distributions are hardly known in the casting community, but clearly deserve wider appreciation and use.

Table 9.2 Percentage Points of the Distribution of Modulus *m* obtained by using the Unbiased Probability Estimators in Table 9.1

N	0.005	0.01	0.025	0.05	0.1	0.9	0.95	0.975	0.99	0.995
5	0.292	0.325	0.381	0.434	0.504	1.630	2.014	2.458	3.169	3.653
6	0.320	0.358	0.418	0.475	0.549	1.555	1.852	2.189	2.694	3.052
7	0.356	0.391	0.445	0.501	0.579	1.502	1.747	2.031	2.462	2.753
8	0.374	0.409	0.470	0.530	0.602	1.480	1.705	1.950	2.293	2.579
9	0.392	0.427	0.488	0.545	0.618	1.444	1.650	1.836	2.126	2.371
10	0.404	0.447	0.504	0.563	0.638	1.419	1.605	1.791	2.051	2.298
11	0.429	0.465	0.529	0.582	0.652	1.399	1.574	1.746	2.003	2.194
12	0.436	0.484	0.539	0.593	0.662	1.380	1.543	1.690	1.892	2.042
13	0.450	0.488	0.550	0.610	0.677	1.362	1.510	1.644	1.837	1.982
14	0.459	0.503	0.560	0.618	0.687	1.350	1.493	1.631	1.792	1.930
15	0.462	0.503	0.568	0.625	0.695	1.334	1.465	1.603	1.769	1.900
17	0.491	0.528	0.594	0.643	0.708	1.324	1.449	1.574	1.735	1.859
20	0.523	0.557	0.611	0.664	0.728	1.299	1.412	1.514	1.644	1.760
22	0.536	0.575	0.635	0.683	0.746	1.282	1.384	1.480	1.610	1.714
25	0.565	0.597	0.648	0.697	0.754	1.266	1.363	1.447	1.568	1.643
27	0.559	0.601	0.652	0.702	0.762	1.254	1.341	1.430	1.538	1.613
30	0.576	0.611	0.667	0.716	0.773	1.241	1.328	1.405	1.493	1.565
32	0.592	0.633	0.684	0.729	0.781	1.234	1.311	1.384	1.480	1.537
35	0.612	0.645	0.690	0.738	0.790	1.226	1.300	1.369	1.453	1.523
40	0.632	0.662	0.708	0.749	0.798	1.207	1.276	1.342	1.424	1.486
45	0.633	0.670	0.723	0.764	0.813	1.196	1.260	1.320	1.388	1.440
50	0.654	0.684	0.734	0.773	0.820	1.190	1.250	1.303	1.374	1.420
55	0.670	0.700	0.748	0.785	0.830	1.183	1.239	1.291	1.355	1.406
60	0.676	0.709	0.749	0.790	0.833	1.174	1.229	1.277	1.332	1.380
65	0.691	0.720	0.762	0.798	0.841	1.168	1.218	1.266	1.321	1.361
70	0.703	0.731	0.769	0.804	0.845	1.159	1.210	1.259	1.312	1.348
75	0.704	0.735	0.776	0.810	0.850	1.158	1.207	1.252	1.304	1.347
80	0.713	0.740	0.780	0.817	0.855	1.150	1.197	1.238	1.289	1.327
90	0.723	0.755	0.790	0.824	0.862	1.141	1.184	1.222	1.273	1.304
100	0.742	0.769	0.805	0.834	0.870	1.132	1.173	1.211	1.250	1.287

9.3 EFFECT OF DEFECTS

In general, any non-metallic discontinuity in the structure, whether a hard, soft, brittle, gas or vapour phase, will probably impair the properties to some degree. Figure 9.10 is an excellent illustration.

However, of course, the more compact the defect, the less damage will be suffered. At the point at which a defect is smaller than the micro-structural features of the alloy (i.e. smaller than the dendrite arm spacing [DAS]), it probably ceases to be important. It is important therefore to make a distinction between the less harmful defects considered in this section and the more extensive planar defects considered in the next section. (Very large planar defects can measure 10−10,000 times the linear dimensions of the DAS.)

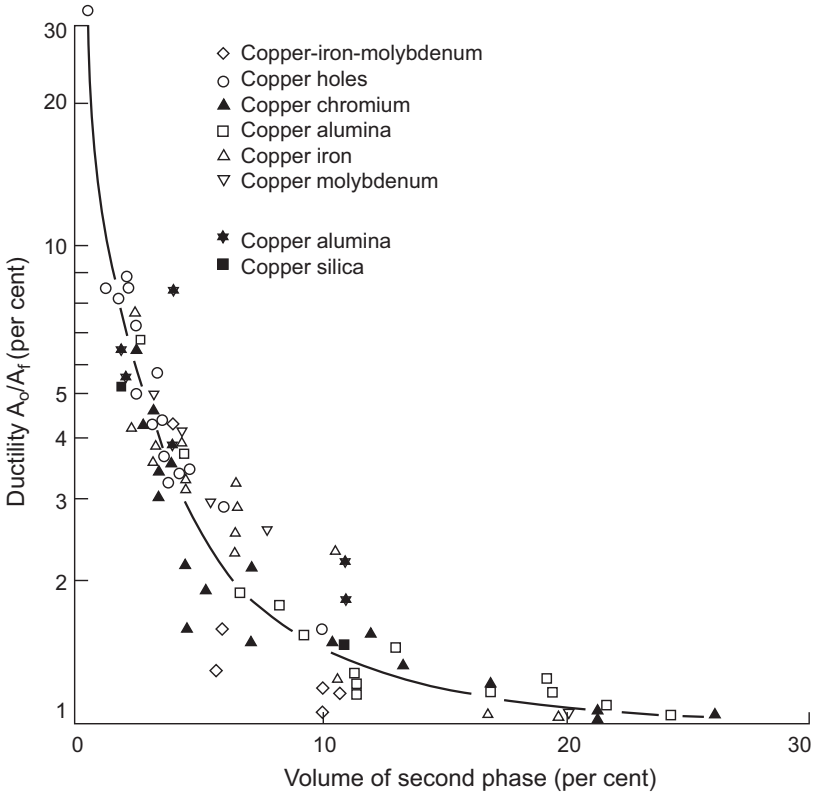

FIGURE 9.10

Ductility of copper containing a dispersion of second phases.

Data from Edelson and Baldwin (1962).

However, the density of defects (the number of defects present in a given volume) is also important, and in some cases will over-ride the effects of the compactness of the defect. We need to keep this in mind because we shall look into the twin aspects of defect size and defect density in the section on properties.

It is noteworthy that defects considered here are not solidification defects. So far as most shaped castings are concerned, apart from a few obvious features as shrinkage porosity and some segregation issues, which are comparatively rare, there is probably no such feature as a *solidification defect*. The only serious defects in castings are *casting defects*. These are all entrainment defects arising from surface turbulence before or during the filling of the mould.

9.3.1 INCLUSION TYPES

Inclusions fall into two major categories: (1) those formed in situ in the liquid or solid matrix by precipitation from solution and (2) those introduced from the outside the liquid metal via an entrainment process, and which therefore have to penetrate the oxide surface.

Those formed atom by atom from the matrix will, of course, enjoy an interface with the matrix which is atomically perfect. This will be an immensely strong interface. Traditional, classical continuum models and the latest molecular dynamics simulations of aggregates of atoms both agree that such interfaces cannot be decohered; their strength

corresponds closely to the ultimate theoretical strength of the matrix, and is therefore in the region of 10–100 GPa. Such inclusions, usually present as desirable second phases, are usually beneficial as strengthening features for the alloy.

The contrast with those inclusions entrained as surface oxide could hardly be more dramatic. Entrained oxide decoheres easily from itself. Similarly, when foreign inclusions become entrained, they arrive in the matrix naturally wrapped in surface oxide, as illustrated in Figure 2.3. As a result of their unbonded wrapping, these inclusions also decohere easily from the matrix. This is the reason for the interesting uniform behaviour of pores and inclusions in copper seen in Figure 9.10. The results for pores and entrained inclusions all fall on the same curve; the higher the defect density, the worse the properties.

Even so, notice that the ductility only approaches disaster levels of 1% at defect densities of more than 10% volume fraction. This is a huge volume fraction. Soberingly, Al alloys are known to have ductilities of 1% or lower with film densities which are so low as to be difficult to estimate, but perhaps in the region of only 10^{-3} vol% (assuming a 1 mm square film 10 nm thick in one cubic mm.).

Whatever the exact numbers, it is clear that films are enormously more damaging than volume defects by a margin of at least several orders of magnitude. In view of this simple deduction, it is difficult to understand the preoccupation which researchers have in identifying compact, chunky inclusions and assuming that these are the initiation sites for cracks, when even a tiny film nearby or in association will effortlessly outweigh its effects. The message is clear: bifilm inclusions (because they act as unbonded cracks) are important and, in densities commonly found in many metals, effectively control properties.

9.3.2 GAS POROSITY

There are several different types of gas porosity, all of which are common in castings. They have to be diagnosed correctly, otherwise a wrong, and consequently ineffectual treatment, may be attempted. The main categories are listed here.

1. Gas precipitated from solution
2. Entrained air bubbles
3. Core blows
4. Micro-blows
5. Layer porosity

Layer porosity is that type of shrinkage porosity that forms in long freezing range alloys under conditions intermediate between those for concentrated macroporosity, and dispersed microporosity. This important intermediate condition is clear from Figure 7.15. Whereas macroshrinkage in the form of a shrinkage pipe, or large central cavity, can be viewed as a compact defect, and dispersed micropores can be viewed as individual compact defects, the intermediate condition is more severe, in the sense that a relatively small volume of porosity has formed itself into an extended defect by concentrating into a sheet, or layer.

To form an opinion of the seriousness of this defect, it is helpful to recall the way in which layer porosity is formed. The pore spreads across a surface of constant tension that exists in the residual liquid in the dendrite mesh. This formation mechanism results in the unique structure of the defect. The layer is not exactly equivalent to a crack because the dendrites are hardly disturbed during its growth; it is only the residual liquid that moves, opening up the planar defect. In fact the dendrites continue to bridge the pore as a dense array, effectively stitching the layer together with closely spaced threads. For this reason, its effect on tensile properties seems to be intermediate between that of individual pores and a fully open hot tear or crack. This intermediate position is seen in its rather mild effects on mechanical properties illustrated in Figure 9.11.

The presence of layers is usually not easily discerned optically on a polished section because there are so many bridging dendrites that the overall pattern is almost hidden, causing the porosity to appear as normal dispersed microporosity. However, it is clearly revealed on radiographs if the view direction is oriented along the plane of the porosity.

A summary of gas pore diagnostic information is given in Table 7.3.

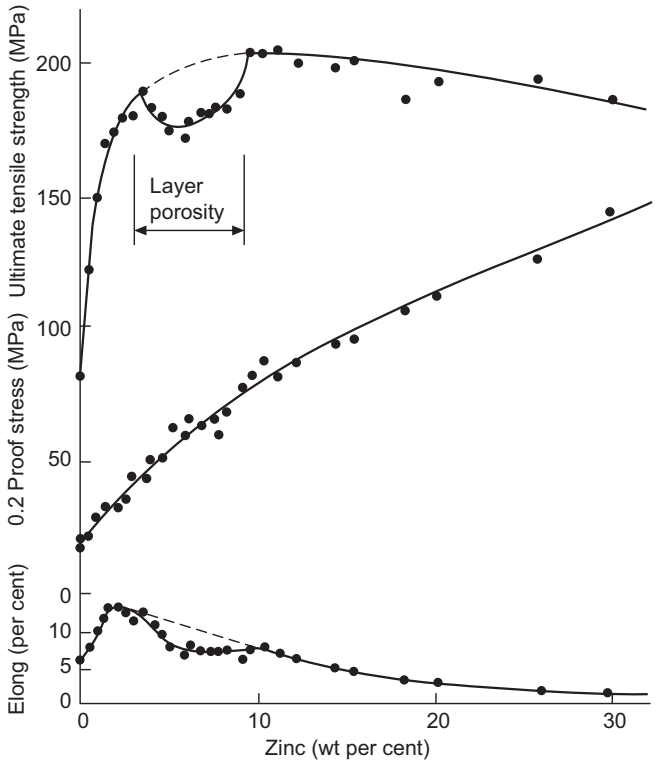

FIGURE 9.11

Effect of layer porosity on the mechanical properties of Mg-Zn alloys.

Data from Lagowski and Meier (1964).

9.3.3 SHRINKAGE POROSITY

Microshrinkage

The effect of shrinkage porosity on mechanical properties is probably practically identical to that of any other kind of porosity. On fracture surfaces, it is common to identify the pore as the origin of the failure. However, we have to keep in mind that, although not obvious to a casual viewer, a bifilm will almost certainly be associated with the pore, probably having initiated the formation of the pore, and will almost certainly be the starting point of the crack leading to failure. The relative likelihood of initiation by the pore or its associated bifilm is easily assessed by comparing the radius of curvature that each provides as a stress raiser. The radius of curvature of a shrinkage cavity will correspond to the curvature dictated by the curvature possible between dendrites of the order of 10 μm for a typical small casting. The curvature formed by the tip of a bifilm would be expected to be in the region between 10 and 1000 times smaller, thus being a significantly more threatening initiation site for a crack propagated by stress.

A further pitfall to bear in mind is that practically all shrinkage defects identified by radiography are actually not shrinkage defects but oxide film defects. A compact, convoluted bifilm, or tangled mass of many bifilms, containing some residual entrapped sprinkling of gas will appear identical to shrinkage porosity on a radiograph. Such attempted identifications should *not* be labelled 'shrinkage' but instead '*appears* to be shrinkage' (with the proviso 'but probably not' added for good measure). In my experience, most so-called 'shrinkage defects' turn out to be oxide defects introduced by poor filling systems.

True shrinkage defects are, in my opinion, rather rare. This is easily understood, because most foundry people understand shrinkage and the necessity for the provision of feeders. Thus most castings are reasonably well fed and are unlikely to show 'true' shrinkage defects, only 'apparent' shrinkage defects which are in fact filling system defects.

For those castings that do suffer some reduced internal pressure as a result of a poor feeding condition, if any part of the liquid is still contact, or nearly in contact, with the outside skin of the casting, the skin might be sucked in, and a shrinkage pore grown by extension of this microscopic pipe drawn in from the outside surface. I have previously called this *externally initiated shrinkage porosity* (Figures 7.13 and 7.17). On a section cut through the casting, it is indistinguishable from an internally initiated porosity. However of course, because it is externally linked, it constitutes a leak to the outside world. It would perform badly as a vacuum component, or would internally corrode, or harbour contamination in a food processing or chemical plant. If machined into from the far side, it would form a through-wall leak.

For other genuine shrinkage conditions in a long freezing range alloy, the microshrinkage pores can take the form of layer porosity (Figure 7.15)—as has already been described in the previous section—as also possibly formed by gas precipitation. As has been repeated mentioned throughout the book, both shrinkage and gas may have cooperated to form the porosity. It is probably not possible to detect the driving source of the porosity, both shrinkage and gas varieties, and the combined variety, would probably all appear identical if formed at the same stage of dendrite development in the casting.

Macroshrinkage (Shrinkage Pipe)

A macroshrinkage pipe, usually from a feeder head, can take the form of a smooth walled cone for a eutectic alloy, or an extensive region of sponge porosity if a long freezing range alloy (Figure 7.8). The sponge appears to be separate interdendritic pores on a section, but the pouring of a coloured liquid through the pores quickly illustrates how interconnected they are.

The various shapes of macro pores are very much influenced by gravity (effectively they float to the top of trapped liquid volumes—or perhaps we should say the residual liquid in the trapped liquid region naturally sits at the bottom of these volumes). Typical shapes are seen in Figures 7.30 and 7.31.

Such macroporosity is simply a sign of inadequate feeding. The rules for good liquid feeding are presented in 'Casting Manufacture'.

9.3.4 TEARS, CRACKS AND BIFILMS

All planar defects such as cracks are capable of constituting extensive faults in the casting, and so are of great concern with regard to its strength, toughness and fatigue resistance. Not only do such features reduce the load bearing area, but increase stress on the residual area even further because of the effect of stress intensification at the crack tip. The overall effect is significant as is clear in Figure 9.12.

Interestingly, the effect of these defects on the yield stress is practically zero. Figure 9.11 illustrates a clear result for Mg-Zn alloys. The effect arises as a result of the reduction in area and notch effects leading to plastic flow around the crack tip which raises the strength by work hardening. The loss of area and the gain in strength match sufficiently well to yield a negligible net change.

A fundamental, but not yet resolved issue, needs to be raised at this point. It is possible that tears, and cracks and bifilms are all the same defect, all being simply bifilms. The difference is merely that tears and cracks are bifilms that are open; tears have opened early, while the casting is still partly liquid, whereas cracks have opened late, after full solidification. Tears open with little or no stress, merely responding to strain, whereas cracks in the solid tend to only open after significant stress has accumulated, and possibly with a loud audible 'crack' as elastic energy is released. Bifilms are of course effectively cracks, but if they remain substantially closed, they can remain undetected and unsuspected. It is frustrating that insufficient research has been carried out to ascertain whether the statement 'all tears and cracks are originally bifilms' is true. However, on balance, it seems to me to be likely to be true.

Hot tears and cold cracks open during cooling as a result of tensile strain and stress respectively in the casting. They typically occur, therefore, across sections and in radii, where they will have an especially damaging effect on the serviceability of the casting. Their diagnostic features have already been discussed in Chapter 8. As open failures, they are naturally more serious defects than a closed bifilm. Although the bifilm can act as a crack when subjected to a tensile stress at right angles to its plane, it may not have developed significant planar morphology by unfurling, and even if

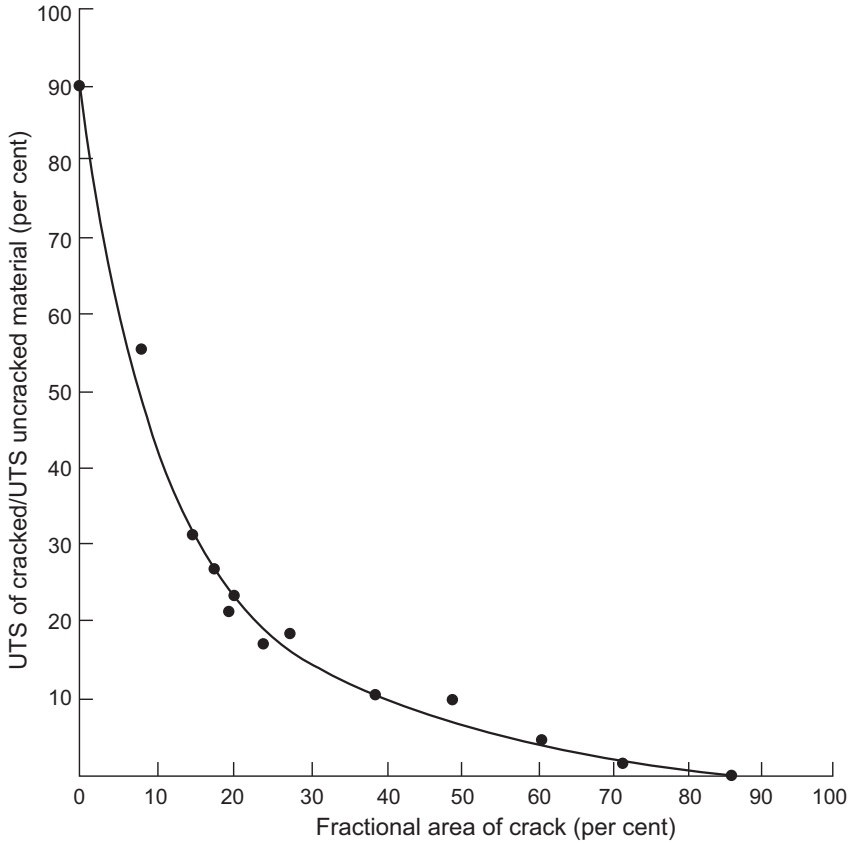

FIGURE 9.12

UTS of a casting as a function of the area of the crack.

From Clyne and Davies (1975).

completely unfurled, and thus not capable of withstanding a tensile stress normal to itself, it will be able to withstand significant shear stress because of friction between the oxide halves, and because of jogs and creases that will provide mechanical obstruction to shear. Thus a closed crack, or closed bifilm, is a crack-like defect, but exhibits some strength under some loading conditions. The open crack or opened bifilm is a seriously weak feature.

Such defects, especially if open, can extend to the whole casting cross-section, in which case, of course, the casting is already broken, and therefore perhaps fortunately identifiable as defective before being put into service!

However, a crack connected to the surface may have formed and opened at high temperature may close again at the surface as the casting cools because of the normal development of compressive stress in the casting surface during the final stages of cooling, as discussed in Section 8.2. This is a standard cooling regime for castings. Thus cracks that are closed, and effectively invisible at the surface, should be expected as the norm. Such cracks, closed tightly under pressure, would be extremely difficult to detect by normal methods such as dye-penetrant testing and radiography. It is possible, therefore, that this is a common but rarely detected defect. It represents a serious concern in safety-critical components. Its detection might require pre-stressing to open the crack whilst being viewed by real-time radiography, or while being investigated by a penetrant dye. The writer is not aware that such testing techniques are ever used. However, for the most important of applications they would be well worth careful consideration. Sophisticated resonance testing would be another discriminating testing technique.

It is worth restating that the extensive tear or crack-like defects are probably not so much initiated by bifilms, but actually *are* the bifilm. These entrainment defects can easily extend over the whole casting cross-section, as we have seen. The visible presence of one of these defects will almost certainly warn of the presence of many more, less easily seen neighbours, and is the reason why it is sometimes futile to attempt to repair such defects by welding for instance.

The lesson remains clear. Intensive inspection and repair is no substitute for correct casting procedures to achieve good metal, quiescently filled.

Bifilms

The double film defect, the bifilm, is formed during the re-aggregation or re-assimilation of a dispersed or fragmented liquid. Thus actions such as the folding-in of the liquid surface, or the mutual assimilation of droplets, all result in the surface oxide film meeting as an impingement of dry face to dry face. Whereas liquid metals during turbulent casting are re-aggregation events of a fragmented liquid, close analogies exist with several solid-state processes such as powder metallurgy and spray forming which are similarly re-aggregation processes, re-forming bulk solids from oxide-covered particulates.

The composition of the surface film is usually an oxide, nitride or pure carbon. The bifilm defect can be extensive, occupying the whole of a cross-section. Alternatively may be small and even negligible, but no one knows how small bifilms can be and still exert some important effect on properties. Similarly, placing and orientation are random, so that either its chance placing, or its orientation, or its size, or all factors together, in a highly stressed region, may or may not be damaging. It is the unpredictable nature of the double film defect that is such a concern. In this way, it contrasts with the bifilms which must exist in powder metallurgy products because here the films are uniformly thin and of a controlled size and dispersion. This is all perfectly predictable.

I am often questioned why a sporadic defect such as a crack always appears at the same place in a particular casting. Clearly, the pattern of stress concentration in the component is fixed. The random distribution of bifilms means that in the case of relatively few bifilms sometimes a bifilm will happen to be sited in the stressed region, and thus be opened by the strain. However, if there is a high concentration of bifilms, as often happens, there will then always be at least one in this region, with the result that all castings will exhibit a similar crack.

Figure 9.13 shows two simple plates 10 mm thick cast in 99.5% Al in the author's laboratory (Runyoro, 1992). They were cast in a vertically parted mould via a bottom gate into the centre of the long side at ingate speeds of above and below 0.5 ms^{-1}, respectively, and were afterwards subjected to a three-point bend test (later work progressed to use the

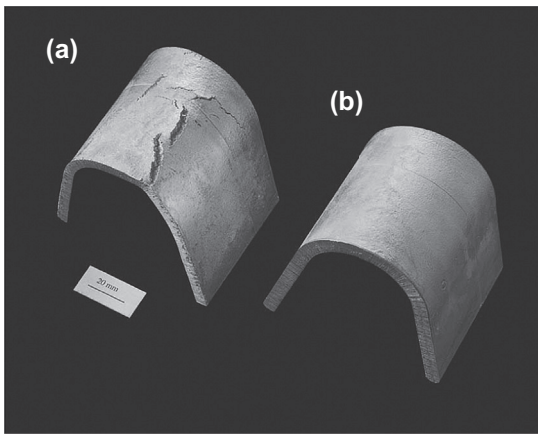

FIGURE 9.13

Plates of 10 mm thick cast in 99.5Al subjected to three-point bending (a) filled at an ingate speed greater than 0.5 m/s and (b) less than 0.5 m/s.

Courtesy Runyoro (1995).

much improved four-point bend test). The turbulently filled casting exhibited several cracks, none of which was along the line of the maximum stress. In fact, the cracks were aligned in *random* orientations. The *randomness* was a strong clue to their origin as the products of surface turbulence because turbulence means randomness, chaos, and essentially unpredictability. The material between the cracks is clearly highly ductile, as would be expected for rather pure cast aluminium. Also, interestingly, under the microscope, the tips of the cracks are found to be blunt. They have been unable to propagate in the ductile aluminium, which constitutes a crack-blunting matrix. It follows that the cracks have not propagated but must have pre-existed as cast, and have merely opened when subjected to bending. All these features are to be expected from entrained bifilms. The test plate (Figure 9.13(b)) cast at a speed at which entrainment is not possible is clearly free from bifilm defects.

If the bifilm is sufficiently large, and if it breaks the surface, then it *may* be detected by normal dye-penetrant methods. However, as a result of the bifilm being naturally tightly closed or forced closed at the surface by surface compressive stress, the dye penetrant approach is not reliable, indicating perhaps only minute pinpoint contact in places. The 'stars at night' appearance of defects on vacuum-cast Ni base alloys when the fluorescent penetrant dye is viewed under ultraviolet light are mostly defects of this kind. This is easily demonstrated by putting on a well-designed filling system, after which the 'stars' all disappear! Bifilm defects are also difficult to detect by radiography unless the incidence of radiation happens to be in or near the plane of the defect, or unless the central region is sufficiently open to constitute an open crack, or the enclosing films sufficiently thick to appear as inclusions.

In contrast to the difficulty of observing bifilms non-destructively, they can sometimes be clearly seen on fracture surfaces. Very thin films require careful study of the fracture surface to reveal their minute characteristic signatures such as the tracery of fine folds. LaVelle (1962) studied the fracture surfaces of aluminium alloy pressure die castings and found layer upon layer of oxide films throughout the structure, giving the fracture a fibrous appearance. In some cases, the surface contact of these extensive defects was minimal, indicating how unreliable their detection by a surface penetrant dye technique could be.

Because film defects are potentially so damaging, and because they are practically impossible to detect by non-destructive methods with any certainty, the only suitable method to deal with this problem is not to attempt to inspect for them, but to set in place manufacturing techniques that guarantee their avoidance. At the present time, no specification calls for specific manufacturing techniques that would eliminate film defects. This unsatisfactory situation has to change.

Only control of the quality of the melt and of the filling of the casting will prevent film defects entering the mould. Once good quality metal is in the mould, measures will be required to prevent the reintroduction of defects by such processes as the outgassing of cores or other forms of surface turbulence after the filter (if any) in the runner. Only by carefully planned and monitored processing will bifilm creation be overcome with confidence.

Again, it bears plentiful repeats: the achievement of good castings lies not in inspection, but in process control.

9.4 TENSILE PROPERTIES

The fracture of metals is a complex subject that we can only touch on with respect to its castings aspects. Even so, the outline of knowledge presented here will be helpful to guide the casting engineer to achieve the best properties for his castings.

9.4.1 MICRO-STRUCTURAL FAILURE

Three main varieties of micro-structures and their mechanical behaviour can be distinguished:

1. Where the matrix of the alloy is ductile, and the second phase, perhaps as hard particles, introduced by mixing (i.e. entrained), the added particles are not bonded to the matrix. When subjected to tensile strain the particles act like pores as seen in Figure 9.10 as a result of their wrapping of unbonded oxide film, as seen in Figure 2.3. This is easily understood; the mix has isotropic properties, and the microscopic failure associated with each particle has no preferred directionality.

2. Where the second phase particles have formed in situ in the alloy, if their formation was not associated with entrained particles, they would be perfectly bonded to the matrix. No fracture within the particles or decoherence at the interface could occur. This is perhaps more clearly seen in the precipitates formed in the solid, such as the GP zones in Al alloys, where debonding is inconceivable. Gall et al. (2000) use atomic simulations to estimate that the force to separate Si from the Al matrix would probably exceed 30 GPa. This is 100 times a typical stress to cause tensile failure of an Al-Si alloy. Thus debonding (and we might also assume, cracking) will be impossible for Si particles.
3. For those second-phase particles that nucleate and grow on entrainment defects such as bifilms, the associated unbonded interface in the bifilm causes interesting specific failure modes. As always, Al-Si alloys are the most intensively studied system comprising an essentially non-metallic second phase, silicon metal, in the soft metallic Al matrix. As such, the findings are instructive because it exhibits behaviour typical of many in other such alloy systems, particularly the cast irons.

When subjected to a tensile load, the silicon particles appear to either fracture or decohere from the matrix. In terms of bifilm theory, this behaviour occurs if the silicon happens to have precipitated on both sides of the bifilm, with the crack in the centre (or only on one side, with the crack between the particle and the matrix).

Some admirable evidence supporting this hypothesis comes from the work of Lopez and his team (Fras, 2007) who painstakingly measured individual particles, noting their orientation to the tensile axis and whether they fractured internally or decohered. Their fascinating results are presented in Figure 9.14.

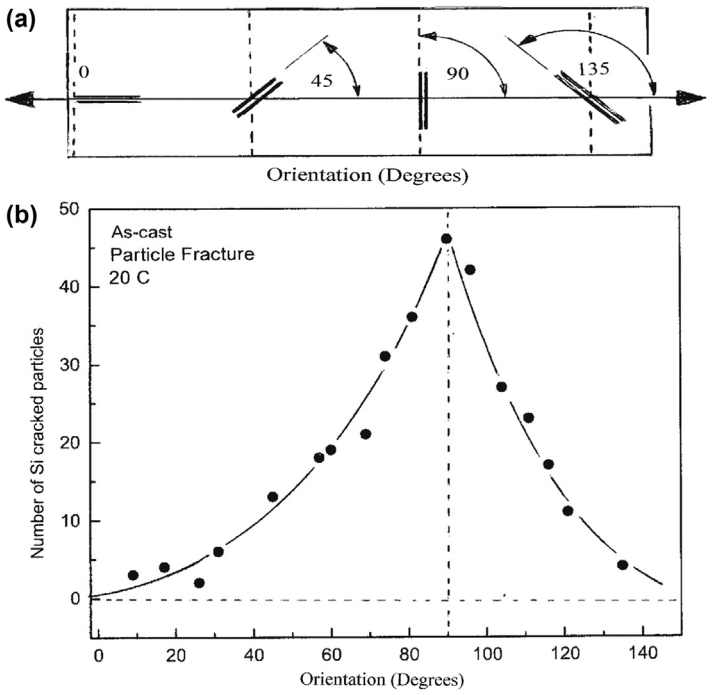

FIGURE 9.14

(a) Silicon particles in Al-Si alloy A319 subject to tensile stress. (b) At room temperature, the particles mainly fracture when at 90° to the stress axis. (c) At 300°C ductile shear at 45° promotes decohesion, in addition to tensile failure continuing near 90°; (d) for alpha-Fe particles at room temperature, their convoluted bifilms lead to fracture at random angles (Fras, Wiencek, Gorny, Lopez, 2007).

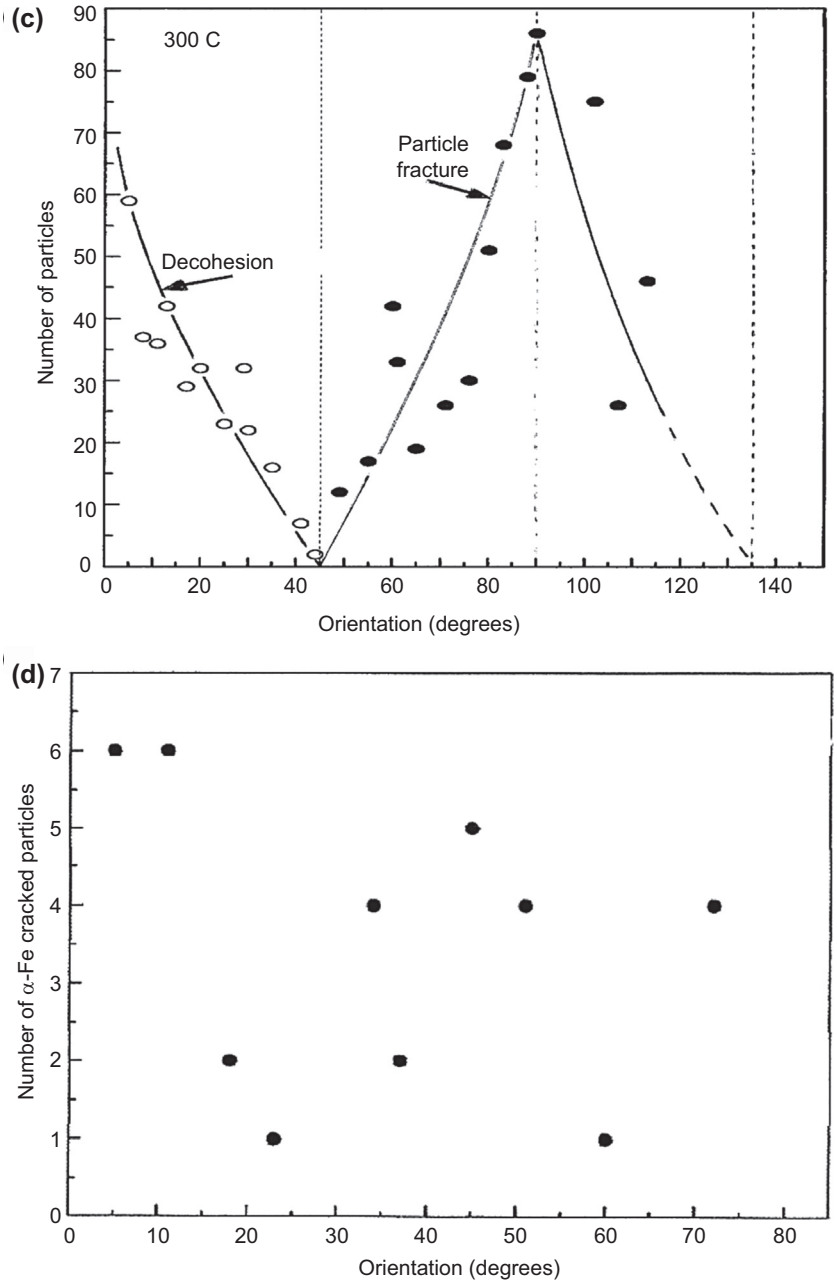

FIGURE 9.14 Cont'd

Clearly, at room temperature, most particles fractured when the stress was at right angles to the plane of the particle. This is no surprise. However, it is interesting that no decohesion is reported for this orientation. In the case of the silicon particles, perhaps the tensile force operates on the extreme edges of the two particles to separate them successfully, whereas when operating on the edges of a vanishingly thin and weak half of the bifilm the strain might tweak the edges a little, but is not expected to pull the bifilm completely clear as in the case of the strong, rigid particle.

At 300°C, the situation becomes more complex. The matrix now softens and can flow plastically under tensile load. Those particles aligned parallel to the stress direction and which have formed on only one side of a bifilm will now be subject to material shearing across and at 45° away from the particle, opening up the unbonded interface. When oriented at 45° to the stress, the maximum resolved shear will be aligned parallel to the length of the particle, so that decohesion is no longer favoured. Fracture of particles starts to occur at increasing angles of orientation, maximising at 90° once again as would be expected.

As an interesting comparison, alpha-Fe particles were also checked for their sensitivity to orientation with respect to the tensile stress direction. As is clear from Figure 9.14(d), there is no favoured direction. This is to be expected in view of the ability of this cubic phase to wrap around convoluted bifilms during its growth, sealing in the convolutions, rather than straightening them as happens with Si particles and beta-Fe particles. The marked difference in behaviour is clearly shown in Figure 6.20.

Turning now to a common feature of fracture surfaces, Figure 2.44(d) shows a typical so-called ductile fracture consisting of a dense array of ductile dimples. At the base of each dimple is a fractured Si particle. If the proposition is that Si particles are strong and resistant to fracture, then surely there must be a bifilm present in every ductile dimple? This reasoning indicates that huge, possibly unreasonably high, numbers of bifilms are present.

In practice, this appears to be only partly true. It seems there is a reasonable explanation of how such numerous fractures could occur from a much smaller population of bifilms as follows. Each bifilm will consist of one smooth side and one side with numerous transverse folds, constituting short transverse cracks. An illustration is seen in Figure 6.20(b) which shows a long beta-Fe particle with one continuous length on one side of the main crack, and separate short lengths of crystal on the other side separated by transverse cracks. This structure is to be expected in all bifilm formation because, during the turbulence of folding in the surface, the impinging of two areas of surface are not likely to each have the same area; the larger surface will be forced to adopt rucks, as transverse folds, while the opposite surface film will remain essentially unfolded. Thus the growth of the beta-Fe crystal will be continuous along one side of the continuously smooth side of the bifilm and will be a series of short lengths on the other side of the bifilm as a result of a natural presence of short transverse cracks.

During the solidification of the Al-Si–coupled eutectic, the bifilms in suspension will tend to be dragged down into the hollows between the advancing Al and Si phases (Figure 9.15). This will occur because the bifilms will be pushed ahead by the Al phase because the oxide is not preferentially ‘wetted’ by the alpha phase, but will preferentially attach to the Si phase, lowering the overall energy of the system. The bifilms will have one smooth side and one with transverse folds (i.e. subsidiary transverse cracks connected to the main longitudinal crack). This is shown in Figure 9.15. If it happens that the transverse cracks are on the side of the Al phase, they will be pushed ahead, effectively flattened against the advancing Si particles as a result of the Al phase tending to ‘push’ the bifilm. Thus the Al phase will not be cracked, explaining the perfection of the plastic shear between Si particles, forming razor-sharp cusps of necked-down material. On the other hand, if the transverse cracks happen to be on the side of the Si particles, the Si will grow around these, incorporating the transverse cracks into the advancing Si crystal. Thus the advancing Si phase will be expected to be cracked repeatedly along its length. If Figure 6.20 is typical, we might expect to see transverse cracks every 10–20 μm which appears reasonably consistent with the observed fractures.

9.4.2 DUCTILITY

Figure 9.10 is a famous result showing the ductility (in terms of reduction of area, RA) of a basically highly ductile material, pure copper, being reduced by the addition of various kinds of second-phase particles, including pores. It is clear that the clean material has a ductility of more than 30%. An RA of 100% (meaning necking down to zero residual area) would be expected for extremely clean copper, but there is a large deleterious effect of the second phases, more or

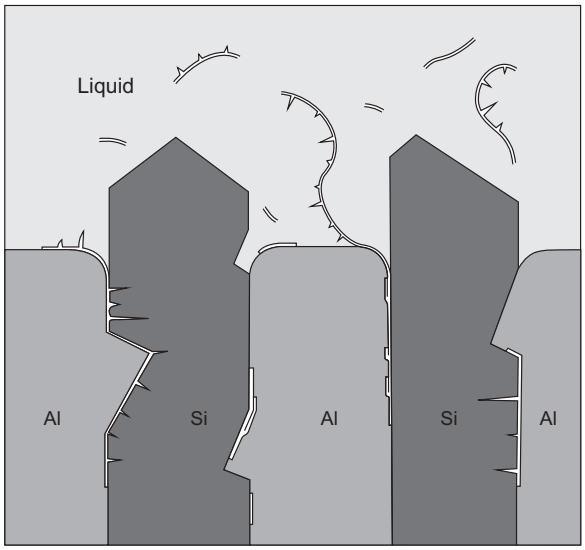

FIGURE 9.15

Bifilms with subsidiary transverse branches are entrained between the Al and Si phases during the growth of the Al-Si eutectic. Branches are pushed back and rejected by the Al phase, but are incorporated in the Si phase, leading to easy Si fracture and decoherence.

less irrespective of their nature. The lack of sensitivity to the nature of the particles or holes is almost certainly the result of the relatively easy decohesion of the particles from the matrix when deformation starts. Thus all particles act as holes.

This result is predictable if the particles are introduced into the melt by some kind of stirring-in process. As the particles penetrate the surface, they necessarily take on the mantle of oxide that covers the liquid metal (Figure 2.3(b)). Thus all immersed particles will be expected to be coated with a layer of the surface oxide, with the dry side of the oxide adjacent to the particle. The absence of any bonding across this interface will ensure the easy decohesion that is observed. In practice, the submerged particles will often remain in clumps despite intense and prolonged stirring (Figure 2.3(c)). This seems to be most probably the consequence of the particles entering the liquid in groups and being enclosed inside a packet of oxide. With time, the enclosing wrapping will gather strength as it thickens by additional oxidation, using up the enclosed air, and so gradually improve its resistance to being broken apart.

In castings, the volume of pores rarely exceeds 1%. (Only occasionally is 2–3% porosity found.) For 1% porosity, Figure 9.10 indicates that the ductility will have fallen from the theoretical maximum (which will be 100% reduction in area for a perfectly ductile material) to approximately 10%, an order-of-magnitude reduction! However, 10% elongation (note we are neglecting that the elongation is not accurately equivalent to RA) is fairly typical, if rather generous, for most light alloys, indicating the possibility of at least 1% by volume (or area) of defects normally present whether detected or not.

Why should an assembly of holes in the matrix affect the ductility so profoundly?

Figure 9.16 shows a simple model of ductile failure. For the sound material, the extension to failure is of the order of the width l of the specimen, because of the deformation of the specimen along 45° planes of maximum shear stress. For the test piece with the single pore of size d, the elongation to failure is now approximately $(l - d)/2$. In the general case for a spacing s in an array of micropores, we have

$$\begin{aligned} \text{Elongation} &= s - d \\ &= 1/n^{1/2} - (f/n)^{1/2} \\ &= \left(1 - f^{1/2}\right)/n^{1/2} \end{aligned} \tag{9.5}$$

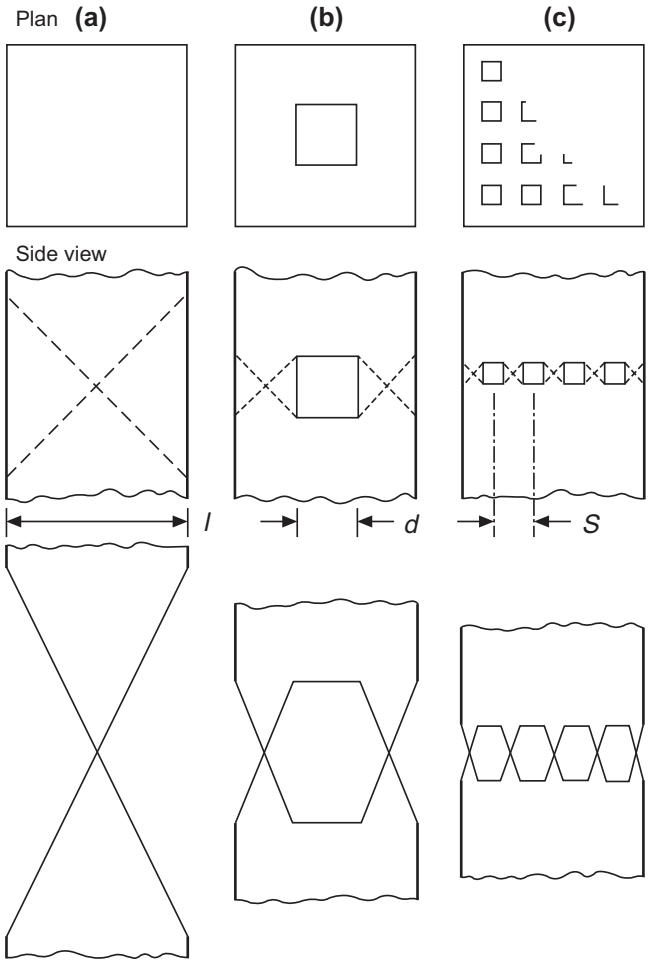

FIGURE 9.16

Simple ductile failure model, representing (a) sound specimen that necks down 100% reduction in area; (b) a single central pore reducing RA to about 50% with a single cup-and-cone fracture; and (c) multiple pores leading to poor elongation with ductile dimple fracture surface.

where n is the number of pores per unit area, equal to $1/s^2$ and f is the area fraction of pores on the fracture surface, equal to nd^2.

Equation (9.5) is necessarily very approximate because of the rough two-dimensional model on which it is based. (For a more rigorous treatment, the reader is recommended to the pioneering work by Thomason (1968) and the more recent work by Huber (2005).) Nevertheless, our order-of-magnitude relation indicates the relative importance of the variables involved. It is useful, for instance, in interpreting the work of Hedjazi (1976), who measured the effect of different types of inclusions on the strength and ductility of a continuously cast and rolled Al-4.5Cu-1.5Mg alloy. From measurements of the areas of inclusions on the fracture surface, Hedjazi reached the surprising conclusion that the film defects were less important than an equal area fraction of small but numerous inclusions. His results are seen in Figure 9.17. One can see that for a given elongation, the microinclusions are about 10 times more effective in lowering ductility. However, he reports that there were between 100 and 1000 times the number of microinclusions compared with

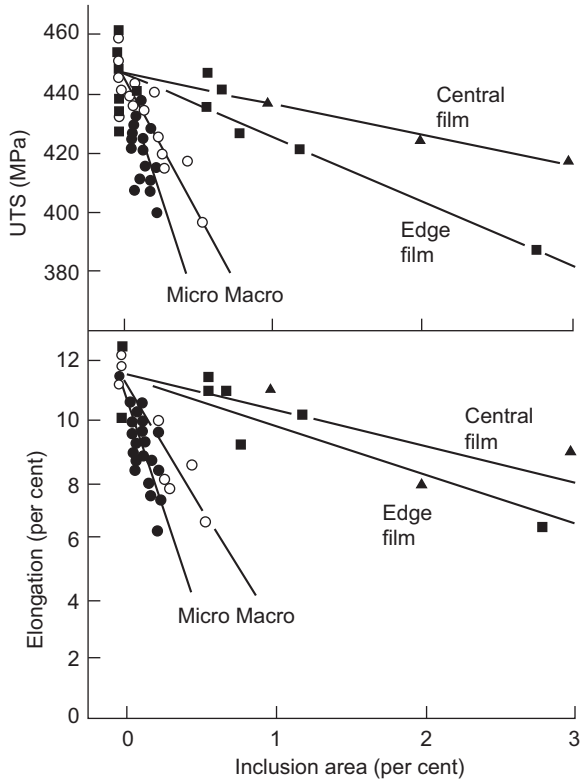

FIGURE 9.17

Strength and ductility of an Al-4.5Cu-1.5Mg alloy as a function of total area of different types of inclusions in the fracture surface.

Data from Hedhazi et al. (1976).

film-type defects in a given area of fracture surface. From Eqn (9.5), an increase in number of inclusions per unit area by a factor of 100 would reduce the elongation by a factor of 10, approximately in line with the observations.

The other observation to be made from Eqn (9.5) is that ductility falls to zero when $f = 1$, for instance in the case of films which occupy the whole of the cross-section of the test piece. This self-evident result can easily happen for certain regions of castings where the turbulence during filling has been high and large films have been entrained. This is precisely the case for the example for the ductile alloy Al-4.5Cu that failed with 0.3% elongation, nearly zero ductility, seen in Figure 2.44(a). This part of the casting was observed to suffer a large entrainment effect that had clearly created extensive bifilms. Elsewhere, other parts of the same casting had filled quietly, and therefore contained no new bifilms, but only the background scatter of old bifilms inherited from the distribution already present in the melt. In this condition the ductility of the cast material rose to a rather mediocre 3.5% (Figure 2.44(b)).

Pure aluminium is so soft and ductile that it is almost possible to tie a length of bar into a knot and pull the knot tight. However, Figure 9.13 illustrates how the presence of bifilms has caused even this ductile material to crack when subjected to a three-point bend test. Notice the material close to the tips of the cracks is highly ductile, so the cracks could not have propagated as normal stress cracks, because the crack tips would have blunted rather than propagated (as confirmed under the microscope). Thus the only way for such cracks to appear in a ductile material like pure

aluminium is for the cracks to have been introduced by a non-stress mechanism. The random accidents of the folding-in of the surface from surface turbulence seems the only likely mechanism, corroborated by the random directions of the cracks, not necessarily aligned along the direction of maximum strain. The *randomness* of their *direction* and *size* is strong confirmation of their origin as the result of a chaotic process such as flow suffering surface turbulence.

Regardless of the inclusion content of a melt, one of the standard ways to increase the ductility of a casting is to freeze it rapidly. This is usually a powerful effect. Figure 2.47 illustrates an approximate 10-fold improvement as the DAS drops from 90 to 30 μm. The effect follows directly from the freezing-in of bifilms in their compact form, reducing the time available for the operation of the various unfurling mechanisms. (There may also be some a contribution from the dendrites pushing the bifilms away from surface regions, effectively sweeping the surface regions clear, and concentrating the bifilms in the centre of the casting where they will be somewhat less damaging to properties as is clearly seen to happen in the channels, mainly the runner and gates, of filling systems of castings. This effect has not been investigated, but may be significantly affected if the bifilms are not quite cleared from the surface regions, but are organised into planar sheets by the columnar grains, as in Figure 2.43(c), and whether therefore the benefits are now dependent on the direction of stress.)

The converse aspect of this benefit is that if the ductility of a casting from a particular melt quality is improved by chilling, this can be probably taken as proof that oxides are still present in the melt. (A simple quality control test can be envisaged based on this proposition.)

The great sensitivity of ductility to the presence of defects in the form of pores or cracks (or any other easily decohered interface such as those obligingly provided by bifilms) is the most powerful limitation to the attainment of good ductility. The awesome spread of ductilities of even aerospace castings is graphically illustrated in Figure 9.18(a) for Al-7Si-0.4Mg alloy by Tiryakioglu (2009a). Because strength is increased by heat treatment, so the elongation of the alloy falls. However, the major effect can be seen to be not heat treatment, but some other arbitrary factor, causing many results to fall lamentably short of their potential. This scatter is attributed to the presence of bifilms. No other conclusion seems possible because aerospace foundries pride themselves on the control of all casting variables. Unfortunately, the one variable which has been unsuspected and has therefore escaped control so far has been turbulence during pouring. Tiryakioglu (2009b,c) produces similar results for the higher strength Al-4.5Cu-type casting alloys A206 and A201, the latter containing 0.7Ag (Figure 9.18(b)). It is clear that excellent properties could be achieved with simple, low-cost Al-Si alloys if they were sufficiently free from bifilms.

Furthermore, the limit shown in Figure 9.18 is only the limit of *uniform* elongation. After the initial extension of the test piece in a uniform manner, it then starts to *neck down*, beginning the *non-uniform* elongation regime. Alexopoulos and Tiryakioglu (2009) show that the total elongation is nearly doubled by the addition of the non-uniform elongation. The elongation associated with necking-down is expected to be an important feature of metals free from bifilms. Zhong and colleagues (2013) suggest it is the work hardening and the strain rate hardening close to the onset of necking that matter for ductility and formability, rather than the overall values of these characteristics. Thus when metals and alloys are produced free from bifilms, they will have a high but as yet unknown elongation, but be expected to achieve routinely 100% RA as a demonstration of their perfection. The RA might become then a more common and discriminating measure of ductility.

Finally, there is the practical challenge of achieving the best ductility from a given batch of alloy. For instance, the ductility falls with aging, but having reached a minimum at the peak hardening response, the ductility then rises once again. Thus occasionally over-aging is recommended equally with under-aging to achieve good ductility. Figure 9.19 illustrates that this is unfortunately not always true for the precipitation hardening of Al alloys. The under-aging treatment optimises ductility for Al-Si-Mg alloys. However, the opposite appears to be true for an Al-Zn-Mg-Cu alloy (Figure 9.20).

9.4.3 YIELD STRENGTH

Steels have a well-defined yield point separating elastic and plastic flow regions so the yield stress can be defined precisely. Al alloys show no such definitive behaviour. The smooth and gradual transition between elastic and plastic behaviour is so difficult to define that it forces us to define an effective yield stress in terms of a ‘proof stress’. We shall

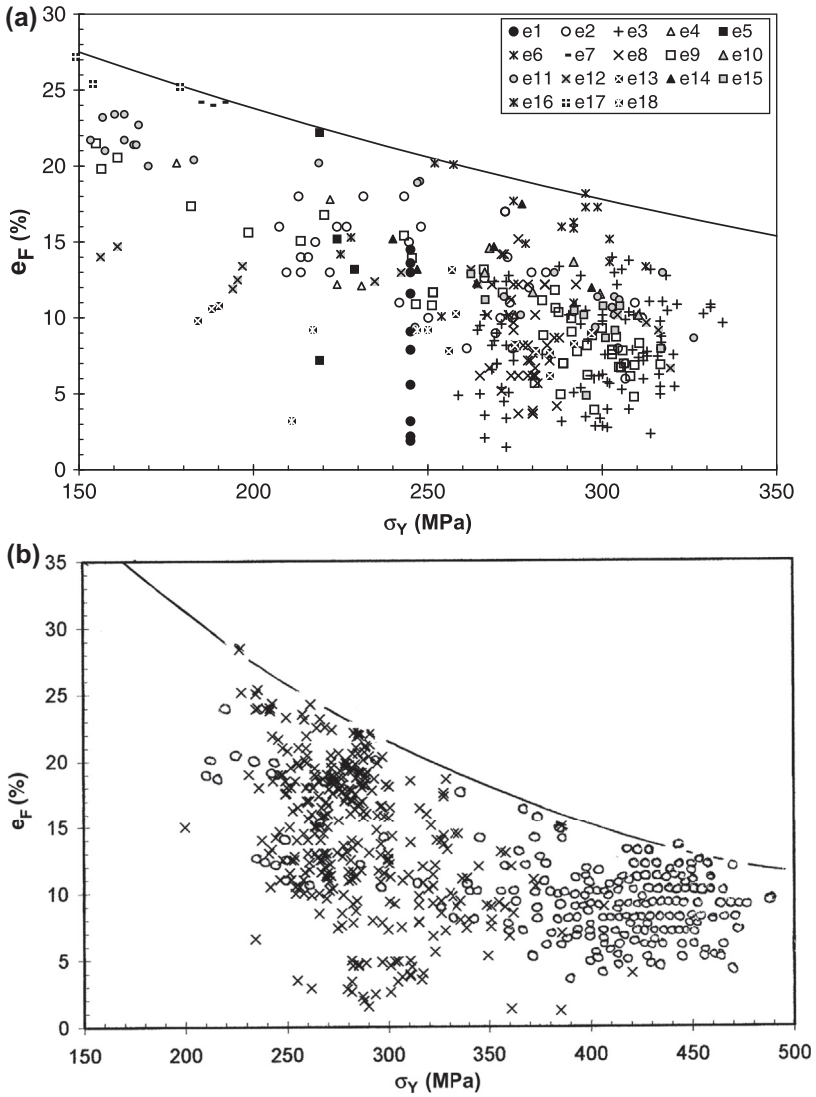

FIGURE 9.18

The scatter of uniform elongation to fracture results for (a) Al-7Si-Mg alloys (356 and 357 types) and (b) Al-4.5Cu alloys (201 and 206 types), reported mostly from aerospace foundries. (Tiryakioglu et al., 2009). Clearly, the attainments of many fall far short of the potential available.

assume that the 0.2% proof stress (0.2 PS) is sufficiently equivalent for our purposes. (The 0.2 PS is that stress at which reversible elastic deformation has just exceeded its limit, and a small amount, 0.2%, of permanent plastic deformation remains on unloading. Some define yield at 0.05 PS and others at 0.1 PS. All these definitions are closely similar to within a few MPa.)

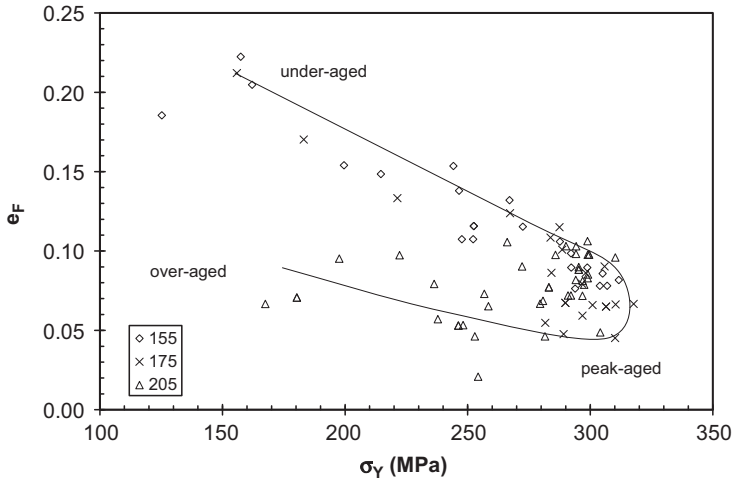

FIGURE 9.19

Elongation versus yield strength for Al-7Si-0.4Mg alloy showing under-aged strengths to be superior to those developed by over-aging (Alexopoulos and Tiryakioglu, 2009).

Whereas both the ultimate strength and the ductility can be greatly damaged by defects, the yield strength is interestingly insensitive to their presence. This behaviour is explained by the load bearing area being reduced by the presence of the defect, thus increasing the stress in the matrix and thereby causing work hardening because of local plastic flow. The increased strength of the matrix as a result of the work hardening to some extent counters the effect of the reduction in load bearing area, keeping the yield point reasonably constant.

This insensitivity of yield to layer porosity is seen in Figure 9.11. The few percent or so loss of area from layer porosity, clearly reducing the ultimate tensile strength (UTS) and elongation, cannot be detected in the scatter of the results for the 0.2 PS. A similar fairly constant yield stress result is seen in Figure 2.47.

In those cases where the yield stress *is* found to be significantly reduced, it is a warning that the material had lost a significant fraction of its load bearing area. In the past it has not been easy to accept that the reduction of 0.2 PS by 90% is the result of a crack occupying 90% of the area, especially when the fault is not easily seen, even on the fracture surface! (Figure 2.44(a) which we have discussed several times before is a clear example showing a fracture of a tensile specimen expected to show 10% elongation but in fact achieved close to zero elongation, corresponding to the 100% loss of area provided by large bifilms. The 0.3% elongation recorded for this sample was found on close examination to have resulted from the interlocking of dendrites either side of the main bifilm crack, giving an extension to failure approximately equal to the DAS.)

Micro-structural Size Effects: The Hall–Petch Relation

As the grain size d of a metal is reduced, its yield strength σ_y increases. The widely quoted formula to explain this result is that due to Hall and Petch (see, for instance, the derivation by Cottrell (1964)):

$$\sigma_y = a + b \cdot d^{-1/2} \tag{9.6}$$

where a and b are constants. The equation is based on the assumption that a slip plane can operate with low resistance across a grain, allowing one part of the grain to slide over the other, and so concentrating stress on the point where the slip plane impinges on the next grain. With the further spread of yielding temporarily blocked, the stress on the neighbouring grain increases until it exceeds a critical value. Slip then starts in the next grain, and so on. The process is exactly analogous to the spreading of a crack, stepwise, halting at each grain boundary.

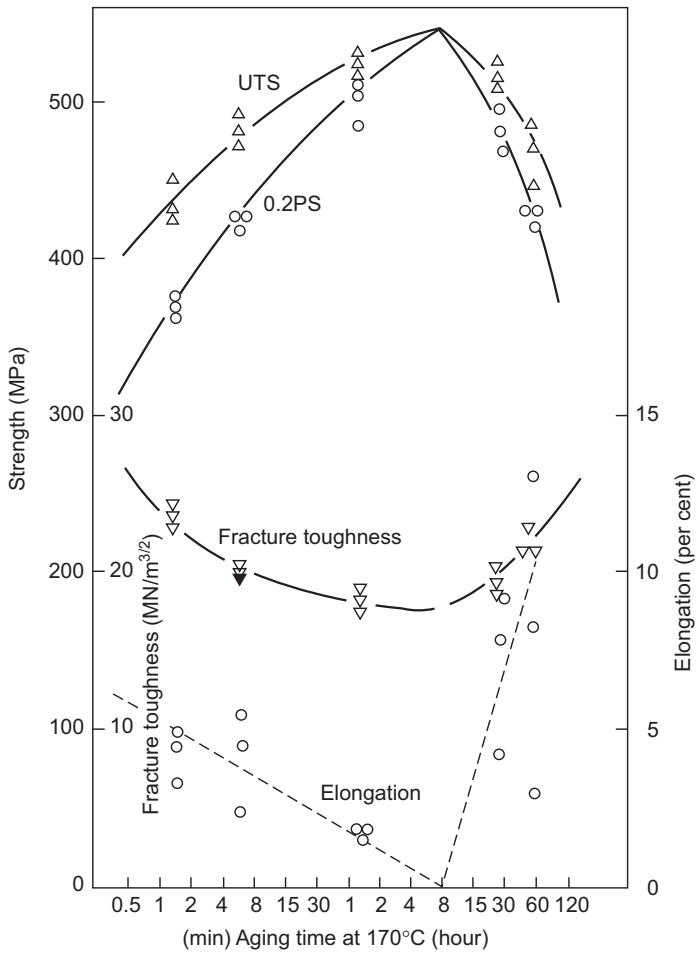

FIGURE 9.20

Mechanical properties of a cast high-strength alloy Al-6Zn-2.7Mg-1.7Cu as a function of effective aging time at 170°C.

Data from Chen et al. (1984).

Although the Hall–Petch relation was originally conceived to explain the effect of grain size, its fundamental power is not limited to this particular mechanism for the hindering of slip planes. For instance, slip can be halted at strong precipitates that might reside in interdendritic regions or inside grains. For instance, Gurland (1970) uses data from the literature to show for several steels in which their strength increases linearly with the inverse of the square root of the grain size for ferritic steels or the inter-particle spacing for pearlitic steels. Similarly, for Al-Si alloys, he shows the relationship between spacing and strength is the same for alloys containing 0–25% Si where the definition of spacing changes from (1) the grain size in pure aluminium, to (2) the dendrite cell size in 1.6–2.5% Si alloys and (3) the planar centre-to-centre nearest neighbour distance between Si particles in 5.3–25% Si alloys.

Both grain size and DAS are important factors affecting the strength of castings, and both rely in different ways on the Hall–Petch relation. We shall deal with these factors separately.

9.4.3.1 Grain size

General

The development of small grains during the solidification of the casting is generally thought to be an advantage. When the grain size is small, the area of grain boundary is large, leading to a lower concentration of impurities in the boundaries. The practical consequences that generally appear to follow from a finer grain size are

1. Improved resistance to hot tearing during solidification.
2. Improved resistance to cracking when welding or when removing feeders of steel castings by flame or arc cutting.
3. Reduced scattering of ultrasonic waves and X-rays, allowing better non-destructive inspection.
4. Improved resistance to grain boundary corrosion.
5. Higher yield strength (because of Hall-Petch relationship).
6. Higher ductility and toughness.
7. Improved fatigue resistance (including thermal fatigue resistance).
8. Reduced porosity and reduced size of pores. This effect has been shown by computer simulation by Conley et al. (1999) and is the consequence of the improved inter-granular feeding and better distributed gas emerging from solution. Improved mass feeding will also help as described in Section 7.1.4.2.
9. Improved hot workability of material cast as ingots.

However, it would not be wise to assume that all these benefits are true for all alloy systems. Some types of alloys are especially resistant to attempts to reduce their grain size, whilst others show impaired properties after grain refinement. Furthermore, this impressive list is perhaps not so impressive when the effects are quantified to assess their real importance. These apparent inconsistencies will be explained as we go.

In addition, important exceptions include the desirability of large grains in castings that require creep resistance at high temperature. Applications include, in particular, ferritic stainless steel for furnace furniture, and high temperature nickel-based alloy castings. Single-crystal turbine blades are, of course, an ultimate development of this concept. These applications, although important, are the exception, however. Because of the limitations of space, this section neglects those specialised applications that require large grains or single crystals and is devoted to the more usual pursuit of fine grains.

Some of these benefits are explained satisfactorily by classical physical metallurgy. However, it is vital to take account of the presence of bifilms. These will be concentrated in the grain boundaries. The influence of bifilm defects is, on occasions, so important as to over-ride the conventional metallurgical considerations. For instance, with the exception of item 5, every other item on the list is controlled by bifilms! For a traditionally educated metallurgist, this is a sobering if not shocking realisation.

For instance, in the case of the propagation of ultrasonic waves through aluminium alloy castings, this was long thought to be impossible. Aluminium alloys were declared to be too difficult. They were thought to prevent ultrasonic inspection because of scatter of the waves from large as-cast grains; no back-wall echo could be seen amid the fog of scattered reflections. However, in the early days of Cosworth Process, with long settling time of the liquid metal, and quiescent transfer into the mould, suddenly back-wall echoes could be seen without difficulty despite the absence of any grain refining action. The clear conclusion is that the scatter was from the gas film between the oxide layers of the bifilms at the grain boundaries.

By extrapolation, it may be that the so-called ‘diffraction mottle’ that confuses the interpretation of X-ray radiographs, and usually attributed to the large grain size, is actually the result of the multitude of thin-section pores, or the glancing angle reflections from the air layer of bifilms at grain boundaries. It would be interesting to compare radiographs from material of similar grain size, but different content of bifilms to confirm this prediction.

The strong link between bifilms and micro-structure, particularly grain size, is illustrated particularly well in Figure 2.44. Images (a) and (b) are the fracture surfaces of test bars taken from different parts of a single casting whose

filling was observed by X-ray video radiography. The large grain size in the turbulently filled test bar (a) contrasts with the fine grain size in the quietly cast bar (b). The large grains are probably the result of reduced thermal convection in the casting because of the presence of wall-to-wall bifilms which obstructed local thermal convection, so that dendrites could grow without thermal and mechanical disturbance that is needed to melt off dendrite arms, leading to grain multiplication. In (b), the presence of numerous pockets of porosity suggests the presence of many smaller bifilms (that cannot be seen directly). These are older bifilms already present in the melt before pouring. The small bifilms will not be a hindrance to the flow of the melt, so that the small grain size is the result of grain multiplication because of convection during freezing.

Unfortunately, nearly all the experimental evidence that we shall cite regarding the structure and mechanical properties of castings is influenced by the necessary but unsuspected presence of bifilms. We shall do our best to sort out the effects so far as we can, although, clearly, it is not always possible. Only new, carefully controlled experiments will provide certain answers. At this time, we shall be compelled to make our best guesses.

Grain refinement

The Hall–Petch equation has been impressively successful in explaining the increase of the strength of wrought steels with a reduction in grain size, and has been the driving force behind the development of high-strength constructional steels based on manufacturing processes, especially controlled rolling or other thermomechanical treatment, to control the grain size. This is cheaper than increasing strength by alloying, and has the further benefit that the steels are also tougher—an advantage not usually gained by alloying.

The extension of these benefits to cast steels has been much less successful as has been related in Section 6.6.

The development of higher-strength magnesium casting alloys with zirconium as the principal alloying element has also been driven by such thinking. The action of the zirconium is to refine the grain size, with a useful gain in strength and toughness. The sharp increase in yield strength as grain size is reduced is seen in Figure 9.21. The zirconium is almost insoluble in both liquid and solid magnesium, so that any benefit from other alloying mechanisms (for instance, solid solution strengthening) is negligible; all the benefit is from the reduced grain size. In fact, the test to ensure that the zirconium has successfully entered the alloy is simply a check of the grain size. Yue and Chadwick (1991) used squeeze casting to demonstrate the impressive benefits of the grain refinement of magnesium castings. This is especially clear work that is not clouded by other effects such the influence of porosity. It appears that magnesium benefits significantly from the effect of small grain size because factor b in the Hall–Petch equation is high. This is the consequence of the grain boundaries being particularly effective in preventing slip, because hexagonal close packed lattices have relatively few slip systems, and only on the basal plane, so that slip is not easily activated in a randomly oriented neighbour.

This behaviour contrasts with that of face-centred-cubic materials such as aluminium, where the slip systems are numerous, so that there is always a slip system close to a favourable slip orientation in a neighbouring grain. Thus although grain refinement of aluminium alloys is widely practised, Flemings (1974) draws attention to the fact that its effects are generally over-rated. In Figure 9.21, for normally attainable fine grain sizes in the range reducing from 1 mm down to 0.1 mm all the Al alloys have small or zero slope, showing small or zero benefit of grain refinement. (Only the Al-Si has a modest slope for reasons explained in the next section.)

The usual method of grain refinement of aluminium alloys is by the addition of titanium and/or boron. The effect has been discussed in Section 6.3.4. The practical difficulties of controlling the addition of grain-refining materials are discussed by Loper and Kotschi (1974), who were among the first to draw attention to the problem of fade of the grain-refinement effect. Sicha and Boehm (1948) investigated the effect of grain size on Al-4.5Cu alloy, and Pan et al. (1989) duplicated this for Al-7Si-0.4Mg alloy. However, both these pieces of work confirm the useful but relatively unspectacular benefits of refinement on strength. These authors suggest that the effects are complicated by the alloying effects of titanium, particularly the precipitation of large $TiAl_3$ crystals at higher titanium levels because the expected linear increase in yield strength with $d^{-1/2}$ is not achieved. It seems likely, once again, that the presence of bifilms is complicating behaviour. The large crystals of $TiAl_3$ suggest that these crystals had precipitated on bifilms, and further suggest that the authors had stirred the melt in an effort to transfer as much Ti into the casting as possible. This counter-productive

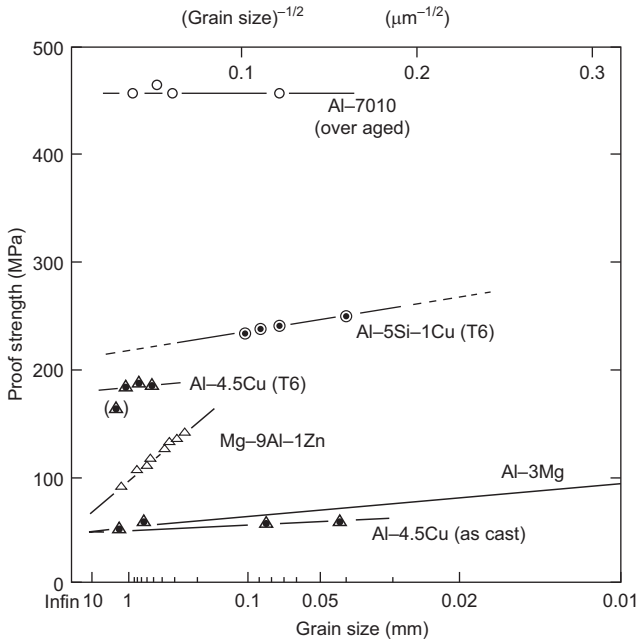

FIGURE 9.21

Hall-Petch plots of yield strength versus grain size$^{-1/2}$ illustrating (a) the relatively poor response of Al alloys contrasted with data for Mg alloys.

Data for 7070, Mg alloy, Al-4.5Cu from T M Yue and G A Chadwick (1991); Al-5Si-1Cu from Wierzbinska (2004); Al-3Mg from Lloyd and Court (2003).

technique eliminates the benefits of the settling of bifilms by the weight of Ti-rich precipitates attached to them as discussed in Section 6.3.3 'Melt cleaning by grain refinement' and Section 14.4.2 'Cleaning by Detrainment'.

It should not be assumed that the advantages, even if small, of fine grain size in wrought steels and cast light alloys automatically extend to other alloy systems. It is worth devoting some space to the difficulties and imponderables elsewhere.

For instance, steels that solidify to the body-centred-cubic form of the iron lattice are successfully grain refined by several additives, particularly compounds of titanium and similar metals, as discussed in Section 6.6 (although not necessarily with benefits to the mechanical properties, as we shall see later). In contrast, steels that solidify to the face-centred-cubic lattice do not appear to respond to attempts to grain refine with titanium and are resistant to attempts to grain refine with most materials that have been tried to date.

The grain-refinement work carried out by Cibula (1955) on sand-cast bronzes and gunmetals showed that these alloys could be grain refined by the addition of 0.06% of zirconium. This was found to reduce the tendency to open hot tears. However, this was the only benefit. The effect on strength was mixed, ductility was reduced, and although porosity was reduced in total, it was redistributed as layer porosity, leading to increased leakage in pressure-tightness tests. Although this was at the time viewed as a disappointing result, an examination of the tests that were employed makes the results less surprising. The test castings were grossly underfed, leading to greatly enhanced porosity. Had the castings been better poured and better fed, the result might have been greatly improved.

Remarkably similar results on a very different casting (but that also appears to have been underfed) were obtained by Couture and Edwards (1973). They found that various bronzes treated with 0.02Zr exhibited a nicely refined grain structure, and had improved density, hot-tear resistance, yield and ultimate strengths. However, ductility and pressure-tightness were drastically reduced. It is possible to conjecture that if the alloy had been better supplied with feed metal

during solidification then pressure-tightness would not have been such a problem. The presence of copious supplies of bifilm defects are to be expected to complicate the results as a consequence of the poor casting technique.

The poor results by Cibula in 1955 have been repeatedly confirmed in Canadian research; Sahoo and Worth (1990), Fasoyinu et al. (1998), Popescu et al. (1998) and Sadayappan et al. (1999) using, mainly, permanent mould test bars. These castings are not badly fed, so that the disappointing results by Cibula cannot be entirely ascribed to poor feeding. It seems likely that bifilms are at work once again.

There may be additional fundamental reasons why the copper-based alloys show poor ductility after grain refinement. Couture and Edwards noted that the lead- and tin-rich phases in coarse-grained alloys are distributed within the dendrites that constitute the grains. In grain-refined material the lead- and tin-rich phases occur exclusively in the grain boundaries. Thus it is to be expected that the grain boundaries are weak, reducing the strength of the alloy by: (1) offering little resistance to the spread of slip from grain to grain, and so effectively lowering the yield point and (2) allowing deformation in their own right, as grain boundary shear, like freshly applied mortar between bricks. However, this seems unlikely to be the whole story because some of the poor results are found in copper-based alloys that contain no lead or tin. A further confusion probably exists because of the probability that the lead and tin phases may precipitate preferentially on bifilms, so that the observed grain boundary weakening effect may not be directly the result of the metallic alloy additions.

Many of the previous studies of copper-based alloys have used Zr for grain refinement. Thus is seems possible that they may have been seriously affected by the sporadic presence of zirconium oxide bifilms at the grain boundaries. Thus the loss of strength and ductility and the variability in the results would be expected as a result of the overriding damage caused by surface turbulence during the casting of the alloys.

The work by Nadella, Eskin and Katgerman (2007), which is referred to elsewhere in this book, beautifully illustrates the current contradictions which arise when the presence of bifilms is overlooked. These workers aimed to use grain refinement reduce the cracking in direct chill (DC) continuously cast Al alloy ingot. When they added Ti-rich grain refiner to the ladle, and then transferred this to the continuous caster, the ingot was grain refined and free from cracks. However, when they added grain refiner to the launder, immediately before the melt entering the continuous casting mould, the ingot was beautifully grain refined, but cracked. This result, baffling to the researchers, is easily understood as the settlement of bifilms by the precipitation of Ti-rich compounds on them, so the melt was cleaned from bifilms before casting. When added to the launder, the sedimentation action was no longer possible, so the bifilms were allowed to enter the casting and initiate cracks.

As the reader will now appreciate, much of our research work on the strengths of cast alloys is, frankly, in a mess. Much of this work will require to be repeated with relatively bifilm-free material. We shall then benefit from understandable and reproducible data for the first time.

9.4.3.2 Dendrite arm spacing (DAS)

DAS can refer to the spacing of the primary dendrite stems in those rather rare cases where no secondary arms exist. More usually, however, the DAS refers to the spacing between the secondary arms of dendrites. However, if tertiary arms are present at a smaller spacing, then it would refer to this.

If the DAS is reduced, then the mechanical properties of the cast alloy are usually improved. A typical result by Miguelucci (1985) is shown in Figure 2.47. Near the chill, the strength of the alloy is high and the toughness is good. As the cooling rate decreases (and DAS grows), the ultimate strength falls somewhat. Although the decrease in itself would not perhaps be disastrous, the fall continues until it reaches the yield stress (taken as the proof stress in this case). Thus, on reaching the yield stress, failure is now sudden, without prior yield. This is disastrous. The alloy is now brittle, as is confirmed by elongation results close to zero.

Because of the effect of DAS, the effect of section size on mechanical properties is seen to be important even in alloys of aluminium that do not undergo any phase change during cooling. For ferrous materials, and especially cast irons, the effect of section size can be even more dramatic, because of the appearance of hard and possibly brittle non-equilibrium phases such as martensite and cementite in sections that cool quickly.

The improvement of strength and toughness by a reduction in DAS is such a similar response to that given by grain refinement that it is easy to see how these two separate processes have often been confused. However, the benefits of the

refinement of grains and DAS cannot be the result of the same mechanisms. This is because when considering DAS no grain boundary exists between the arms of a single dendrite to stop the slide of a slip plane. A dislocation will be able to run more or less without hindrance across arm after arm, since all will be part of the same crystal lattice. Thus, in general, it seems that the Hall–Petch equation should not apply. Also, of course, Hall–Petch can only explain an increase in yield with an improved refinement, whereas refined DAS offers also offers an improved ductility.

Why then does a reduction in DAS increase both strength and toughness?

This question appears never to have been answered.

Classical physical metallurgy has been unable to explain the effect of DAS on mechanical properties. Curiously, this important failure of metallurgical science to explain an issue of central importance in the metallurgy of cast materials has been consistently and studiously overlooked for years.

In the first edition of *Castings* the author suggested that the answer seemed to be complicated, and to be the result of the sum of several separate effects, all of which seem to operate beneficially. These beneficial processes are listed and discussed in the following sections. However, after these effects have been reviewed and assessed, it will become clear that the major benefit from a refinement of DAS remains largely unexplained.

We shall arrive at what seems to be an inescapable conclusion: the action of bifilms will be presented as the dominant effect, explaining for the first time the widely appreciated benefits of small DAS in castings, as we shall see.

Residual Hall–Petch hardening

It might be supposed that there was some residual Hall–Petch effect affecting strength. A perfect atomic lattice between adjacent dendrite arms would allow slip to progress from arm to arm without problem. This seems largely true for relatively pure Al and its solid solution alloys such as the low magnesium Al-Mg alloys and many of the wrought alloys that are relatively low in solute. Thus there are fundamental reasons why the effect of Hall–Petch hardening should be negligible in these Al alloys, and in many other solid solution, single-phase alloys (also including of course many stainless steels). The small or negligible benefit to the single-phase Al alloys is seen in Figure 9.21 for 7010, Al-4.5Cu and Al-3Mg alloys.

Slight faults during growth will cause the dendrite arms within a grain to become slightly misoriented. This will result in a low-angle grain boundary between the arms. The higher the degree of misorientation, the greater the resistance will be to the passage of a slip plane.

When studying the structure of a cast alloy under the microscope, most dendrite arms are seen to be, so far as one can tell by unaided observation, fairly true to their proper growth direction. Thus any boundary between the arms will have an almost vanishingly small misorientation, presenting a minimal impediment to slip across the boundary. However, it is also usually possible to see a proportion of arms at slight deviations of several degrees, perhaps as a result of mechanical damage. If mechanical disturbance during freezing is increased, for instance by stirring or vibration, then the number of misaligned arms, and their degree of misalignment, would be expected to increase.

Thus one might expect some small resistance to slip even from rather well aligned dendrites because of the lack of perfection; the result of the existence of subgrains within the grains. Some contribution from Hall–Petch hardening might therefore be expected to be present at all times.

For those alloys that have interdendritic precipitates, however, there may be a positive action to arrest slip between dendrite arms. This is true in Al-Si alloys, as is evident from the modest increase in strength noted in the impressive early work by Gurland (1970) and later by Wierzbinska and Sieniawski (2004) noted in Figures 9.22 and 9.23. Interestingly, for the Al-5Si-1Cu alloy, there is a maximum potential benefit of about 15 MPa if very efficiently grain refined, plus a further maximum benefit from the refinement of DAS by chilling that might yield about 30 MPa. Thus by taking maximum advantage of refinement of grains and dendrites a total addition to strength could be 45 MPa. In practice, one would expect to achieve something rather less than this in most casting conditions, so that benefits to strength of Al-Si higher than 5–7%Si are not especially impressive, but worth having.

Comparing the benefits achievable in a single-phase solid solution alloy such as Al-3Mg, Figure 9.22 illustrates that only about 10 MPa might be achieved by rapid solidification, but no benefit from grain refinement would be expected as a result of grain boundaries being easily traversed by slip planes in such materials. For most practical purposes, this benefit is negligible.

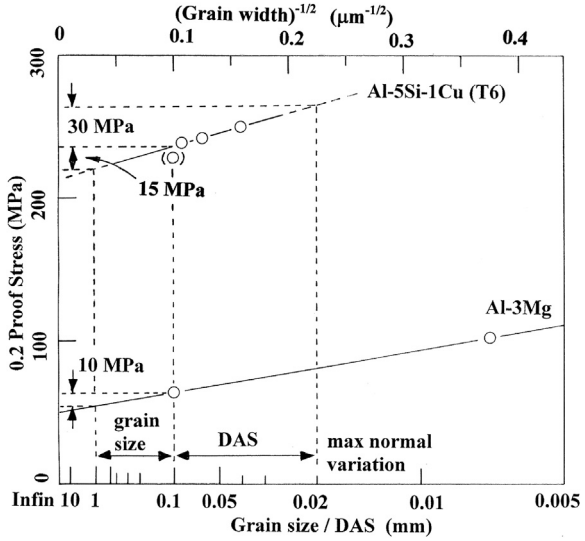

FIGURE 9.22

The poor strengthening effect of up to approximately 10 MPa for the best grain size reduction of Al-3Mg, with nothing for DAS refinement for this solid solution alloy compared with 15 MPa for DAS plus 30 MPa for grain refinement of Al-Si alloys.

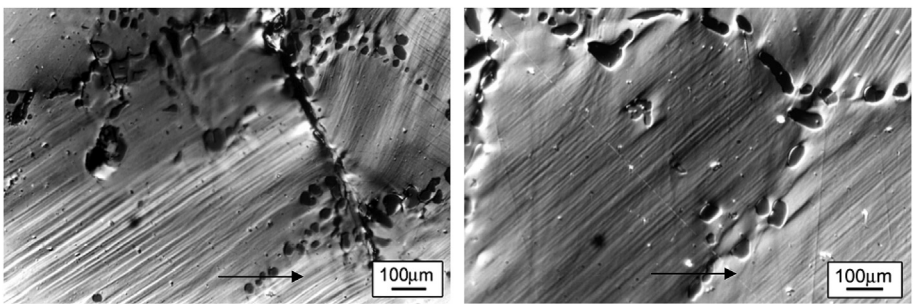

FIGURE 9.23

Change of slip band direction and intensity at interdendritic boundaries in Al-5Si-1Cu alloy (Wierbinska and Sieniawski, 2004).

We can conclude that in general, although the Hall–Petch mechanism is likely to be a contributor to increased strength, in most castings it will be negligibly small.

The final fact that eliminates the Hall–Petch effect as a major contributor to the DAS effect is the fundamental fact that Hall–Petch strengthening affects only the yield strength. Figure 2.47 and many similar results in the literature indicate that yield strength is hardly affected by DAS. The main effect of changes in DAS is seen in the ductility and ultimate strength values which Hall–Petch is not able to explain.

Restricted nucleation of interdendritic phases

As the DAS becomes smaller, the residual liquid is split up into progressively smaller regions. Although in fact these interdendritic spaces remain for the most part interconnected, the narrowness of the connecting channels does make them behave in many ways as though they were isolated.

Thus as solutes build up in these regions, the presence of foreign nuclei to aid the appearance of a new phase becomes increasingly less probable as the number of regions is increased. As DAS decreases, the multiplication of sites exceeds the number of available nuclei, so that an increasing proportion of sites will not contain a second phase. Thus, unless the concentration of segregated solute reaches a value at which homogeneous nucleation can occur, the new phase will not appear.

Where the second phase is a gas pore, Poirier et al. (1987) have drawn attention to the fact that the pressure due to surface tension, becomes increasingly high as the curvature of the bubble surface is caused to be squeezed into progressively smaller interdendritic spaces. The result is that it becomes impossible to nucleate a gas pore when the surface tension pressure exceeds the available gas pressure. Thus as DAS decreases, there becomes a cutoff point at which gas pores cannot appear. Effectively, there is simply insufficient room for the bubble! The model by Poirier suggests that this is at least part of the reason for the extra soundness of chill castings compared with sand castings. Later work by Poirier (2001) and the theoretical model by Huang and Conley, assuming no difficulty for the nucleation of pores, confirm the improvement of soundness with increasing fineness of the structure.

In summary, therefore, we can see that as DAS is reduced, the interdendritic structure becomes, on average, cleaner and sounder. These qualities are probably significant contributors to improved properties.

Restricted growth of interdendritic phases

Meyers (1986) found that for unmodified alloys of the Al-7Si system the strength and elongation were controlled by the average size of the silicon particles, but where the particles were uniformly rounded as in structures modified with sodium, the strength and elongation were controlled by the number of silicon particles per unit volume. These conclusions were verified by Saigal and Berry (1984), using a computer model. This important conclusion may have general validity for other systems containing hard, plate-like particles in a ductile matrix.

The highly deleterious effect of iron impurities in these alloys is attributed to the extensive plate-like morphology of the iron-rich phases. Vorren et al. (1984) have measured the length of the iron-rich plates as a function of DAS, and find, as might be expected, the two are closely related; as DAS reduces, the plates become smaller. From the work of Meyers, Saigal and Berry, we can therefore conclude that the strength and toughness should be correspondingly increased, as was in fact confirmed by Vorren. Ma and coworkers (2008) measure the lengths of the β-Fe particles in Al-7Si-0.4Mg alloy as a combined assessment of the increase of both Fe content and cooling time, plotting strength properties as a function of this length (Figure 9.24). They show how ductility is reduced dramatically, tensile strength is somewhat reduced, but yield strength is hardly affected.

It seems likely that although there may be an element of cause and effect in the restriction of the growth of second phases by the dendrite arms, the major reason for the close relation between the size of secondary phases and DAS is that both are dependent on the same key factor: the time available for growth. Thus local solidification time controls the size of both dendrite arms and interdendritic phases.

The reason underlying the importance of the large iron-rich plates in Al alloys is proposed in this work to be the result of the presence of oxide bifilms inside the plates, as has been stated in Section 6.3, and will be referred to later.

Improved response to heat treatment

To summarise the effect of DAS on heat-treatment response: as DAS is reduced, so (1) the speed of homogenisation is increased, allowing more complete homogenisation, giving more solute in solution and so greater strength from the subsequent precipitation reaction. (2) The speed of solution is also increased, allowing a greater proportion of the non-equilibrium second phase to be dissolved. The smaller numbers and sizes of remaining particles, if any, and the extra solute usefully in solution, will bring additional benefit to strength and toughness.

Even when the second-phase particles are equilibrium phases, the high temperature homogenisation and solution treatments have a beneficial effect, even though the total volume of such phases is probably not altered. This is because

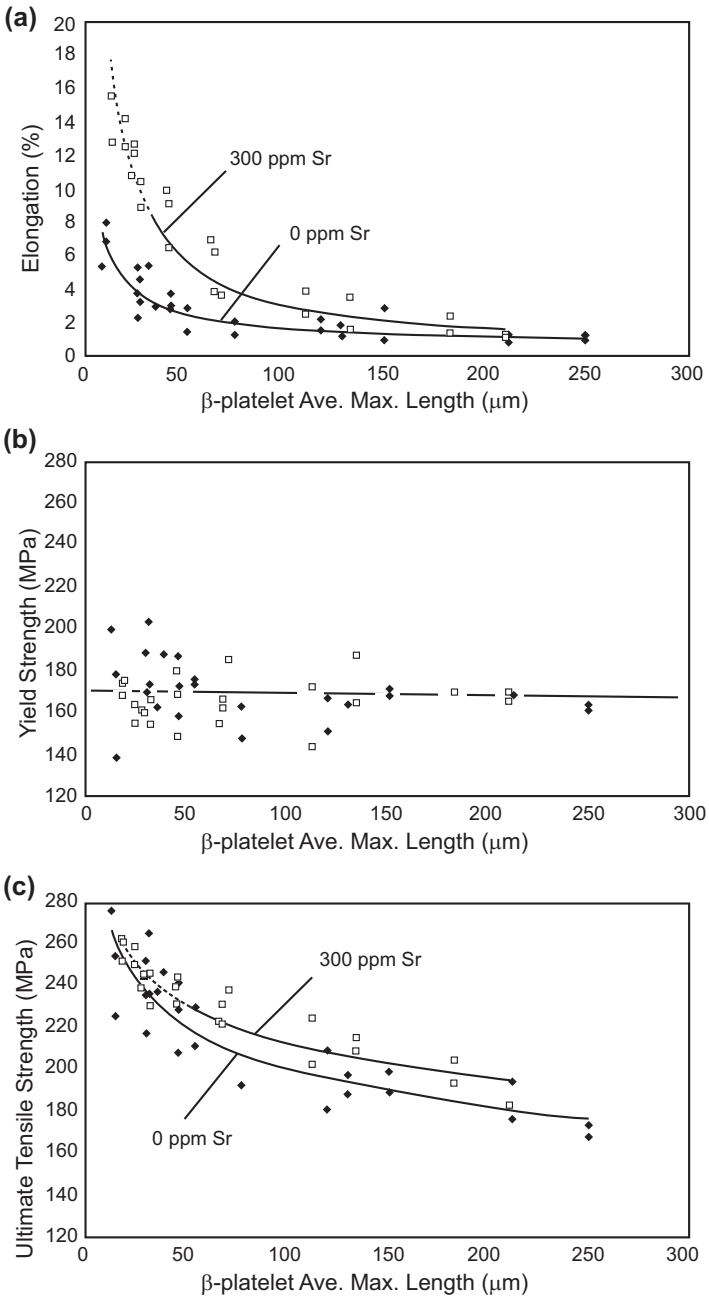

FIGURE 9.24

(a) Elongation; (b) yield strength; and (c) tensile strength of Al-7Si-0.4Mg alloy with 0 ppm and 300 ppm Sr as a function of average maximum length of β-Fe particles (Ma, Samuels, Dot and Valtierra, 2008).

the inclusions tend to spherodise; their reduced aspect ratio favours improved toughness as discussed previously. Any remaining pores will also tend to spherodise, with similar benefit.

There is no doubt, therefore, the improved response to heat treatment is a valuable benefit from refinement to DAS arising from the reduced presence of interdendritic phases (although, ironically, this effect is seen to reduce any Hall–Petch contribution) and possibly the additional solute now in solution. These real improvements to properties if heat treatment is carried out are a separate and additional factor to the important factor described later.

We need to keep in mind, however, that the improvements in properties as a result of refined DAS are enjoyed whether heat treatment is carried out or not. Thus there remains some other major factor at work, so far not considered. We consider this now.

Effect of bifilms

The following examination of the effect of bifilms in the liquid alloy suggests that their effect on properties, as indicated by the DAS, is expected to be dominant.

Rather than consider that refined DAS improves properties, it is more accurate to start with the view that the properties of castings should initially be good, but are degraded as DAS coarsens. This revised viewpoint is helpful as is explained later.

The importance of the presence of bifilms only becomes seriously damaging as solidification time is extended. This is due to the fact that the bifilms arrive in the casting in a compact form, tumbled into compactness by the bulk turbulence during the filling of the mould cavity. In this form, their deleterious effects are minimised. They are small and rounded. Their effectiveness as defects grows as they slowly unfurl, gradually enlarging to take on the form of planar cracks up to approximately 10 times larger diameter than the diameter of their original compact shape. As we have seen in Chapter 2, there are several driving forces for this straightening phenomenon. These include the precipitation of gas inside, or second phases (particularly iron-rich phases in Al alloys) outside, or the action of shrinkage to aid inflation, or the action of growing grains to push and thereby organize the films into interdendritic or inter-granular planes. All these mechanisms extend and flatten the bifilm cracks so as to reduce properties.

The bifilms are seen therefore to evolve into serious defects, given time. Time is a crucial factor. Thus, if there is little time, the defects will be frozen into the casting in a compact form of diameter in the range of 0.1–1 mm or less in smaller castings. However, given time, the bifilms will open to their full size. This might be as large as 10–15 mm across in an Al alloy casting of 10–100 kg weight. In Al-bronze castings and some stainless steel castings weighing several tonnes bifilms in the size range of 50–100 mm are not uncommon. These constitute massive cracks that seriously degrade properties.

The fall of ductility with increasing DAS becomes clear therefore. It is not the DAS itself that is important. *The DAS is merely the indicator of the time available* for the opening of bifilms. The DAS is our independent clock. It is the opening of the bifilms into extensive planar cracks that is important in degrading properties.

The time required for the complete opening of bifilms depends, of course, on the rate at which they can open. This in turn depends on how ravelled the bifilm is, and depends on the various driving forces available for opening. Thus the defects will open at variable rates depending (1) somewhat on their geometry, but faster for (2) higher concentration of gas in solution, (3) poorer conditions for feeding, and, in aluminium alloys, (4) higher iron contents.

A practical example is given in Figure 9.25. Sketch (a) shows the opening of bifilms in a poorly fed region whose solidification is delayed by its heavy section. In other regions of the casting the bifilms have no time to open, and are therefore frozen-in as compact and relatively harmless defects. The mechanical properties are good in the rapidly solidified regions, and poor in the slowly solidified and poorly fed regions. Sketch (b) illustrates the benefit of keeping some pressure on the solidifying liquid, in this case by the planting of a feeder onto the casting. The opening of the bifilms is thereby resisted to some extent, and improved properties are retained by the solidification under pressure, even though the pressure is quite modest. Sketch (c) illustrates the case where the metal is superbly clean. The properties are good everywhere regardless of cooling conditions and regardless of pressurisation from a feeder. (The reader will notice some solid feeding, however, which would be avoided by the pressurisation provided by a good-sized feeder.)

We can therefore make an interesting prediction for results such as those presented in Figure 2.47. The prediction is: if there were no bifilms in the liquid metal, the curves of UTS and Elongation to failure versus DAS would both be nearly horizontal lines. It is possible that a slight downward slope might be expected as a result of other factors, such as interdendritic regions becoming less clean, as discussed earlier. However, apart from such minor effects, properties

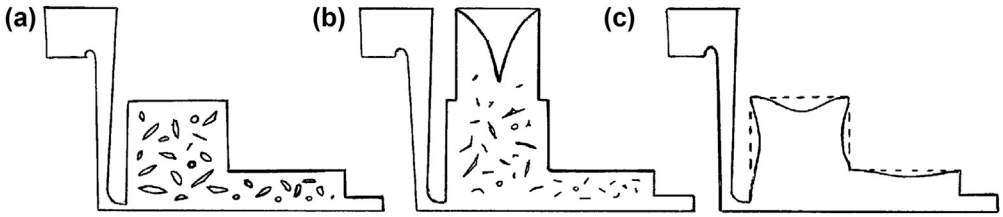

FIGURE 9.25

(a) Opened bifilms resulting from a lack of feeding leading to poor ductility; (b) improved ductility from maintenance of pressure by a feeder; and (c) excellent ductility irrespective of feeding or pressure in the absence of bifilms (however, possible external sinks in heavy sections as shown).

would become essentially *insensitive* to changes in DAS. In other words, in the absence of bifilms, properties would remain high regardless of how slowly or quickly the casting solidified.

Good evidence that this is true, that properties of clean metals are substantially independent of DAS, comes from widely different sources:

1. For steels, Polich and Flemings (1965) showed that low-alloy steels that had been subjected to directional solidification in an upward direction, encouraging the floating out and pushing ahead of bifilms, exhibited a constant elongation despite DAS increasing from 20 to 150 μm. Conversely, conventionally solidified equiaxed versions of the same steel, in which bifilms would not have separated, showed a fall in ductility as DAS increased (Figure 9.26).
2. From early experience with the Cosworth Process, when Cosworth Engineering made its racing car engines from castings poured in conventional foundries, at least 50% of all the cylinder heads (four-valves-per-cylinder designs) failed by thermal fatigue between the neighbouring exhaust valve seats. In 1980, when cylinder heads became available for the first time from the new process, characterised by quiescent transfer and counter-gravity filling, the failures fell immediately to zero. The DAS was hardly changed, and was in any case considerably larger than that available from permanent mould casting, for which resistance to thermal fatigue at that time was poor and variable. Thus DAS was not controlling in this case. It is difficult to avoid the conclusion that the action of bifilms was crucial in this experience.

   The action of some casting customers specifying DAS to avoid thermal fatigue in critical locations like the exhaust valve bridge in cylinder heads is seen therefore to miss a valuable potential benefit. Certainly control of DAS will be important for casting systems that provide poor filling control and thus contain a high density of bifilms. However, in a process, such as Cosworth Process, specifically designed to provide good quality metal, it is almost certainly an unnecessary complication and expense. In general, for casting processes as a whole, it would be more constructive to specify the reduction in bifilms by good processing techniques. This would achieve benefits throughout the whole casting, not merely in those designated regions where a limited DAS has been specified.
3. The new ablation process (Section 17.14) completely separates any observable effect of DAS from properties. DAS can be huge if the application of the cooling water is delayed, allowing the dendrites to grow and coarsen. However, the properties can still be remain high if the residual eutectic liquid is frozen quickly, thus retaining the bifilms small size, the Fe-rich particles having no time to grow and straighten the bifilms and so reduce properties. Properties could remain adequate even when working with melts that were known to contain large populations of bifilms. Figure 9.27 is an example for an Al-7Si-0.4Mg-0.4Fe alloy showing the eutectic phase so fine as to be difficult to resolve, and Fe-rich platelets so small, approximately 1 μm or less long, that they are difficult to find even at the highest optical magnifications (Tiryakioglu, 2009).

9.4.4 TENSILE STRENGTH

UTS is a somewhat dated mouthful, yet nicely descriptive, for its equivalent, the tersely modern, economic, tensile strength (TS). It is a composite property composed of the total of (1) the yield stress plus (2) additional strengthening

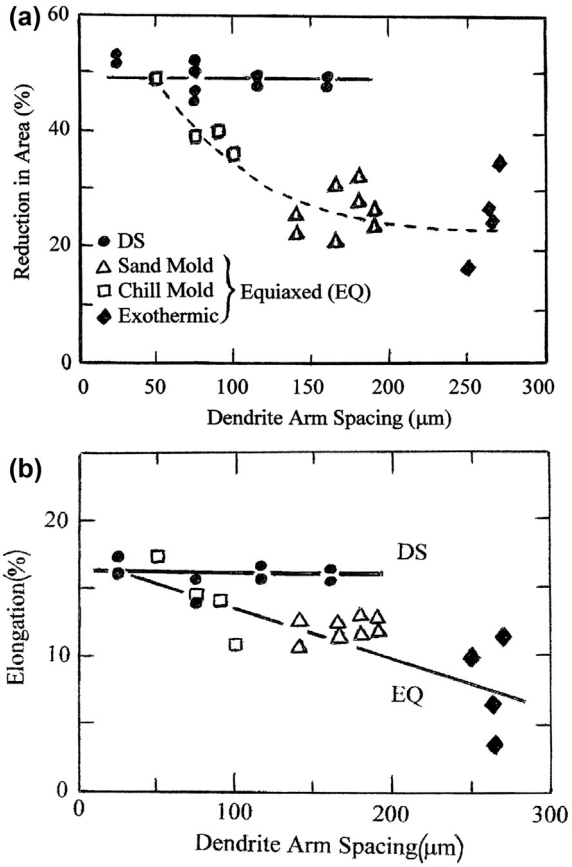

FIGURE 9.26

Vertically oriented DS low-alloy steel is expected to be relatively free from bifilms, and thus DAS has no influence on ductility; conventional equiaxed solidification traps bifilms, permitting DAS to control ductility measured as RA (a) and Elongation (b) by Polich and Flemings (1965).

from work hardening during the plastic yielding of the material before failure. These two components make its behaviour more complicated to understand than the behaviour of yield stress or ductility alone.

TS equals the yield, or proof, stress when (1) there is no ductility, as is seen in Figure 2.47 and Figure 9.20, and (2) when the work hardening is zero. The zero work hardening condition is less commonly met, but occurs often at high temperatures when the rate of recovery equals or exceeds the rate of hardening.

The problem of determining the TS of a cast material is that the results are often scattered. The problems of dealing with this scatter are important, and are dealt with at length in Section 9.2 'The statistics of failure'. Section 9.2 is strongly recommended reading.

Generally, for a given alloy in a given heat treated condition, proof strength is fixed. Thus as ductility is increased (by, for instance, the use of cleaner metal, or faster solidification) so TS will usually increase, because with the additional plastic extension, work hardening now has the chance to accumulate and so raise strength. The effect is again clear in Figure 2.47. For a cast aluminium alloy, Hedjazi et al. (1975) show that TS is increased by a

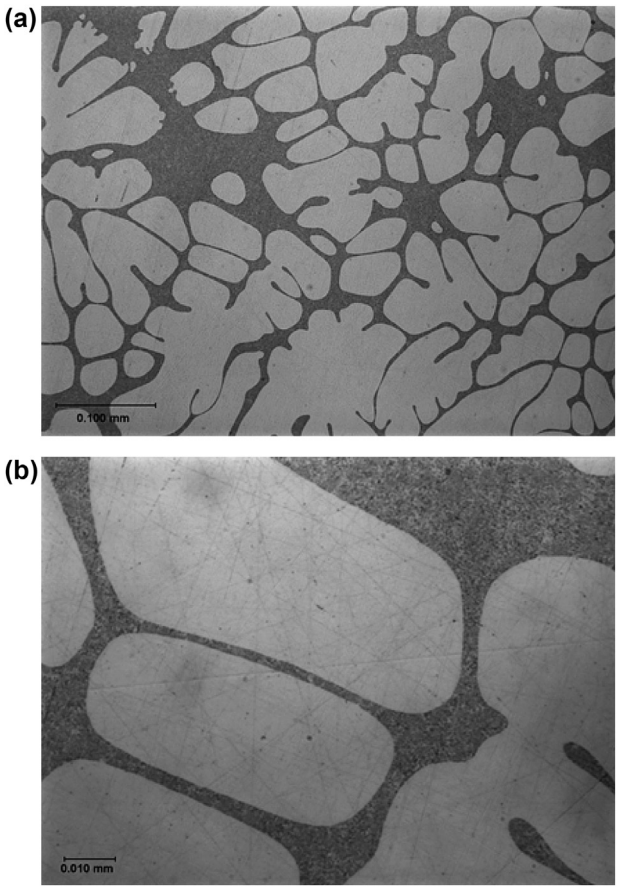

FIGURE 9.27

Ablation cooled Al-7Si-0.4Mg-0.4Fe alloys at nominal (a) 200 × and (b) 1000 × magnification, showing Si particle size and spacing approximately 1 μm, and β-Fe particles too small to be easily found.

Courtesy Alotech.

reduction in defects, as shown in Figure 9.28. The response of the TS is mainly due to the increase in ductility, as is clear from the linear response, and the shift of the properties mainly to the right, rather than simply upwards, for cleaner material.

The rather larger effect that layer porosity is expected to have on ductility will supplement the smaller effect because of loss of area on the overall response of TS. Figure 9.11 shows the reduction in TS and elongation in Mg-Zn alloy systems where the reduction in properties is modest. In Figure 7.34, the TS of an Al-11.5 Mg alloy shows more serious reductions, especially when the porosity is in the form of layers perpendicular to the applied stress. Even so, the reductions are not as serious as would be expected if the layers had been cracks, a result emphasising their nature as 'stitched', or 'tack welded' cracks, as discussed in Section 9.3.2.4.

When the layers are oriented parallel to the direction of the applied stress, then, as might be expected, Pollard (1965) has shown that layer porosity totalling even as high as 3% by volume has a practically undetectable effect on properties.

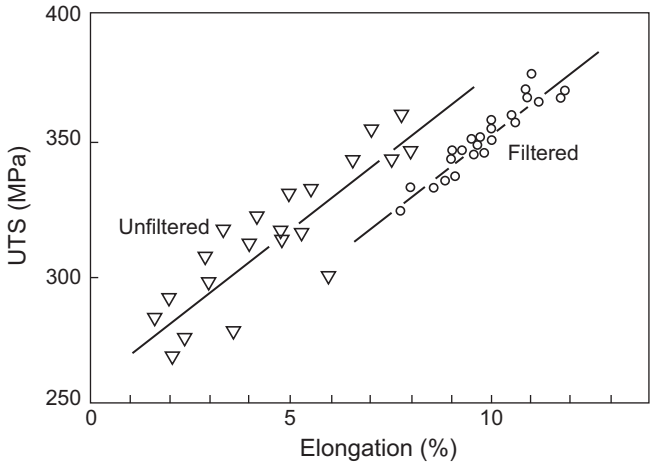

FIGURE 9.28

Mechanical properties of Al-4.5Cu-1.5Mg alloy in the unfiltered and filtered conditions, illustrating the strong response of ductility.

Data from Hedjazi et al. (1975).

Finally, it is clear that cracks or films occupying the majority of the cross-section of the casting will be highly injurious for TS as they are for ductility. The self-evident general understanding that the TS falls to zero as the crack occupies progressively more of the area under test is quantified by Clyne and Davies (1975) in the Figure 9.12.

9.5 FRACTURE TOUGHNESS

Fracture toughness is a material property that is generally independent of the presence of gross defects (although could be affected by a dense population of small defects, as will become clear). This is because it is assessed by the force required to extend a crack that has been artificially introduced in the material usually by extending a machined notch by fatigue. Thus fracture toughness measures the properties of the matrix at the point at which the notch is placed, i.e. it is a material property. It is not a property like tensile strength or ductility in which the crack finds its own start location, ensuring failure from the largest defect. When preparing the toughness assessment test piece, the machining of a notch into the specimen at a pre-fixed location would be unlikely to encounter a major defect by chance.

Fracture toughness is the material property that allows the prediction of the shapes and sizes of defects that might lead to failure. It is a basic tenet of fracture mechanics that fracture may begin when the stress-intensity factor K exceeds a critical value, the fracture toughness K_{1C}. A detailed presentation of the concept of fracture toughness is beyond the scope of this book. The interested reader is recommended to an introductory text like that by Knott and Elliott (1979). Here we shall simply assume some basic equations and the experimental results.

Stress intensity K as well as fracture toughness has the dimensions of stress times the square root of length, and is most appropriately measured in units of $\mathrm{MNm^{-3/2}} = \mathrm{MPa\ m^{1/2}}$. (Care is needed with units of this property. Fracture toughness is sometimes measured less conveniently in $\mathrm{Nmm^{-3/2}} = \mathrm{MPa\ mm^{1/2}}$ that differ by a factor of $(1000)^{1/2} = 31.6$.) For a penny-shaped crack of diameter d in the interior of a large casting, the critical crack diameter at which failure will occur is approximately:

$$d = 2K_1C^2/\pi\sigma^2 \tag{9.7}$$

from which, for an aluminium alloy of fracture toughness 32 MPa $m^{1/2}$ at its yield point of 240 MPa, the critical defect size d is 11 mm. For an edge crack, Eqn (9.7) is modified by a factor of 1.25, giving a corresponding critical defect size of 9 mm, indicating that edge cracks are somewhat more serious than centre cracks, but in any event defects of about a centimetre across would be required, even at a stress at which the casting is on the point of plastic failure. These are comparatively large defects, which is reassuring in the sense that such large cracks may have a chance to be found by non-destructive tests before the casting going into service. However, they underline the conclusion that most current radiography standards which state 'no linear defects' of any size, or which reject aluminium alloy castings for flaws of only approximately 1 mm in size, may not be logical.

The important message to be learned from the concept of fracture toughness is that the maximum defect size that can be tolerated can be precisely calculated if the fracture toughness and the applied stress are both known.

Equation (9.7) can be used to indicate that at the limit, when the applied stress σ equals the yield stress σ_y, the greatest resistance to crack extension that can be offered by a material is controlled by the value of K_{1C}/σ_y (units most conveniently in $m^{1/2}$). This parameter is a valuable measure of the defect tolerance of a material.

Figure 9.29 shows how the permissible defect size in ductile irons is large for low-strength irons, but diminishes with increasing strength because of the fall of fracture toughness. Thus for the stronger irons the permissible defect size is below 1 mm. This is particularly difficult to detect and sets a limit to the stress at which a strong ductile iron casting may be used with confidence.

Steels can have high fracture toughness, with correspondingly good tolerance to large defects at low applied stress. However, because they are used in highly stressed applications, the permissible defect size is reduced, as Eqn (9.10) indicates. Jackson and Wright (1977) discuss the serious problem of detecting flaws when the permissible size is small. At the time of writing, most non-destructive testing methods have been found wanting in some respect. However, the technology of non-destructive techniques has improved significantly and is expected to continue to improve, allowing the detection of smaller defects with greater certainty, and so extending the range over which castings can be stressed whilst

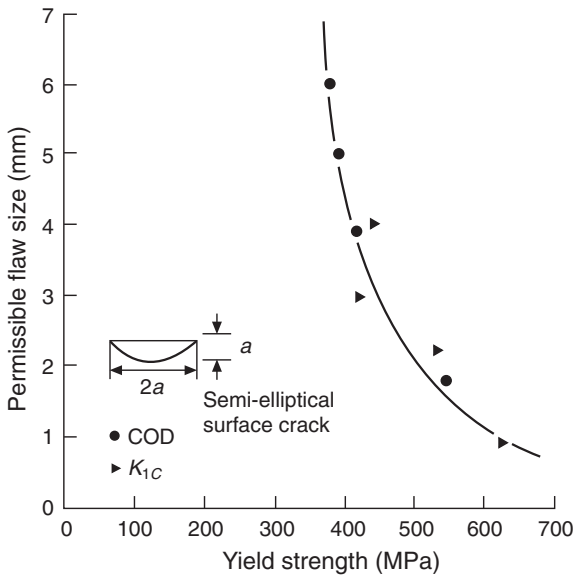

FIGURE 9.29

Permissible edge defect sizes in ductile irons of increasing strength.

Data from Seetharamu and Srinivasan (1985).

reducing the risk of failure. In this respect, the most significant advance is probably the development of sophisticated resonance testing described in Section 19.8.

Nevertheless, Jackson and Wright's conclusion is good advice: choose an alloy with a large critical flaw size, which can be detected, and measured accurately. Also, if the working load is fluctuating, it will be necessary to calculate from crack propagation rate curves the time for a flaw to grow to the critical size. This can then be compared with the design life of the component.

To be safe, they recommend the following assumptions:

1. A string of cracks is equivalent to one long crack.
2. A group of flaws is one large flaw of size comparable with the envelope that circumscribes them.
3. Unless clearly seen to be otherwise, all flaws have a sharp aspect ratio.
4. All flaws reside on the surface.

A casting designed on this basis is likely to be somewhat overdesigned, but perhaps not so much as if there had been no use of the principles of fracture mechanics.

There has been relatively little work carried out on the fracture toughness of cast Al alloys. Tiryakioglu and Hudak (2008) have therefore developed a relation between round notched tensile strength σ_{NT} and fracture toughness K_{1C}, both normalised by dividing by the yield stress σ_y, as shown in Figure 9.30(a) for Al-7Si-0.6Mg alloy. The direct comparison between σ_{NT} and K_{1C} is given in Figure 9.30(b) showing limits of accuracy at 5% and 1% error to within 95% confidence. The best fit line is given by

$$K_{Ic} = \beta\sigma_{NT} \tag{9.8}$$

where $\beta = 6.33 \times 10^{-2}\ \mathrm{m}^{0.5}$ with $R^2 = 0.72$ and standard mean deviation 1.48 MPa^2 m. Round tensile test specimens with a circumferential sharp notch are easy and quick to produce, so the important parameter, K_{1C}, is suddenly made much more accessible.

So far all the discussion has related to linear elastic fracture mechanics (LEFM), in which the fracture resistance of a material is defined in terms of the elastic stress field intensity near the tip of the crack. In fact, the fracture toughness parameter K_{1C} is valid only when the region of plastic yielding around the tip is small.

For lower-strength materials, plastic deformation at the tip of the crack becomes dominant, requiring the application of yielding fracture mechanics (YFM) and the concept of either (1) crack opening displacement (COD or δ) or (2) the J integral, as a measure of toughness.

The critical COD is the actual distance by which the opposite faces of the crack separate before unstable fracture occurs. This critical opening is known as δ_c. The critical flaw size is given by:

$$d_c = c\left(\delta_c/\varepsilon_y\right) \tag{9.9}$$

where c is a material constant and ε_y is the strain at yield. For materials that are on the borderline for treatment by LEFM or YFM, Jackson and Wright (1977) indicate that a unified test technique can be used to determine K_{1C} or δ_c from a single test piece, and that the following useful relation may be employed

$$\delta_c/e_y = \left(K_{1C}/\sigma_y\right)^2 \tag{9.10}$$

Hence the ratio δ_c/e_y in YFM is comparable with $(K_{1C}/\sigma_y)^2$ in LEFM, i.e. it is a measure of the defect tolerance of a material. It deserves to be much more widely used in the design and specification of castings.

The transition between K_{1C} and COD, when properly applied, is seen to give consistent predictions of the critical defect size. The results in Figure 9.29 for ductile irons show a region of smooth overlap between the two approaches.

Although the COD has a clear physical basis, in both its formulation and its application, there are empirical assumptions that are difficult to justify by the rigorous application of mechanics at this time. For this reason, more attention is being given to the use of the J integral in structural-integrity assessment, especially in the United States. J is a crack-tip driving force that, under certain conditions, can be applied to elastic–plastic situations to describe the onset

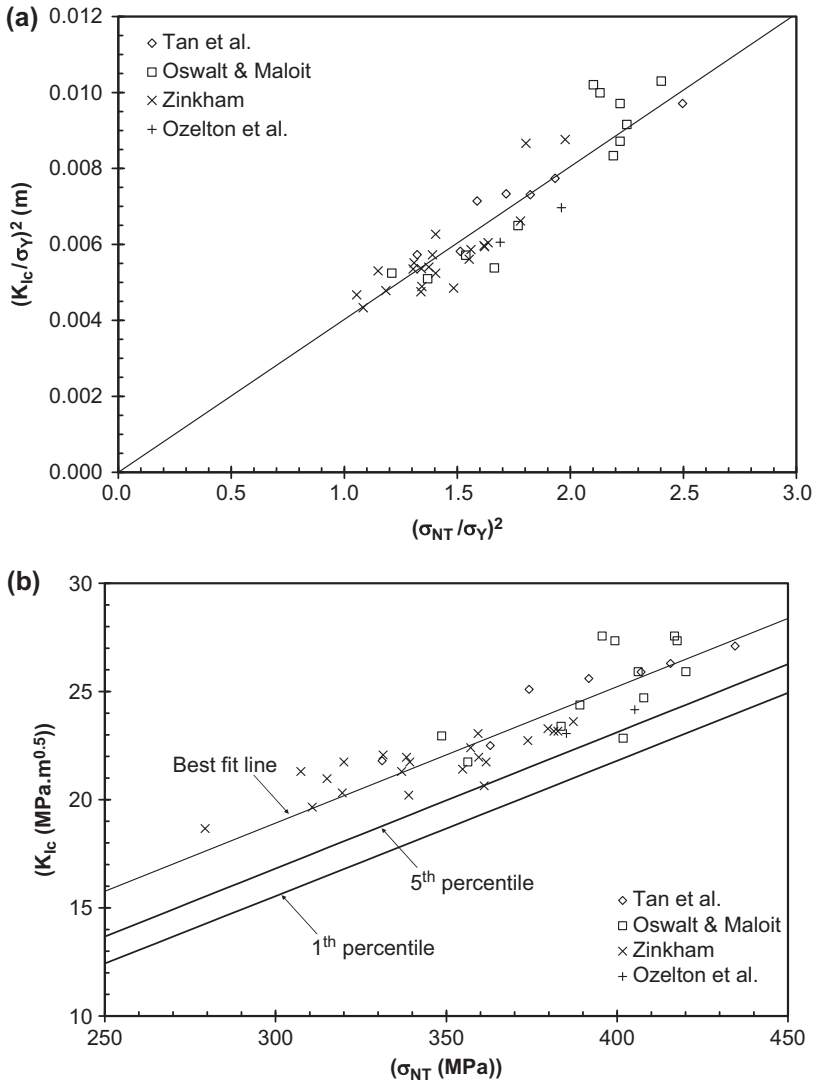

FIGURE 9.30

(a) Relation between $(K_{1C}/\sigma_Y)^2$ and the square of notch tensile strength σ_{NT}/yield strength σ_Y. The best fit line goes through the origin, suggesting a convincing relationship. (b) K1C values from all studies is plotted versus notch-tensile strength (lower bounds at 95% and 99% confidence limits are also shown). (Tiryakioglu, 2008.)

of stable crack growth. For a given geometry of loading, size of test piece and size of defect, J is related directly to the area under the load–displacement curve obtained for the cracked body, where displacements are measured at the loading points.

A general overview of the fracture toughness and strength of cast alloys is given in Figure 9.31. This indicates the rather poor properties of flake irons, and the excellent properties of some steels, nickel alloys and titanium alloys. Ductile

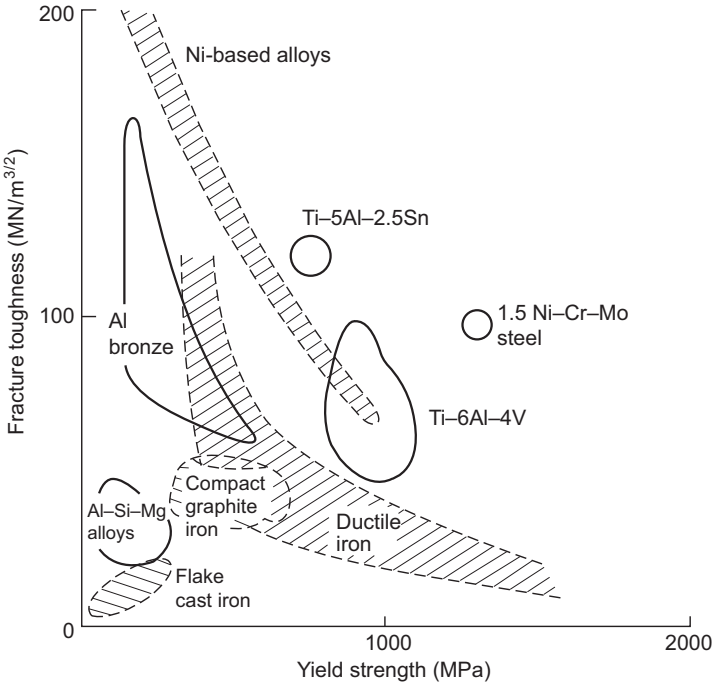

FIGURE 9.31

Map of fracture toughness versus yield strength for various cast alloys.

Data from Speidel (1982) and Jackson and Wright (1977).

irons occupy an interesting middle ground. In general, it seems that most groups of alloys can exhibit either high strength and low toughness or high toughness and low strength. The result is the hyperbolic shape of the curve as seen for ductile irons. As more results for other alloys are determined, Figure 9.31 will be expected to develop into a series of overlapping hyperbolic regimes containing the various alloy systems.

Figure 9.32 shows how the fracture toughness values can be translated into permissible flaw diameters, assuming a central penny-shaped crack, and a given level of applied tensile stress. Lalpoor and colleagues (2009) work out from computed stresses the sizes of critical flaws in a continuously cast high-strength Al alloy 7050, finding that the diameters of critical penny shaped cracks are in the region of 20–50 mm. Because spontaneous failures of these products are relatively common (and expensive of course) it is clear that such large cracks do exist. It seems inescapable that these are bifilms introduced during the initial fall of the melt into the mould; the rest of the mould filling action is practically perfect and not capable of introducing such defects.

Figure 9.20 presents interesting results for the mechanical properties of a high-strength aluminium alloy that is not normally poured to make shaped castings. In this work, it was cast and given a range of heat treatments covering the peak response condition. In the optimally hard state, it had an elongation close to zero and would not normally be used in this condition because a designer or user would be nervous about brittle failure. It is in the nature of brittle failure (i.e. failure without general plastic deformation) that there is no benefit from either (1) the redistribution of stress or (2) any prior warning of impending failure by the general plastic yielding of the casting. Nevertheless, the fracture toughness is clearly little influenced by aging and retains a respectably high value regardless of the low ductility. This means that any crack or other defect will always have to exceed a certain critical size before failure occurs, even if such failure is eventually of a brittle character, and therefore probably catastrophic.

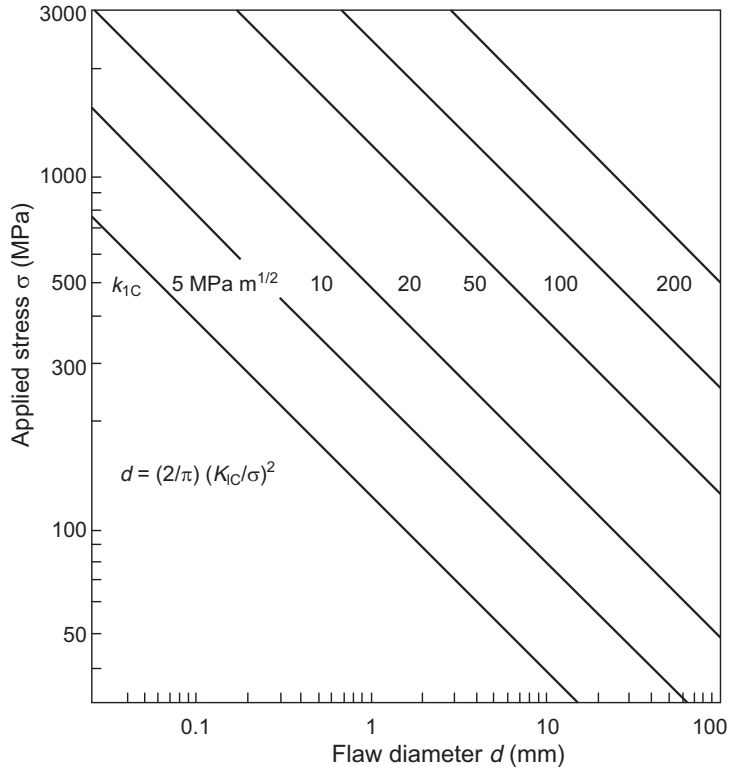

FIGURE 9.32

Relation between fracture toughness, applied stress and the critical defect size for failure in a material containing a central circular flaw.

This general behaviour is confirmed by Vorren and colleagues (1984) for the more common casting alloy Al-7Si-0.5Mg: although these researchers find the fracture toughness falls with increasing iron content in the alloy, the fall is significantly less than the fall in ductility, assessed by the reduction in area.

In those cases where general deformation of the casting cannot be tolerated, therefore, the use of fracture toughness is a more appropriate measure of the reliability of the casting than ductility. It seems that for many years, we have been using an inappropriate parameter to assess the reliability of many of our castings.

9.6 FATIGUE

9.6.1 HIGH CYCLE FATIGUE

A huge volume of work exists on the fatigue of castings. Therefore this lightweight and shallow condensation hardly scratches the surface of a profound and increasingly mature discipline. We shall endeavour to mention some of the more important issues.

Initiation

A historically classical study of fatigue in a cast alloy Al-7Si-0.5 Mg was carried out by Pitcher and Forsyth (1982). These workers were able to show that in general the fatigue performance of cast alloys was poor because the initiation of

the fatigue crack during stage 1 of the fatigue process was short. This observation appears to have been confirmed for cast Al alloys many times, for instance recently by Wang, Apelian and Lados (2001), who found *zero* time was required for crack initiation and that the fatigue life was the time merely for propagation of the crack. With the wisdom of hindsight, we can conclude that this was almost certainly a consequence of the presence of bifilms. Thus the cast specimens were effectively pre-cracked. This conclusion is strongly indicated by the rather poor casting technique used for the preparation of test specimens and additionally confirmed by the appearance of pores that appeared to be associated with films in some of their micrographs. Thus the size of initiating defects in their castings effectively eliminated stage 1.

Stage 2 of the fatigue process is a small forward movement of the crack for each tensile part of the stress cycle. This stepwise propagation across the majority of the section leaves a characteristic pattern of 'beach marks' as seen in Figure 9.35(f). By counting back from the thousands of beach marks from the final mark at which the remaining cross-section was too small to withstand the load, and so failed catastrophically, it can be deduced that the initiation of the fatigue crack probably started on the first cycle.

However, Pitcher and Forsyth found that stage 2 of the growth of the crack was remarkably slow compared with high-strength wrought alloys. The slow rate of crack propagation seemed to be the result of the irregular branching nature of the crack, which appeared to have to take a tortuous path through the as-cast structure. This contrasts with wrought alloys, where the uniformly even micro-structure allows the crack to spread unchecked along a straight path. With the wisdom of hindsight, we can speculate that the crack followed randomly oriented and branching bifilms, as would have occurred if the sample shown in Figure 2.40(b) had been subjected to fatigue.

The results by Polich and Flemings (1965) on the solidification of steels are highly informative. They found that steels directionally solidified (DS), in which the growth direction was upwards, had properties significantly better than those solidified in a non-directional equiaxed mode. We can speculate that the equiaxed mode would have trapped bifilms between the growing grains, whereas the vertical solidification would have allowed bifilms to float clear, and even if encountered by the front, would have a chance to be pushed ahead and thus avoid incorporation in the solid. The absence of bifilms in the DS material is corroborated by the insensitivity of its ductility to wide changes in DAS (in contrast to equiaxed material) as seen in Figure 9.26. Furthermore, these authors found the properties of the DS material were also insensitive to the direction of grain growth, so that grain direction and grain boundary direction was, it seems, unimportant to the properties and the development of cracks. This important counter-intuitive finding further confirms that only the presence of bifilms at grain boundaries influences properties, and that otherwise, boundaries are practically as strong as the matrix so that cracks are hardly influenced by the presence of boundaries. (Despite widespread glib assertions of the weakness of grain boundaries, they are clearly strong; otherwise, all our bridges would be in the rivers.)

One conclusion to be drawn from the work indicating that initiation takes no time but crack propagation is slow, is that if initiation can be delayed, then fatigue lives of cast metals might be extended considerably, perhaps in excess of those of wrought alloys.

An indication of the general validity of this conclusion is confirmed by Pitcher and Forsyth, who shot-blasted their specimens to generate residual compressive stresses in the surface. This did help to slow initiation, and total fatigue lives were improved. For sand castings, fatigue life was increased to that expected of chill cast material as shown in Figure 9.33. (It is a pity that the important high-stress/low-cycle part of the fatigue curve is often not investigated. It is interpolated here between the high-cycle results and the TS values; i.e. the single cycle to failure result.) Chill-cast material is subject to a similar substantial improvement when shot blasted. For steel castings, Naro and Wallace (1967) also found that shot peening considerably improved the fatigue resistance.

Although the improvement of fatigue resistance as a result of the compressive surface stresses introduced by shot peening is perhaps to be expected, the effect of grit blasting is less easy to predict, because the fine notch effect from the indentations of the grit particles would impair, whereas the induced compressive stresses would enhance fatigue life. From tests on aluminium alloys, Myllymaki (1987) finds that these opposing effects are in fact tolerably balanced, so that grit blasting has little net effect on fatigue behaviour.

Effect of defects

Improvement is expected if cast defects are eliminated, so that the fatigue crack now needs to be initiated, thus introducing a lengthy stage 1. Figure 9.33 illustrates the case of a pearlitic ductile iron where consistently improved

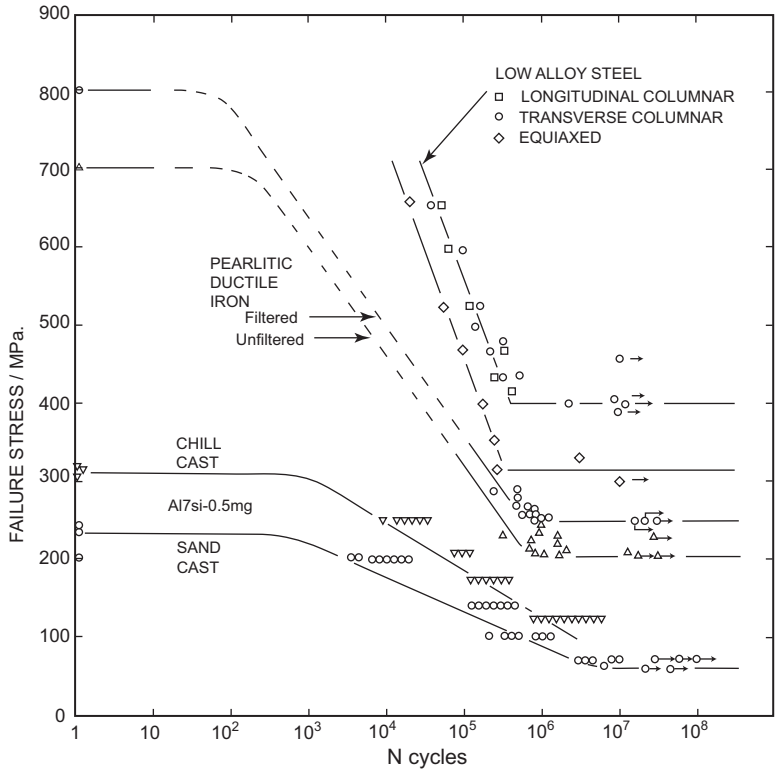

FIGURE 9.33

Fatigue data for an Al alloy (Pitcher and Forsyth, 1982), a pearlitic ductile iron (Simmons and Trinkl, 1987) and a low-alloy steel (Polich and Flemings, 1965).

performance was obtained from the use of material with a reduced density of defects produced by filtering in the mould. The elimination of thermal fatigue cracking in the early Cosworth Process Al-7Si-0.4Mg alloy cylinder heads is another instance of the importance of the elimination of defects, so as to introduce a long stage 1 to the fatigue crack formation.

This industrial experience has now been confirmed by a careful laboratory study by Nyahumwa, Green and Campbell (1998, 2000) on Al-7Si-0.4Mg alloy castings. To vary the number density and size of oxide film defects in the castings, test bars were cast using bottom gated filling systems with and without filtration. Test pieces were machined from the castings and were fatigue tested in pull–pull sinusoidal loading at maximum stresses of 150 and 240 MPa under stress ratio $R = +0.1$.

The use of the pull–pull mode of testing (positive R ratio) is important for two reasons. (1) The fracture surface is undamaged (in contrast to the hammering that normal reversing load fatigue specimens suffer) and so can be studied under the scanning electron microscope (SEM) in great detail. This is most important when searching for elusive features such as oxide films, and probably has been a significant factor explaining how such extensive defects have been overlooked until recently. (2) In service conditions in many castings, the existence of residual tensile stress is a common feature because of inappropriate quenching practice after solution heat treatment. Some residual stress is to be expected even in carefully quenched castings. Thus fatigue failure is most likely to occur in regions already experiencing

significant tensile loads. Thus pull–pull testing conditions will represent such regions more accurately. It follows that fatigue testing in laboratories using reversed loading (push–pull, with negative R ratios) should be reconsidered in favour of pull–pull (positive R ratio).

Test bars of an Al-7Si-Mg alloy (2L99) were cast in chemically bonded silica sand moulds. Two batches of test bars were cast using (1) a bottom-filling unfiltered system through which a liquid metal entered the ingate at a velocity greater than 0.5 ms^{-1}, and (2) a bottom-filling filtered system through a ceramic foam filter with 20 pores per inch (corresponding to an average pore diameter of approximately 1 mm); in this system, a liquid metal entered the ingate at a velocity less than 0.5 ms^{-1}. An SEM examination was carried out on the fracture surfaces of every one of the 64 failed specimens to ascertain the crack initiator in every case. This was a huge exercise, probably never attempted previously.

Fatigue life data obtained from the filtered and unfiltered castings tested at 150 and 240 MPa are plotted in Figure 9.34. The probability of failure for each of the specimens in a sample was defined as the rank position divided by the sample size (i.e. the test results were ranked worst to best in ascending order; so, for instance, the 20th sample from the bottom in a total of 50 samples exhibited a 40% probability of failure).

Figure 9.35 shows the three main types of fracture surface observed: (a) oxide film defects which were categorised either as young, thin film or older, thicker film, based on the thickness of folds; (b) slip mechanisms indicated by a typical faceted transgranular appearance; and (c) fatigue striations, often called beach marks, denoting the step by step advance of the crack. Later examination of the so-called slip planes indicated a mix of what appeared to be a true slip plane, and a fairly flat plane formed from a straightened oxide film.

There was much to learn from this work. Figure 9.34 shows that for the unfiltered castings, most failures initiated from defects, sometimes pores, but usually oxides. The oxides were a mix of young and old. Only three specimens were fortunate to contain no defects. These exhibited 10 times longer lives, and finally failed from cracks that had initiated by the action of slip bands that created interesting facets on the fracture surface. Thus these specimens had lives limited by the metallurgical properties of the alloy, although even in this case, an ‘ultimate’ attainment of life could not be assumed since it seems likely that entrainment defects had initiated the slip bands (Tiryakioglu, Nyahuwa and Campbell, 2011)

The filtered castings (bold symbols in Figure 9.34) were expected to be largely free from defects, but even these were discovered to have failed mainly as a result of defects, the defects consisting solely of old oxides that must have passed through the ceramic foam filter. There were no young oxides and no pores. A check of the equivalent initial flaw size (determined from the square root of the projected area of fatigue defect initiators) showed that 90% were in the range 0.1–1.0 mm, with a few as large as 1.6 mm. Thus most would have been able to pass through the filter without difficulty.

Again, those few samples of cast material free from oxides displayed an order of magnitude improved life, the best of which agreed closely with the best of the results from the unfiltered tests. This agreement confirms the relatively defect-free status of these few results.

The detrimental effect of mixed oxide films in the unfiltered castings is reflected by the lower fatigue performance compared with that of the filtered castings containing old oxide films. This indicates that the old oxide films, which were observed to act as fatigue crack initiators in the filtered castings, were less damaging than mixed oxide films. Clearly, we can conclude that the young films are more damaging, almost certainly as a result of their lack of bonding. This contrasts with the old oxide films that have probably benefited from the closing and partial re-bonding of the interface. This observation is consistent with the expectation that pores would be associated with new films, whose bifilm halves could separate to form pores, but not with old films, whose bifilm halves were (at least partly) welded closed.

These findings are confirmed in general by the results at the higher stress 240 MPa (Figure 9.34(b)) The fatigue failures of unfiltered castings are initiated from a mixture of pores, and old and new oxides; the 33 filtered castings initiated from 29 old oxides, three pores and one slip plane; and the 33 unfiltered and HIPped tests initiated from 32 old oxides and one slip plane. The various types of fracture surface are shown in Figure 9.35.

The presence of facets on the fracture surface is interesting. Whereas it has been usual to ascribe the formation of facets only to a slip plane mechanism, Tiryakioglu et al. (2011) have suggested that some facets appear to have formed from straightened bifilms. There appear therefore to be two forms of facets which are quite distinct: (1) the slip plane–generated facets have nearly flawless mirror-smooth planes with sharply defined edges and steps as seen in

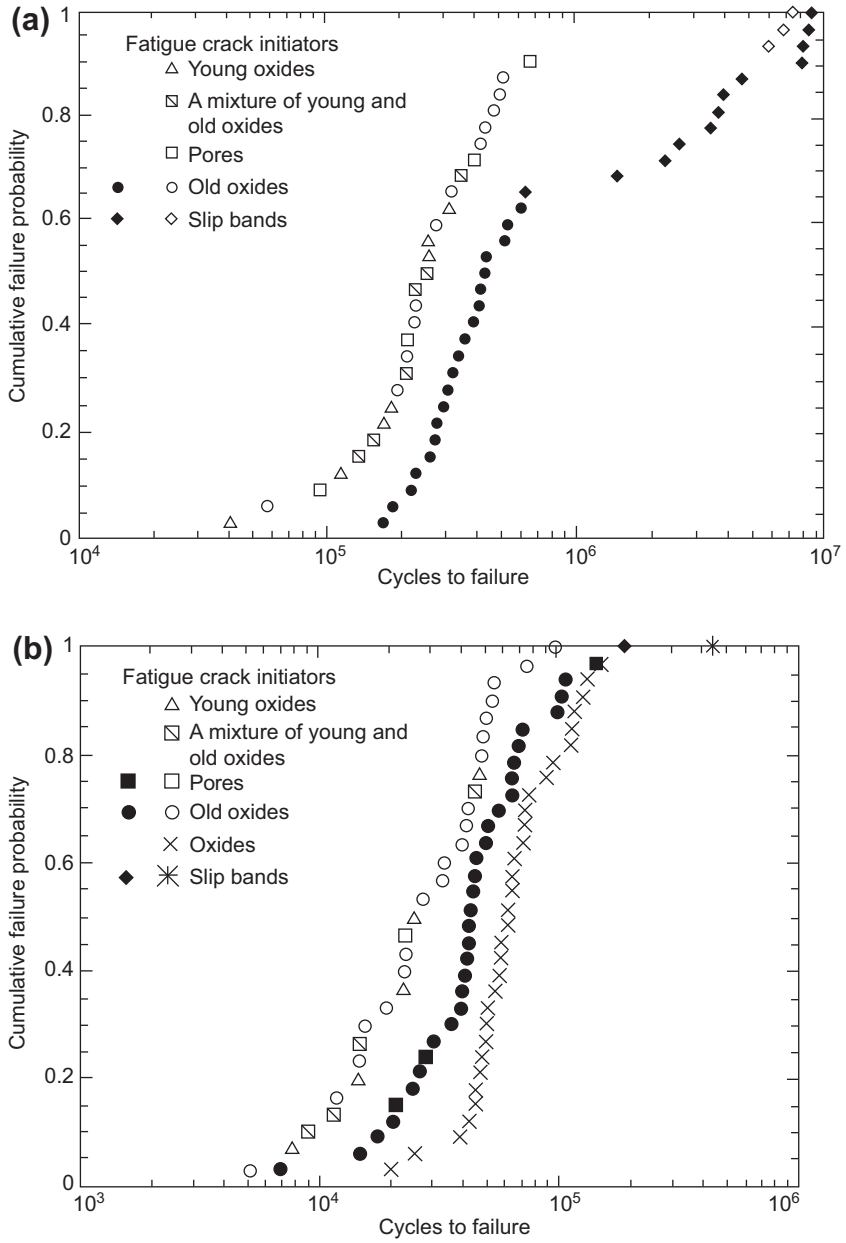

FIGURE 9.34

Fatigue life of unfiltered (open symbols), filtered (solid symbols) and unfiltered and HIPped (cross and star symbols) of Al-7Si-0.4Mg alloy castings tested in pull–pull at R = +0.1 and (a) 150 MPa and (b) 240 MPa (Nyahumwa et al., 1998, 2001).

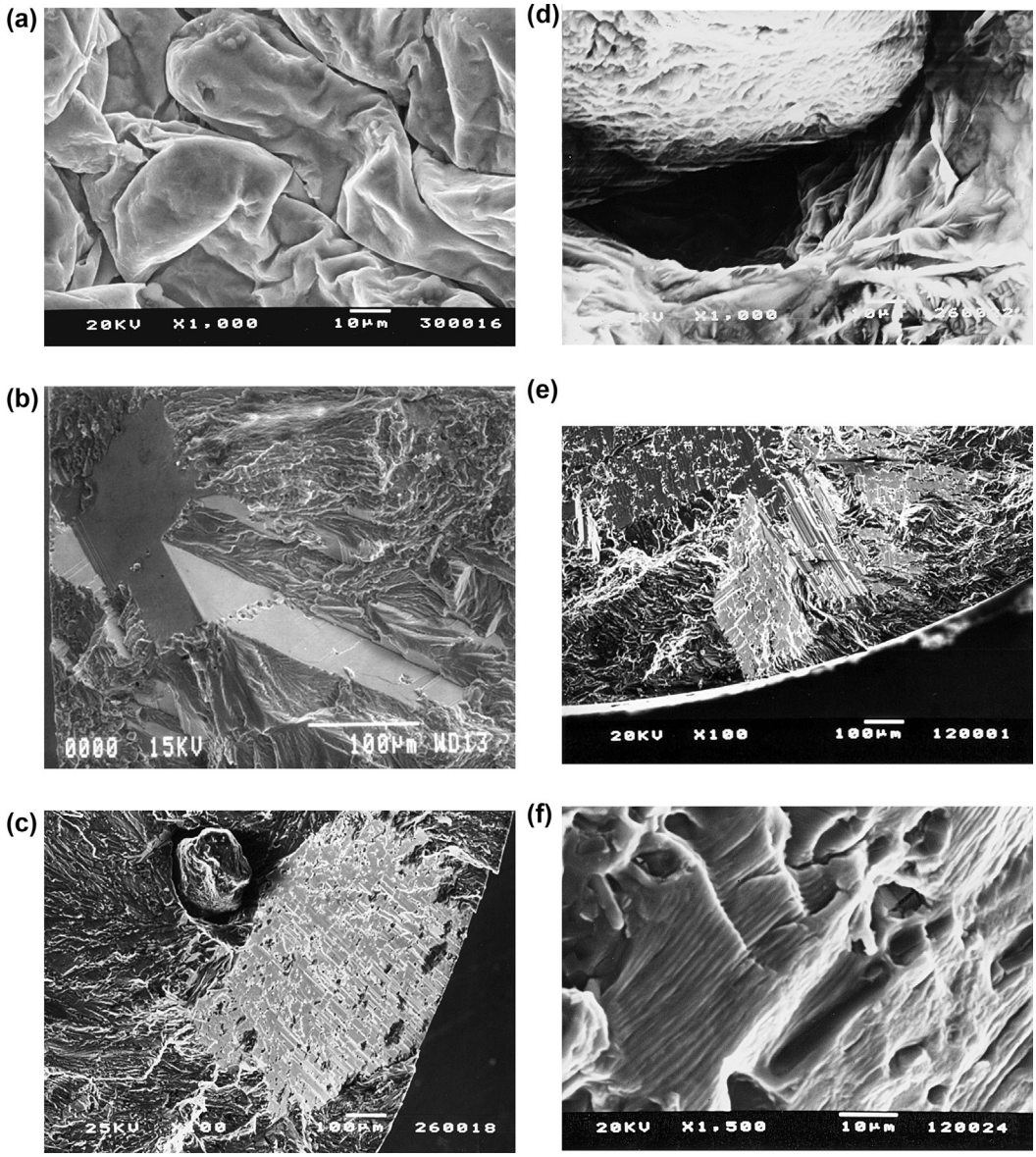

FIGURE 9.35

Fatigue fracture surfaces illustrating (a) oxide initiator; (b) slip plane–generated facets; (c) bifilm facet with failure probably initiated from entrained sand particle; (d) close-up of sand particle showing it to be enveloped by an oxide film as a result of its entrainment; (e) mixed slip plane and bifilm facets; (f) 'beach mark' striations from the stepwise advance of the fatigue crack (Nyahumwa et al., 1998, 2001).

Figure 9.35(b). (2) The straightened bifilm originated plane is less smooth, with no sharp steps or edges, but edges in places extending out from the facet to become contiguous with a crumpled oxide film, and its surface covered with small pores as would be expected to have been entrained together with the bifilm as is shown in Figure 9.35(c) and 9.35(e). Figure 9.35(c) and the higher magnification Figure 9.35(d) illustrate that the oxide wrapping of the entrained grain of silica sand appears to be the contiguous with the planar film, strongly suggesting these two oxide films are one and the same film, the area beyond the sand grain having been straightened by the advance of dendrites. Interestingly, both forms (1) and (2) act as cracks, and both are of size dictated by the grain size of the casting, thus these authors found that their effect on fatigue life was effectively identical. Clearly, when these are observed the fatigue life is usually long, but may not represent an 'ultimate limit' as has previously been supposed.

Other workers (for instance Wang et al., 2001) using Al-7Si-0.4Mg alloy have in general confirmed that for a defect of a given area, pores are the most serious defects, followed by films of various types. This is to be understood in terms of pores having zero tensile strength, but bifilms may be partly welded, but in any case always have some degree of geometrical interlocking as a result of their convoluted form as is clear from Figure 2.41.

However, the pre-eminence of pores in fatigue failure is not to be taken for granted. Nyahumwa found films to be most important in his work on this alloy. He had the advantage of having the latest techniques to search for and identify the full extent of films, whereas it is not known how thorough previous studies have been, and films are easy to overlook even with the best SEM equipment. In contrast, Byczynski (2002) working with the same techniques in the same laboratory as Nyahumwa found that pores were the most damaging defects in the more brittle A319 alloy used for automotive cylinder blocks. This difference may be the explicable by the differences in ductility of the two alloys that were studied. Nyahumwa's alloy was ductile, and so required the stress concentration of bifilms acting as cracks. Byczynski's alloy was brittle, so that cracks could more easily occur from pores.

Thus we may tentatively summarise the hierarchy of defects that initiate fatigue in order of importance: these are pores and/or young bifilms, followed by old bifilms. It would be expected that in the absence of larger defects, progressively finer features of the micro-structure would take their place in the hierarchy of initiators. However, it seems that such an attractively simple conceptual framework remains without strong evidence, even doubtful, at this time as is described later.

The considerable work now available on Al alloys illustrates the present uncertainties. In Al alloys, it has been thought that silicon particles may become active in the absence of other initiators. However, the action of bifilms is almost certainly involved in the occasional observations of the nucleation of cracks from these sources. For instance, the observed decohesion of silicon particles from the matrix (Wang et al., 2001, part I) is difficult to accept unless a bifilm is present, as seems likely. The initiation of cracks from iron-rich phases occurs often if not exclusively from bifilms hidden in these intermetallics (Cao and Campbell, 2002). The initiation of fatigue from eutectic areas, and reported many times (for instance Yamamoto and Kawagoishi, 2000 and Wang et al., 2002, part II) is understandable if bifilms are pushed by growing dendrites into these regions. The fascinating fact that Yamamoto and Kawagoishi observe silicon particles sometimes initiating fatigue cracks and sometimes acting as barriers to crack propagation strongly suggests bifilms are present sometimes and not at other times, as would be expected. It is not easy to think of other explanations for this curious observation.

Performance

Figure 9.36 is intended to illustrate the panorama of performance that can be seen in castings. The poor results can sometimes be seen in pressure die castings, in which the density and size of defects can cause failure to occur on or even before the first cycle (some test pieces from a poor pressure die casting fell to pieces in the hand before being loaded into the testing machine). However, it is to be noted that the unpredictability of this process sometimes will yield excellent results if the defects are, by chance, or by manipulation, in an insensitive part of the casting, or where perhaps the bifilms are aligned parallel to the stress axis. The uncertainty of the effects of the certainly present bifilms in pressure die castings is the key reason why it is never easy to select such castings for safety critical applications.

In terms of this panorama in Figure 9.36, the results of Nyahumwa are presented as 'fair' and 'good', respectively, showing a few tests that exhibit outstandingly good lives, reaching 10^7 cycles. Clearly, a series of ideal castings, free from defects, would display identical lives all at 10^7 cycles. The important lesson to draw from Figure 9.36 is that most engineering designs have to be based on the minimum performance. It is clear, therefore, that even the castings

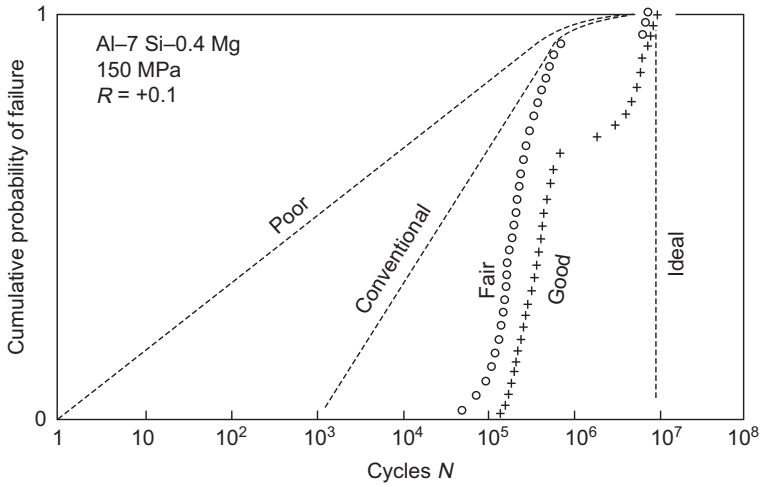

FIGURE 9.36

Schematic overview of the extreme range of fatigue performance found in structural Al alloy castings. There is recent evidence that the 'ideal' performance should be shifted substantially to the right (Tiryakioglu, Campbell and Nyahumwa, 2011).

designated 'good' in this figure have a potential to increase their lowest results by at least two orders of magnitude, i.e. 100 times. It means that for most of the aluminium alloy castings in use today, we are probably using a maximum of only 1% of their potential fatigue life. To gain this hundredfold leap in performance, we do not need different or more costly alloys, we merely need to eliminate defects.

The sobering density of defects in many special steels arises as a result of the appalling way in which the steels are cast. Whereas large tonnages of steels are cast by continuous casting, and so tolerably well cast, smaller quantities of special steels are cast into ingots. The process is shown in Figure 12.1. The dreadful mix of liquid metal and air creates masses of bifilm in steels with solid oxides such as the 1%C1.5%Cr steels for roller-bearing applications. The bifilm networks created during the pouring of the ingots have been widely interpreted as fatigue cracks (Figure 9.37) and certainly lead to fatigue failures by parts of the bearing surface spalling away. The contact pouring of ingots would solve this problem as seen in Figure 12.1.

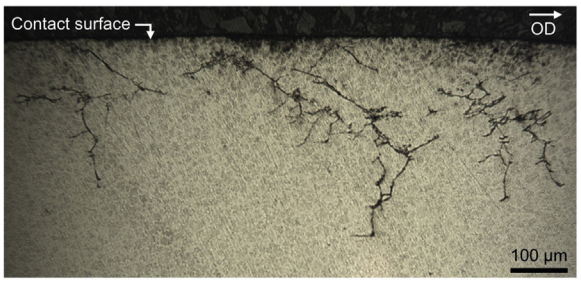

FIGURE 9.37

Bifilm cracks leading to the fatigue failure of the main steel roller bearings in a windmill.

Courtesy Martin Evans (2012).

As a closing update on the current understanding of the key aspects of fatigue, Tiryakioglu (2009) finds that the size distribution for fatigue-initiating defects in Al-7%Si-Mg alloys is described by an extreme value distribution known as the Gumbel distribution (and not Weibull or lognormal as has been commonly assumed). In addition, the fatigue life model based on the Paris–Erdogan equation with no crack initiation stage provides respectable fits to the data he has been able to test so far. A new distribution function combining the size distribution of fatigue-initiating defects and fatigue life model provides fits to data that could not be rejected by goodness-of-fit tests, in contrast to two-parameter Weibull. Tiryakioglu has gone on to explain the use of Weibull and other distributions, providing helpful examples and illustrations of comparisons between different distribution models (Tiryakioglu, 2010, 2011).

9.6.2 LOW CYCLE, HIGH STRAIN AND THERMAL FATIGUE

Thermal fatigue is a dramatically severe form of fatigue. Whereas normal *high-cycle fatigue* occurs at *stresses* comfortably in the elastic range (i.e. usually well below the yield point) *thermal fatigue* is driven by thermal *strains* that force deformation well into the plastic flow regime. The maximum stresses, as a consequence, are therefore well above the yield point.

Thermal fatigue is common in castings in which part of the casting experiences a fluctuating high temperature whilst other parts of the casting remain at a lower temperature. The phenomenon is seen in grey iron disc brakes and aluminium alloy cylinder heads and pistons for internal combustion engines, particularly diesel engines and air-cooled internal combustion engines. It is also common in the casting industry with the crazing and sometimes catastrophic failure of high-pressure die-casting dies made from steels and gravity dies (permanent moulds) and ingot moulds made from grey cast iron.

The valve bridge between the exhaust valves in a four-valve per cylinder diesel engine is an excellent example of the problem, and has been examined in detail by Wu and Campbell (1998). In brief, the majority of the Al alloy casting remains fairly cool, its temperature controlled by water cooling. However, the small section of casting that forms a bridge, separating the exhaust valves, can become extremely hot, reaching a temperature in excess of 300°C. The bridge therefore attempts to expand by $\alpha\Delta T$, where α is the coefficient of thermal expansion and ΔT is the increase in temperature. For a value of α about 20×10^{-6} K^{-1} for an Al alloy, we can predict an expansion of $300 \times 20 \times 10^{-6} = 0.6\%$. This is a large value when it is considered that the strain to cause yielding is only about 0.1%. Furthermore, because the casting as a whole is cool, strong and rigid, the bridge region is prevented from expanding. It therefore suffers a plastic compression of about 0.6%. If it remains at this temperature for a sufficient time (an hour or so) stress relief will occur, so that the stress will fall from above the yield point to somewhere near zero.

However, when the engine is switched off, the valve bridge cools to the temperature of the rest of the casting, and so now suffers the same problem in reverse, undergoing a tensile test, plastically stretching by up to 0.6%.

The starting and stopping of the engine therefore causes the imposition of an extremely high strain and consequent stress on the exhaust valve bridge. For those materials, such as a poorly cast Al alloy, that has perhaps only 0.5% elongation to failure available, it is not surprising that failure can occur in the first cycle. What perhaps is more surprising is that any metallic materials survive this punishing treatment at all. It is clear that modern, well cast cylinder heads can undergo thousands of such cycles into the plastic range without failure.

The experience from the early days of setting up the Cosworth Process provided an illustration of the problem as described earlier. In brief, before the new process became available, the Cosworth cylinder heads intended for racing were cast conventionally via running systems that were probably well designed by the standards of the day. However, approximately 50% of all the heads failed by thermal fatigue of the valve bridge when run on the test bed. These engines were, of course, highly stressed, and experienced few cycles before failure. From the day of the arrival of the castings, otherwise substantially identical in every way, but made by the new counter-gravity process, no cylinder head ever failed again. The presence of defects is seen therefore to be critical to performance, particularly when the metal is subjected to such extreme strains as are imposed by thermal fatigue conditions.

Thermal fatigue tests can be carried out in the laboratory on nicely machined test pieces resembling a tensile test piece. One of the interesting observations is that for some ductile Al alloys, the repeated plastic cycling for those

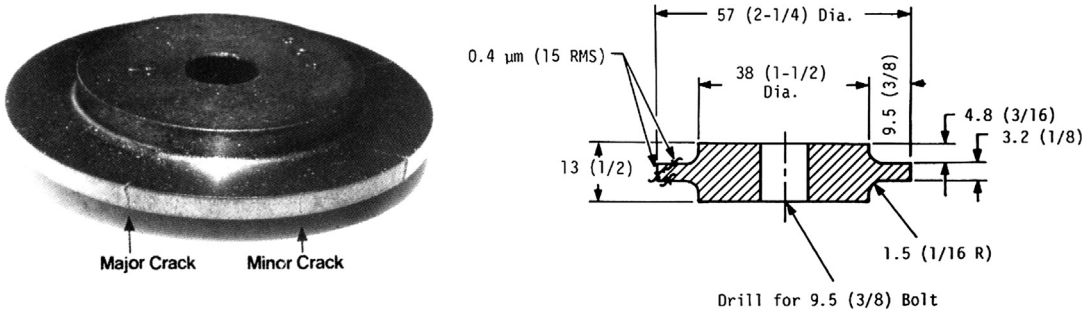

FIGURE 9.38

A simple and low-cost thermal fatigue specimen (Roehrig, 1978).

specimens that survive hundreds or thousands of cycles causes them to deform into shapeless masses. This gross deformation appears to be resisted more successfully for higher strength alloys (Grundlach, 1995). However, such tests require sophisticated and costly equipment which limit the number of investigations that can be carried out and rate at which results can be achieved.

There are, however, other forms of test pieces that are to be recommended for their extreme simplicity. Roehrig (1978) described three such tests, the simplest of which is shown in Figure 9.38. Such simple test pieces provide their own strain and stress development without the need for costly equipment. A typical testing scenario might be a stack of finned disc samples, bolted together through the central hole. The stack is immersed in a fluidised bed of alumina grit at near 1000°C for 5 s followed by transferring into a second bed at near 100°C for 120 s. These conditions may be selected for the simulation of stresses in a particular design or new alloy intended for an automotive brake disc. Some samples and some alloys fail after only a few cycles, whereas others survive for 1000 cycles or more. Other tests described by Roehrig are designed to simulate conditions specifically in cylinder heads, and some raise the severity of the cooling by water quenching. Such tests are excellent to optimise the selection of alloy for a particular casting requiring a specific thermal cycle resistance.

9.7 ELASTIC (YOUNG'S) MODULUS AND DAMPING CAPACITY

In an engineering structure, the *elastic modulus* is the key parameter that determines the *rigidity* of the design. Thus steel with an elastic modulus of 210 GPa is very much preferred to the light alloys aluminium (70 GPa) and magnesium (45 GPa). However, of course, the specific modulus (the rigidity modulus divided by density) gives a somewhat more favourable comparison because they are all closely similar at about 26 $MPam^3kg^{-1}$.

Because the elastic properties of metals arise directly as a result of the interatomic forces between the atoms, there is little that can normally be done to increase this performance. Alloying, for instance has practically no effect.

The one exception worth noting to this general rule is the alloy system Al-Li, which creates such a large volume fraction of Al-Li intermetallics that the elastic modulus is raised by about 10%. At the same time, the density is reduced by about 10%, resulting in an overall increase in specific elastic modulus of 20%. This relatively modest increase in stiffness seems to be an example of the highest that can be expected for most engineering metals.

It was all the greater surprise to the author, therefore, when he arranged for a computer simulation to be carried out on the largest bell in the United Kingdom. This was Great Paul, the 17,000 kg bell in St Paul's Cathedral, London. The investigators, Hall and Shippen (1994), found that agreement with the fundamental note and the harmonics could only be obtained by assuming that the elastic modulus was only 87 GPa, not 130 GPa expected for alloys of copper. This alarming 33% reduction was almost certainly the consequence of Great Paul being full of defects, mainly porosity and bifilms. This is true for most bells because, unfortunately, they are top poured via the crown of the bell. (The Liberty Bell

in the United States is a famous example of a crack opened from the massive bifilm constituted by the oxide flow tube that can be seen to have formed around the sinuous flow of the falling metal stream, starting high on the shoulder of the bell, and continuing down the side to its lip.) At the time of writing, the one bell foundry in the world known to the author (Nauen, Tonsberg, Norway) that uses bottom gating for its bells, placed mouth upwards, claims that it has never suffered a cracked bell, and its bells sound for twice as long as conventional bells. The longevity of the sound is understandable in view of the reduced quantity of bifilms to be expected, so reducing the loss of energy by internal friction between the rubbing surfaces of the bifilms as the bell vibrates.

It is clear, therefore, that many castings will suffer from a lower elastic modulus than expected because of their high content of bifilms. Furthermore, because elastic modulus is very rarely checked, this fact is not widely known. For the future, the full stiffness of the material will be gained only if the metal quality is good, and if the casting is poured with a minimum of surface turbulence.

The effect of a high density of bifilms in castings reducing the elastic modulus of the cast material is an interesting hypothesis that has a widely known and accepted metallurgical analogy that lends convincing comparison. The example is that of flake cast irons compared with steels. The graphite flakes in cast irons act as cracks because they are unable to withstand significant tensile stress (they may actually have formed around cracks if the bifilm theory presented in Chapter 6 is correct, which I think it is!). The iron, behaving like a steel matrix laced with a multitude of cracks, finds its modulus reduced from 210 GPa to only 152 GPa, a reduction of 28%, a value comparable to the reduction expected for many defective cast materials. In addition, of course, flake graphite irons are renowned for their excellent damping capacity, its absorption of vibrations and deadening of noise making it an ideal choice for the beds of machine tools.

Sand cast plates of Mg alloy ZE41A-T5 showed variations in elastic modulus in the as-cast condition that could be plotted on a Weibull distribution, with measurements generally in the 6–37% range below the theoretical 44.7 GPa (Xinjin Cao, 2009).

Further Examples Cannot Be Resisted

Zildjian cymbals, much prized by percussionists and drummers, own much of their unique sound and mechanical resilience (lesser cymbals can turn inside out when struck) to the fact that their original cast preform is tested by striking to see if the material has a ring in its cast state. If it does not, it is remelted. Clearly, this example confirms our expectations that the effects of the presence of bifilm defects survive in some alloys, even after the extensive working, applied in this case by forging and spinning into a thin disc.

The writer reveals his age when he admits to recalling the wheel tapper, moving along the side of the rail track, tapping the wheels of the train with his long handled hammer. He was checking that the 'ring' was correct. A cracked wheel would give a different note. Less romantically, but perhaps more reliably, the wheel tapper has now been superseded by the use of automated checking by ultrasonics while the wheels are rolled in a special checking station.

Ultimately, therefore, although there are fundamental reasons why the elastic modulus of many castings and their alloys cannot be improved, the reader may be able to raise the elastic modulus of a badly poured casting by 20–30% with negligible cost, exceeding the achievements of the famous Al-Li alloy which cost a fortune to develop.

Elastic properties of castings can now be measured quickly and with great precision using such modern tools as vibration frequency spectrum analysis, as described in Section 19.8.

9.8 RESIDUAL STRESS

Unseen and often unsuspected, residual stress can be the most damaging defect of all. This is because the stress can be so large, outweighing all the benefits of heat treatment and expensive alloying, and outweighing even the effects of all other defects.

Residual stress is usually never specified to be low. This is a grave indictment of the quality of component specifications and of standards in general. It is also practically impossible to measure in a non-destructive way in the interior of a complicated casting. However, it can be controlled by correct processing—another vindication of prudent, intelligent manufacture compared with costly, difficult and potentially unreliable inspection.

Also, of course, as will be noted in due course, in rare instances, residual stress can be manipulated to advantage. However, in the general case it should be assumed for the sake of safety that somewhere in the finished part, the retained stress will be in opposition to the strength of the casting. It can be viewed as subtracting from the casting's strength. Alternatively, it can be viewed as adding to the applied stress. Either way, a high residual stress means that the casting can be subjected to a total stress near to its point of failure even when relatively trivial loads are applied. Unfortunately, a conservative assessment of residual stress would have to assume that it reached the yield stress. This condition is expected to be common.

The remedy is, of course, either (1) the avoidance of stress-raising treatments such as quenching castings into water following solution treatment (and so accepting the somewhat reduced strengths available from safer quenchants such as forced air) or (2) the application of stress relief as already discussed (remembering, of course, that stress relief will effectively negate much or all of the strength gained from heat treatment). Either way, again, the use of the casting with lower internal stress and lower strength is vastly safer, more predictable and more reliable than a high strength casting with high internal stress.

As an example of a part that suffered from internal stress, a compressor housing for a roadside compressor in Al-5Si-3Cu alloy (the UK specification LM4) was thought to require maximum strength and was therefore subjected to a full solution treatment, water quench and age (T6 condition). Two housings exploded in service. Fortunately, on these occasions, no one was near at the time so no one was hurt. The manufacturer was persuaded to carry out a heat treatment that would reduce the internal stress, but also, of course, reduce the strength. This was strenuously resisted, but finally very reluctantly agreed. However, on testing the parts to destruction, the implementation of a heat treatment not to increase strength but merely to provide stress relief (a TB7 treatment) after casting, followed by air cooling, gave a part with only half the strength of the fully heat treated 'strong' casting, but double the burst pressure. No failures have occurred since.

This sobering lesson is expanded as rule 9 in the 10 *Rules for Casting* dealt with in Chapter 10.

9.9 HIGH TEMPERATURE TENSILE PROPERTIES

Creep

The gradual deformation of metals under load at high temperatures has been traditionally viewed as taking place in three stages:

1. Primary creep is the rapid early phase that gradually reduces in rate, eventually leading into stage two.
2. Secondary creep is the steady-state regime, in which creep rate is constant.
3. Tertiary creep is the final stage in which the rate of strain increases because of the growth of microscopic internal pores and tears that gradually link to cause the fracture of the whole component.

However, the reader should be aware that this traditional view is strongly criticised by Wilshire (see Wilshire and Scharning, 2008; Williams et al., 2010), who proposes a revolutionary single mechanism and single equation to fit all parts of the extension versus time creep curve. Wilshire's argument is that primary creep is subject to a decreasing rate, whereas tertiary creep is subject to an accelerating rate, so that the so-called secondary creep is merely a region in which these two mechanisms overlap to give a minimum creep rate. Wilshire's approach allows an accurate interpolation and extrapolation from relatively few experimental data points for several quite different metals and alloys, suggesting it is a valuable new fundamental interpretation of creep behaviour. We shall not delve deeper into the creep theory, but for our purposes, it is simply important to know that creep happens, and what we as founders might do to improve creep performance.

Components are said to have failed by creep if, during this slow deformation process, they exceed some critical size or shape. An example might be a turbine blade, whose length grows under the centrifugal stress so that it eventually scrapes the outer casing of the engine (although nowadays both blades and casings are designed to accept such problems). Alternatively, creep failure under tension might mean the fracture of the component at the end of tertiary creep.

Bifilms at grain boundaries are prime sites for the initiation of such catastrophic failures. Failure of the Ni-base alloy 718 described by Jo and colleagues (2001) appears to be precisely such a process initiated by oxide or nitride bifilms, judging from the micrographs published by these authors, although confirmatory evidence from the appearance and chemistry of the fracture surfaces was not carried out.

During the early development of the Pegasus engine for the Harrier Jump Jet 25, polycrystalline Ni-based alloy turbine blades that had previously been scrapped because of their content of porosity were subjected to HIPping, and were fitted to a test engine alongside sound blades to evaluate whether hipping might be a satisfactory reclamation technique for blades that otherwise would be scrapped. The HIPped blades failed within a few hours, damaging the engine and forcing a rapid shutdown of the test. The failures had occurred by creep cavitation at the grain boundaries of recrystallised regions in the centre of the castings. Almost certainly the original porosity would be caused by films rich in aluminium oxide entrained by the severe turbulence that is usual during the vacuum casting process. (The vacuum is known to contain plenty of residual air to ensure the formation of an oxide or nitride film on the liquid metal.) The great stability of the films, formed at the high casting temperature, would ensure that they were resistant to any re-bonding action during HIPping. The recrystallisation would have happened because of the large plastic strains that were a necessary feature of the collapse of the porosity. The grains would grow, expanding until they reached local barriers such as bifilms. Thus the bifilms, effectively unbonded, and so acting as efficient cracks, were automatically located at the grain boundaries from where the failures were seen to occur.

Superplastic Forming

In a related phenomenon of superplastic deformation, creep is deliberately induced at a high rate as a deformation process often involving several 100% of elongation. It is mainly useful for the shaping of sheet metals. The forming process is limited by the opening of microscopic voids, usually at grain boundaries, a process referred to in this field as ‘cavitation’. A typical example in Mg alloys is shown in Figure 9.39. The voids grow, causing the mechanical properties of the material to deteriorate, and progressively link, eventually leading to complete failure.

Several Al alloys can be produced in a superplastic condition. Al-Zn alloys are commonly used, although superplasticity has been developed in many Al alloys including Al-Li and Al-Mg varieties.

Chang (2009) describes how his Al-4.5Mg alloy cavitated at grain boundary precipitates of Al_6(Mn,Fe) and Mg-Si particles, strongly suggesting these particles occupied sites on bifilms that happened to be in grain boundaries.

Even more direct evidence of a bifilm-controlled failure mechanism in this alloy is provided by the work of Kulas and coresearchers (2006). Their SEM observations confirmed that voids opened at grain boundary intermetallics during grain boundary sliding. The intermetallics seem to have formed on oxide bifilms, because close examination of the voids by these authors indicated the presence of ‘filaments’ aligned with the deformation direction, stretching across the voids. The filaments were not analysed (indeed, this would have been a problem because they were clearly extremely thin, perhaps only 100 nm or less) and did not receive further comment by the authors, but can hardly be anything other than alumina films; the remnants of the bifilms causing the failure.

Similar observations can be listed for steels. During creep at 540°C of a power plant steel (Perets, 2004) containing 2.25Cr, 1Mo, 0.15C, carbides form on grain boundaries, where cracks and pores are observed, together with decohesion of the matrix from the carbides. A 12Cr steel studied by Wu and Sandstrom (1995) showed cavity initiation so early in their creep tests that they concluded the cavities were probably already present before testing. A super-austenitic stainless steel studied by Fonda (2007) using micro-tomography revealed that every sigma particle was associated with at least one void.

Intermetallic compounds are generally infamous for their brittle behaviour. However, in his studies of Fe_3Al Frommeyer (2002) reports amazing superplastic behaviour with elongations of 350%, indicating there seems to be nothing fundamentally wrong with the formability of this intermetallic. His work could not contrast more with that reported later for the same intermetallic by Yu and Sun (2004). They produced this material by vacuum melting and vacuum pouring into a sand mould, but experienced the ingots cracking and sometimes falling into pieces during hot forging which they attributed to the large, coarse grains. It seems certain that the fractures were the result of alumina bifilms from the turbulence of the pour because pour heights are high in typical vacuum furnaces. Figure 16.30 illustrates the problem. The large bifilms produced during the filling of the mould would have suppressed convection in the

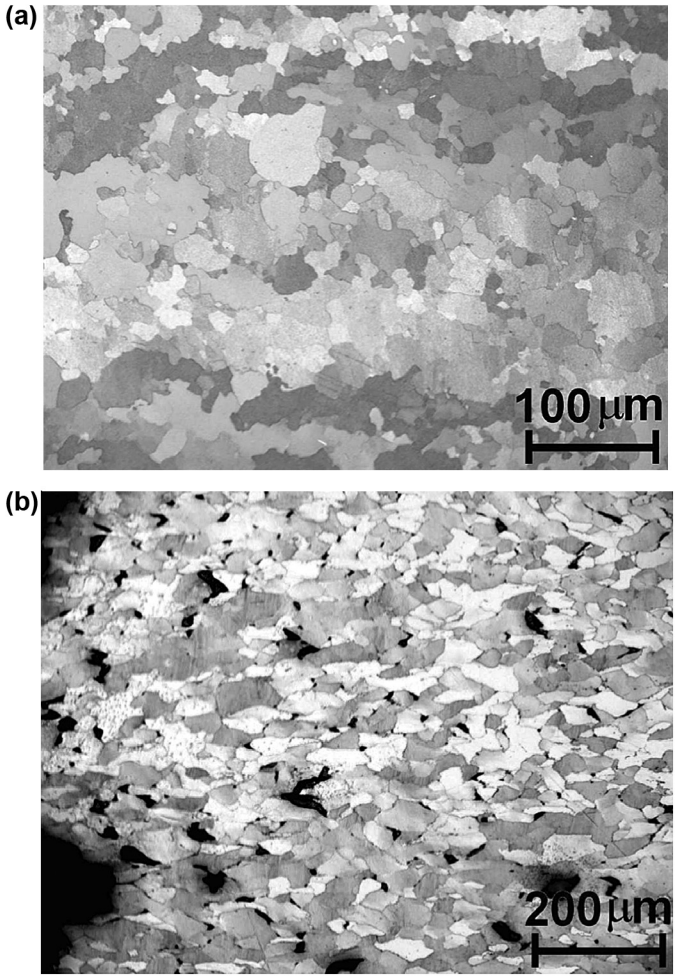

FIGURE 9.39

Castings, solution treated, extruded 30:1 and finally subjected to tensile strain at 10^{-3} s^{-1} at 200°C (a) Mg and (b) Mg-0.9Al alloy showing so-called cavitation; pore growth from the decoherence of grain boundaries.

Courtesy Stanford et al. (2010).

solidifying ingot and lead to the undisturbed growth of large grains, instead of the fine grains produced from grain multiplication in normal convection currents.

The implication of these creep and superplastic failures by the gradual accretion of grain boundary voids is that they would not occur if bifilms were not present. The failure mechanism would then probably be 100% ductile failure leading to 100% RA. If true, the prospects for improvement in these materials are awe inspiring.

9.10 OXIDATION AND CORROSION RESISTANCE

During the cooling of the casting in the mould, and to some extent after it has been extracted from the mould, and especially during high temperature heat treatment, air can gain access to and can attack the interior of the casting via

surface-connected bifilms. Similarly, if the casting experiences a corrosive environment, internal access of the corrodant can lead to a variety of problems. The role of the bifilm is central to the understanding of these important problems.

9.10.1 INTERNAL OXIDATION

When a metal such as an aluminium alloy is heat treated, the external surface naturally develops a thick oxide skin. However, in addition, some researchers have noted the development of internal oxides.

How is this possible? Oxygen is insoluble in aluminium and its alloys, and so, in principle, is not able to penetrate the alloy.

Clearly, such internal oxidation can only occur if the oxidising environment has access to the interior through some kind of hole. Surface-connected shrinkage porosity might create such a hole linked to extensive internal cavities. However, reasonably adequate pressurisation of the solidifying metal in the casting by proper feeding will prevent the formation of surface-connected porosity. Much more probable is access via bifilms connected to the outside surface. In the case of machined castings, particularly test bars, the machined surface will certainly cut into many bifilms, opening up many points of access for penetration by gas or liquid and attack deep into the interior of the casting.

It is easy to understand therefore that when working with an Al-4Mg alloy subjected to a solution treatment at 520°C for several hours Samuel and coworkers (2002) expected to find the usual benefits including not only the taking of solutes into solution, but fragmentation and spherodising of intermetallics, resulting in an improvement in mechanical properties. However, they reported the development of spinel (the $Al_2O_3 \cdot MgO$ mixed oxide) in the interior of the casting, and the reduction in tensile properties.

In the author's laboratory, Fenn and Harding (2002) treated some as-cast ductile iron test bars at 950°C for 1 h to eliminate carbides to allow them to be machined. The tensile properties turned out to be unexpectedly low, especially the ductility. Elongations in the region of 20% or more for this grade were to be expected, because ductile iron, as its name implies, is expected to be reliably ductile. It was a shock therefore to discover that elongations were highly scattered in the range of only 1–10%. Many specimens appeared to fail brittlely. SEM studies revealed thick uniform carpets of oxide on the fracture surfaces (Figure 9.40). These oxides clearly did not have the appearance of entrained films, and did not contain the content of Mg that would be expected if the oxides were bifilms entrained in the liquid metal during casting. It seems that the oxygen had penetrated the core of the bifilm and was added to the original magnesium silicate from which the original bifilm was constituted. The additional oxide appeared to be nearly pure iron oxide, as would be expected from a solid-state reaction. At the relatively low temperature of 950°C (low compared with the casting temperature of about 1450°C), the magnesium in solution in the solid alloy would be fixed, being unable to diffuse to the surface of the bifilm to enhance the magnesium concentration in the oxide. A further confirmation of the solid-state thickening of these oxides is that the graphite nodules appear through holes in the carpet. Clearly, the iron oxide cannot thicken above the nodules, giving the curiously dimpled or quilted appearance of the surface of the oxide seen in Figure 9.40(a). In Figure 9.40(b), the nodules themselves appear to be disintegrating as might be expected as their graphite oxidised away.

These internal oxidation problems are almost certainly common in cast alloys that have been subjected to heat treatment.

The same effect will occur, of course, automatically during the cooling of the casting in the mould. Additional oxidation of the originating bifilm will occur for surface-connected bifilms, thickening the film and possibly masking its original form. The original composition of the oxide may also be diluted and/or hidden by overgrowth of new oxide resulting from the solid-state reaction.

The solution to the avoidance of such internal oxidation is the avoidance of bifilms. Although this would be a complete solution, it may not be always practical. A next-best solution might be one of the many techniques to keep the bifilms closed, because, clearly, any action to open the bifilm, for instance by shrinkage, will enhance the access routes to the interior. It follows that a well-fed casting (i.e. pressurised by the atmosphere) or a casting artificially pressurised internally during solidification (as provided by some casting processes) will be less susceptible to the ingress of air during high temperature treatment. It will therefore retain its mechanical properties relatively unchanged (whether originally good or bad of course).

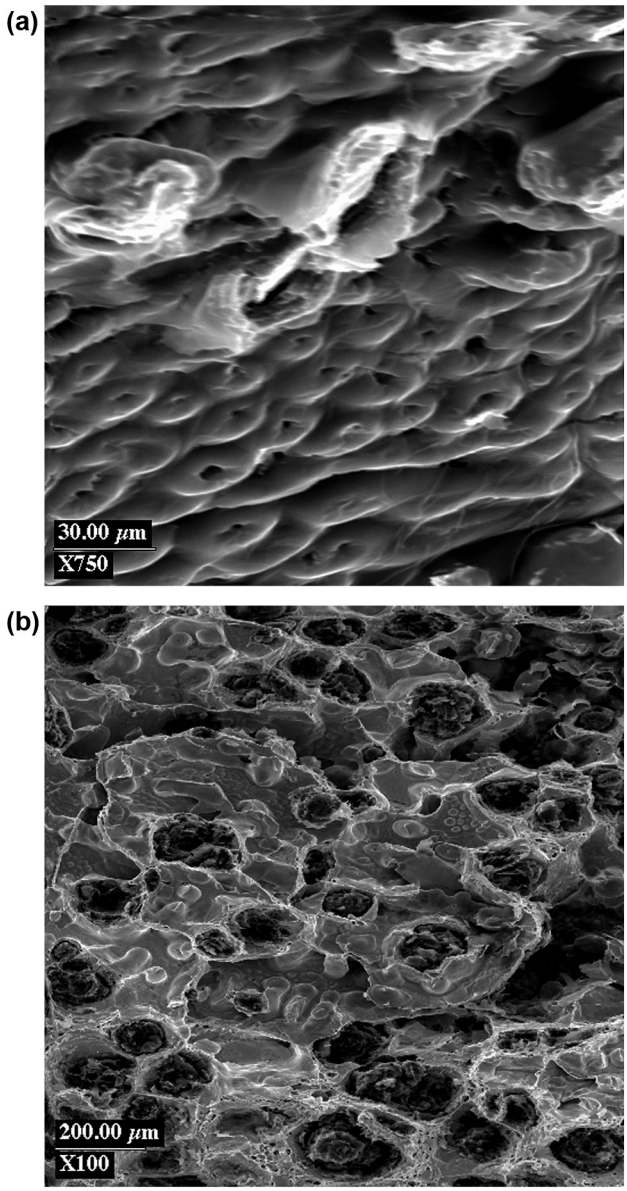

FIGURE 9.40

Fracture surface of a ductile iron damaged during annealing at 950°C for 1 h by internal oxidation of a surface-connected bifilm, showing (a) the formation of a carpet of solid-state-grown oxide and (b) oxidation of graphite nodules (Fenn and Harding, 2002).

9.10.2 CORROSION

Corrosion of metals, particularly aluminium alloy castings, and wrought products such as alloy plate and sheet, is a troublesome feature that has attracted much research in an effort to understand and control the phenomenon. Naturally, no comprehensive review of such a vast discipline can be undertaken here. The reader is referred to some recent reviews (Leth-Olsen and Nisancioglu, 1998). The purpose of this section is to present the evidence that a large number, possibly most corrosion problems, not only in shaped castings, but also in wrought alloys, arise from casting defects.

All corrosion pits that the author has seen are the sites where bifilms happen to meet the surface. In the absence of bifilms, it is proposed that there would probably be no corrosion of metals from surface pits. Corrosion might still be expected, but would probably be vastly reduced, having to occur uniformly over the whole surface of the metal. Alternatively, if localised sites were favoured, localised corrosion might continue to occur on a reduced scale from other inclusions, grain boundaries, or from dislocations that intersect the surface.

Many of the current theories of the corrosion of metals have been principally concerned with environmental attack on an essentially continuous unbroken planar substrate, regarding the surface of the metal as a uniform re-active layer (Leth-Olsen and Nisancioglu, 1998). The result has been that theories of filiform and inter-granular corrosion of aluminium alloys are at a loss to explain many of the observed features of these phenomena because these corrosion processes clearly do not exhibit uniformity of attack; the attack is extremely localised and specific in form.

The presence of bifilms generated in the pouring process has not, of course, been considered up to now as a factor contributing to the severity of corrosion. It will become clear in this section how bifilms help to explain many of the observed features of metallic corrosion. The link occurs because bifilms are, of course, often connected to the surface, allowing them to be detected sometimes by dye penetrant techniques. Similarly, in a corrosive environment, such bifilms will allow the local ingress of corrosive fluids between their unbonded inner surfaces (Figure 9.41). The presence of different varieties of second phases precipitated on the outer surfaces of bifilms will be expected to act as a further enhancement of the corrosion process by the creation of an electrochemical corrosion couple, explaining the major differences observed, for instance, between Al alloys of different Fe, Mn and Cu contents.

The stages of corrosion, leading to some pits formed by cathodic action involving alkaline dissolution, and other pits formed by anodic action leading to acidic dissolution, are illustrated schematically in Figure 9.42(a) and (b).

Direct and clear observations of oxide film tangles associated with corrosion sites have been made by Nordlien and Davenport (2000) and Afseth and coworkers (2000). Figures 9.43 and 9.44 are typical examples of sea water corrosion of a wrought Al alloy.

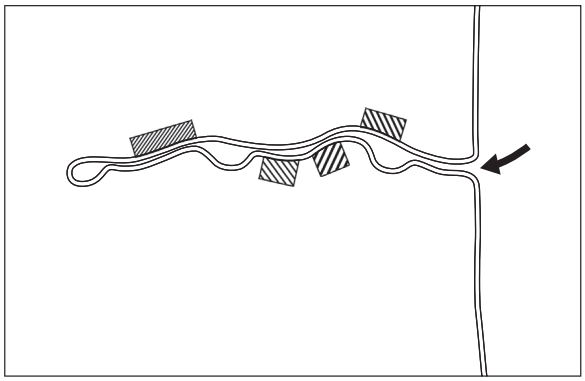

FIGURE 9.41

An image of a surface-connected bifilm, decorated with pockets of air and precipitated compounds of various kinds, is effectively open to the environment and makes an effective and complex corrosion cell if any aqueous corrodant such as sea water or rain water enters.

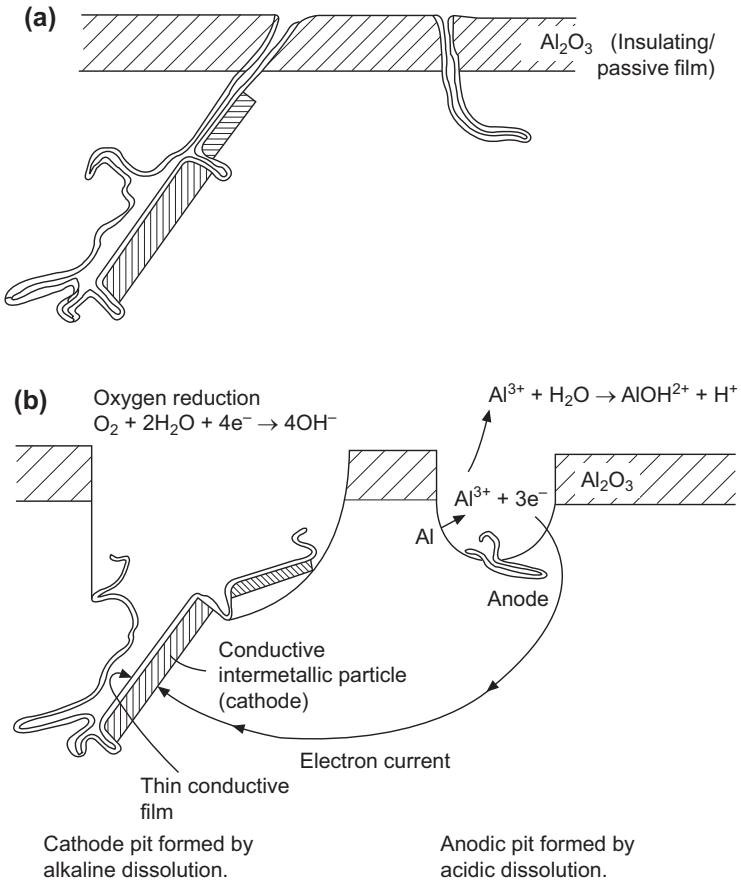

FIGURE 9.42

Mechanism of pitting corrosion from surface-connected bifilms (a) before and (b) during corrosion.

Adapted from Bailey and Davenport (2002).

9.10.3 PITTING CORROSION

Although there are many instances in which the corrosion of metals occurs uniformly across the whole surface, the special case of concentrated corrosion at highly localised sites, generating deep pits, is sometimes a serious concern. Most of the studies of pitting corrosion have been carried out on steels. Because we cannot in this short work survey this vast subject, we shall take only Al and its alloys as an example, following the review by Szklarska-Smialowka (1999), and see how pitting corrosion relates to the cast structure.

The main message of this section is that, in general, the familiar corrosion pit is not, originally, the product of corrosion. It pre-exists as a bifilm which emerges at the free surface of the metal. This pre-existence appears to have been generally overlooked until now because the originating defect is usually practically, if not actually, invisible. The corrosion process develops the pit into a highly visible and deleterious feature.

The corrosion proceeds as illustrated in Figure 9.42. The intermetallic particle precipitated on the bifilm acts as a cathode, with the electrical current passing through the electrolyte to anodic areas of the surface. It has been generally

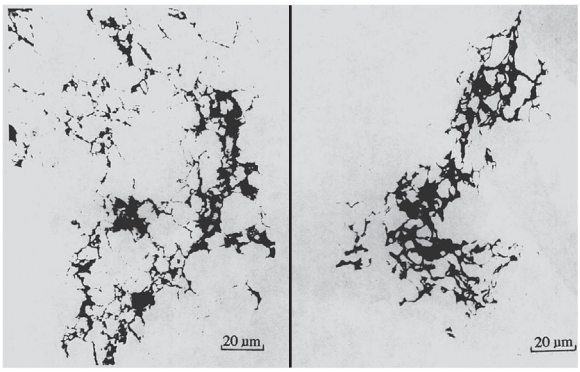

FIGURE 9.43

Two views of forged 7010-T736 alloy subjected to seawater corrosion.

Courtesy Forsyth (2000).

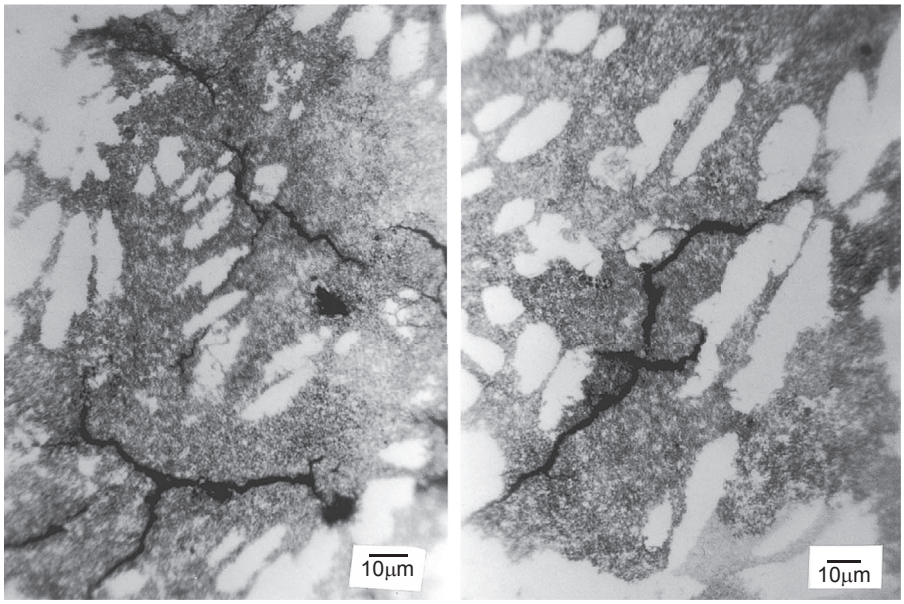

FIGURE 9.44

Typical polished and etched 7010 alloy in the solutionised condition subjected to seawater corrosion illustrating the interdendritic nature of the cracks.

Courtesy Forsyth (2000).

thought that the intermetallic particles provide the conductive path through the insulating alumina film. However, it is probable that the bifilm itself is sufficiently thin to be conductive, or will have been fractured during the cooling of the casting, so aiding this effect. The cathodic pit is the bifilm pit containing the intermetallic, whereas the anodic pits may be part of the same bifilm pits but distant from the intermetallic, or may be quite separate surface-intersecting bifilms that do not happen to contain intermetallics.

Oxygen is reduced at the cathode, demanding electrons, and so forming hydroxyl ions according to

$$O_2 + 2H_2O + 4e^- = 4OH^-$$

The alkaline conditions created by the hydroxyl ions assist to dissolve the material around the intermetallic, enlarging the pit. Conversely, at the anodic pit, conditions are acidic because of the generation of hydrogen ions as follows

$$Al = Al^{3+} + 3e^-$$

$$Al^{3+} + H_2O = AlOH^{2+} + H^+$$

Thus this pit also enlarges as matrix material is dissolved. The electrical circuit is, of course, completed by electrons travelling though the aluminium matrix from the anode pit to the cathode pit.

The random nature of the creation of such defects, being linked to the action of surface turbulence at several stages of manufacture of the sheet, explains why the corrosion behaviour is so variable, changing in severity from one supplier of metal to another and from one production batch of alloy to the next. Also, of course, every pit will be different because of the random nature of the oxide tangles. The tangled geometry is indicated in Figures 9.43 and 9.44. This randomness has been a major problem to investigators.

The bifilms are expected to survive, and may even grow during plastic deformation, with their residual entrained air continuing to oxidise any newly created elongation of the defect until supplies of air are exhausted. Further extensions of the defect may then weld. Thus surface-linked cracks, possibly plated with intermetallics, will be expected not only characteristic of castings but also of wrought products.

In their studies of the effect of corrosion on the wrought alloy Al 6061 in the T6 heat treated condition Almaraz et al. (2014) notice that fatigue crack initiation was frequently associated with two or more corrosion pits, which greatly aided crack nucleation. These authors admitted that they could not understand why the effect was so severe. When researching etch pit formation in DC ingots, Jaradeh and Carlberg (2011) observed oxides associates with porosity (the clear signatures of bifilms) which developed into circular etch pits in NaOH solution. Interestingly, the numbers of pits corresponded reasonably well with the numbers of oxides in the liquid metal counted by Prefil.

9.10.4 FILIFORM CORROSION

In a standard corrosion scratch test, filiform corrosion takes the form of a high surface density of superficial corrosion paths, called filaments, which propagate extensively over the next few days from a scribe mark on a test plate. The corrosion proceeds away from the scratch along filamentary lines aligned with the original rolling direction. They travel under any protective layer such as paint, occasionally tunnelling beneath the metal surface, only to break out at the metal surface once again after a few millimetres or so. The lengthwise growth and subsequent sideways spreading of the filaments eventually causes any protective coating, such as a paint layer, to exfoliate. The length of filaments has been found to be generally in the 1–10 mm range. However, reviewers confirm (Leth-Olsen and Nisancioglu, 1998) that quantification of the phenomenon suffers from significant scatter that has hampered these studies.

The concentration of corrosion at strictly localised sites (the filaments) is clear. However, it is important to observe that the great majority of the metal surface remains completely free from attack (despite the long and deep breach of the protective coating by the scratch). Also clear is the different behaviour of different casting batches of nominally identical material, on different occasions giving filaments shallow or deep, or short (1 mm) or long (10 mm).

Growth of filaments stops when the length reaches some value between 1 and 10 mm. This has been suggested to be the result of chloride depletion in the head of the filament (Leth-Olsen and Nisancioglu, 1998), but is clearly more likely that the corrosion has reached the end of that particular bifilm.

In his review of the subject, Nordlien (1999) describes how the filaments of corrosion can grow at up to 5 mm per day. They occur on all families of aluminium alloys (1000, 2000, 3000, 5000, 6000, 7000 and 8000 series) and on all product forms (sheet, foil, extrusions).

Interestingly, a surface of rolled aluminium alloy sheet can be sensitised to the formation of filiform corrosion (in corrosion jargon it is 'activated') by annealing at 400°C. This effect can be understood as the growth of oxidation products on the internal surfaces of cracks that will assist to open the cracks (see Section 9.10.1). The deactivation by etching probably corresponds to the preferential attack and removal of surface cracks and laminations. Re-activation by subsequent annealing seems likely to be the result of the opening of slightly deeper defects by oxidation. The removal of defects by etching removes only a few micrometres of depth of the surface. Considering the defects are commonly 1–10 mm in size, there will be no shortage of new defects to open on subsequent re-activation cycles.

In severe cases of surface corrosion, the frequent observations of delamination (Leth-Olsen and Nisancioglu, 1998) can be understood as the lifting of irregular fragments of bifilm that lie just under the metal surface. Other related observations of blistering (see Chapter 19.2) can also be understood as the inflation of just-subsurface bifilms by hydrogen evolved from the chemical reaction between the corrodant and the intermetallic compounds associated with the bifilm.

9.10.5 INTER-GRANULAR CORROSION

Inter-granular corrosion in its various forms is also proposed here to be associated in some cases with the newly identified bifilm defects, as a result of the natural siting of bifilms at grain boundaries in the cast structure.

Metcalfe (1945) records studies of the intercrystalline corrosion of the heads of rivets in an Al-Mg alloy from an aircraft that has been flown near marine environments. He concludes that the effect is one of stress corrosion cracking. Undoubtedly, there would be residual stress that may have played a part in the failures that are described. More especially so because the cracks were observed to follow grain boundaries sensitised by prolonged in-service aging, and the convoluted form of the crevices was due to the fact that the flattened grains themselves were distorted in this fashion by the complex flow pattern of the worked metal. Even so, a look at a section of one of the decapitated rivets in his work reveals a convoluted crack that can hardly have been propagated by stress. The stress would have been reduced to near zero after the spread of the first crack across the neck of the rivet. In fact, there is the trace of a crack which has repeatedly turned, spreading back and forth across the neck of the rivet at least five or six times. This type of crack is typical of a folded oxide defect. Its presence would ensure the stability of the convoluted form of the grain boundaries, which it would pin. Furthermore, in this vintage of alloy, a high density of entrainment defects would be the norm. The defect has provided an easy path for the attack of corrodant.

Forsyth (1995, 1999) describes seawater corrosion leading to intergranular cracking in 7010Al alloy. Corroded surfaces that have been polished back through the worst of the surface layer are presented in Figure 9.44. The inter-granular and transgranular cracks were, once again, typical of the localised tangled arrays of films that are normal in aluminium alloys produced via the melting and casting route. The cracks exhibit the typical irregular branching and changes of direction on several different size scales, often unrelated to the general size of the grain size of the matrix. Alloy material between such damaged regions was recorded to be completely free from attack. These observations are difficult to explain without the existence of random entrainment defects from the original casting.

When etching to reveal the dendrite structure, the cracks were seen (Forsyth, 1999) to be confined to the inter-dendritic regions (Figure 9.44) as is expected from the dendrite pushing of oxide bifilms. The defects are therefore concentrated in the residual liquid in the interdendritic regions, and in grain boundaries.

Forsyth (1999) also investigated the corrosion of 7010 alloy in seawater as a result of machining or bruising of the surface. In the case of bruising, the deformation of the surface would be expected to open any entrained defects at or near the surface, creating highly localised and deeply penetrating inter-granular pathways for attack.

Forsyth also draws attention to the especially damaging nature of the attack, in that despite rather little dissolution of material, complete blocks of material could be removed simply by the penetration of the attack along narrow planes in different directions. This observation corroborates his earlier report (Forsyth, 1995) in which subsequent anodising of the surface led to the incorporation of unanodised grains of metal in the corrosion debris remaining from such localised attack. The metal grains remained unanodised because they were found to be electrically isolated from their surroundings. This would not be surprising if double oxide films, separated by their inter-layer of air, surrounded the grains.

9.10.6 STRESS CORROSION CRACKING

Stress corrosion cracking (SCC) is a particularly serious form of failure. It seems to occur in conditions in which both stress and corrosive environment combine. It is often unexpected, involving the corrosion of minute amounts of material, but producing extensive and sometimes disastrous cracks. There remains much research but few conclusive results. The problem remains a mystery.

Once again, the presence of bifilms might prove to be the unsuspected major influence in most of the research conducted so far. Two very different examples are presented later, one for a Mg alloy and the other for an austenitic stainless steel.

Winzer and Cross (2009) describe the stress corrosion cracking of Mg alloys containing β particles ($Mg_{17}Al_{12}$). They describe how the consensus of opinion is growing that β particles are associated with the transgranular crack propagation and suggest several mechanisms that might be involved without reaching any conclusions. However, the simplest explanation seems to be the association between β particles and bifilms. Bifilms will certainly be present, and β particles will be expected to form on them, and the bifilm crack will provide a route for the corrodants. It all seems so straightforward. However, it has yet to be proven.

Andresen and colleagues (2009) carried out work on an austenitic stainless steel intended for application as a core component in a nuclear light water reactor. The corrodant in this case was deaerated, demineralised water. Once again, the authors admit to inconclusive results. However, the technique for the production of their samples (as roundly criticised by me in a published letter – Campbell, 2010), including vacuum induction melting and casting followed even more inappropriately by vacuum arc remelting guarantees a generous population of oxide bifilm defects. Several of the SEM images of the fracture surfaces showed clear examples of oxide films that had been formed on the melt. On occasions, these filled the field of view of the image and so could be deduced to be at least approximately 0.1–0.2 mm in size.

Further evidence of SCC initiated by bifilms was found by Lu and coworkers (2014) for an austenitic stainless steel in water at temperatures in the 250–320°C range. The SCC crack formed preferentially at the bottom of a corrosion pit (indicating that the initiator was a bifilm) and propagated along the phase boundary between austenite and ferrite (a typical location for a bifilm, arising from the ferrite initiating preferentially on bifilms to reduce its strain energy of formation).

In conclusion, it seems there is considerable evidence that in the absence of bifilms, some types of corrosion and possibly stress corrosion cracking might be reduced or eliminated. The elimination of bifilms would revolutionise metals and improve the quality of our lives in many ways.

9.11 LEAK-TIGHTNESS

Leak-tightness has usually been dismissed as a property hardly worthy of consideration, being merely the result of ‘porosity’.

However, of all properties specified that a casting must possess, such as strength, ductility, fatigue resistance, chemical conformity etc., leak-tightness is probably the most common and the most important. This might seem a trivial requirement to an expert trained in the metallurgy and mechanical strengths of materials. However, for the foundry engineer, it is a critical requirement not to be underestimated.

A cylinder head for an internal combustion engine is one of the most demanding examples, requiring it to be free from leaks across narrow walls separating pressurised water above its normal boiling point, very hot gas, hot oil at high pressure, and all kept separate from the outside environment. A failure at a single point is likely to spell failure for the whole engine. In this instance, as is common, leakage usually means ‘through leaks’, in which containment is lost because of a leak path completely through the containing wall.

However, leakage sometimes refers to surface pores that connect to an enclosed internal cavity inside a wall or boss. Such closed pores give problems in applications such as vacuum equipment, where outgassing from surfaces limits the attainment of a hard vacuum. Problems also arise in instances of castings used for the containment of liquids, where capillary action will assist the liquid to penetrate the pore. If the pore is deep or voluminous, the penetrated liquid may be

impossible to extract. This is a particular problem for the food processing industry where bacterial contamination residing in surface-connected porosity is a concern. Similarly, in the decontamination of products used in the chemical, pharmaceutical or nuclear industries, aggressive mechanical and chemical processes fail to achieve 100% decontamination almost certainly as a result of the surface contact with bifilms and possibly with shrinkage cavities. Such industries require castings made from clean metal, transferred into moulds with zero surface entraining conditions. Only then would performance be satisfactory.

It is true that leaks are sometimes the result of shrinkage porosity, especially if the alloy has a long freezing range, so that the porosity adopts a sponge or layer morphology. Clearly, any form of porous metal resulting from poorly fed shrinkage will produce a leak, especially after machining into such a region.

Leaks are seldom caused by gas porosity i.e. bubbles of gas precipitated from solution in the liquid metal. The following logic provides an explanation.

Gurland (1966) studied the connections between random mixtures of conducting and non-conducting phases by measuring the electrical resistance of the mixture. He used silver particles in Bakelite, gradually adding more silver to the mix. He found the transition from insulating to conducting to be quite abrupt, in agreement with stochastic (i.e. random) models. The results are summarised as follows.

% Ag	% Conducting
1	0
1.73	50
2.5	100

In the case of about 1–2% gas porosity in cast metals, the metal must surely therefore be permeable to gas. Why is this untrue? It is untrue because the distribution of gas pores is not random as in Gurland's mixtures. Gas pores are distributed at specific distances, dictated by the diffusion distance for gas. In addition, the pores are kept apart by the presence of the dendrite arms. Thus leakage from connections between gas pores cannot occur until there are impossibly high porosity contents in the region of 20–30% by volume (see Figure 7.36).

The only possible exception to this rule is the relatively rare occurrence of wormhole-type bubbles formed by the simultaneous growth of gas bubbles and a planar solidification front. Such long tunnels through the cast structure naturally constitute highly effective leak paths (see Figures 7.38 and 7.39). Fortunately they are rare, and easily identified, so that corrective action can be taken.

In the author's experience, most leaks in light-alloy and aluminium bronze castings are the result of oxide inclusions. These fall into two main categories:

1. Some are the result of fragments of old, thick oxide films or plates which are introduced from the melting furnace or ladle, in suspension in the melt, and which become jammed, bridging between the walls of the mould as the metal rises. The leak path occurs because the old oxide itself suffered an entrainment event; as it passed through the surface, it would take in with it some new surface oxide as a thin, non-wetting film covering. The leak path is the path between the rigid old oxide fragment and its new thin wrapping.
2. The majority of leaks are the consequence of new bifilms introduced into the metal by the turbulent filling of the mould. A clear example in an iron casting is shown in Figure 19.7. These tangled layers of poorly wetted surface films, folded over dry side to dry side, constitute major leak paths through the walls of castings. The leaks are mainly concentrated in regions of surface turbulence. Such regions are easily identified in Al alloys as areas of frosted or grey striations down the walls of top-gated gravity castings outlining the path of the falling metal. The remaining areas of walls, away from the spilling stream are usually bright and clear, free from any visible oxide striations and are free from leaks. The reader should be able to confirm, and take pride in, the identification of an aluminium alloy casting which has been top-poured from a distance of at least 100 m! Unfortunately, this is not a difficult exercise, and plenty of opportunity exists to keep oneself in training in most light alloy foundries! It is to be hoped that this regrettable situation will improve.

An example of a sump (oil pan) casting, top poured into a gravity die (permanent mould), is shown in Figure 9.45. The leakage defects in this casting are concentrated in the areas that have suffered the direct fall of the melt. The surface oxide markings are seen on both the outside and inside surfaces of these parts of the casting walls (Figure 9.45(a) and (b)). Other distant areas where the melt has filled the mould in a substantially uphill mode are seen to be clear of oxide markings and free from leaks. The precise points of leakage are found by the operator who inverts the casting, pressurises it with air and immerses it under water. He is guided by the stream of air bubbles emerging from leaks, and deals a rapid

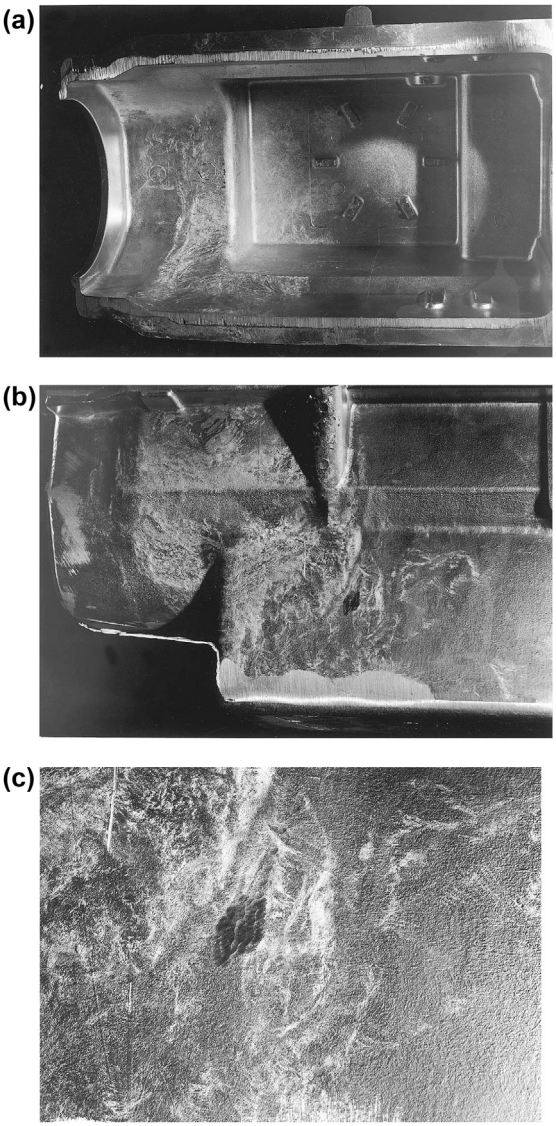

FIGURE 9.45

Views of (a) the inside and (b) outside of a top-poured ail pan (sump) casting showing the light traces of entrained oxides and (c) the corresponding leak defects repaired by peening, seen in close up.

series of blows from a peening gun. This hammering action deforms the surface locally to close the leak. The peening marks are seen in close up in Figure 9.45(c).

The linkage between oxide films and leakage problems was noted by Burchell (1969), when he attempted to raise the hydrogen gas content of aluminium alloys by stirring with wood poles, dipped in water. The porosity of the castings increased as was intended to counter feeding problems, but so did the number of leaks. Burchell identified the presence of oxide films on the fracture surfaces of tensile test bars that were cast at the same time.

It is unfortunate therefore that the folded form of entrained surface films creates ideal opportunities for leak paths through the casting. This source of leakage is probably more common than leaks resulting from other kinds of porosity. Although shrinkage porosity is often blamed for leaks, this seems to be the result of the common mis-diagnosis of bifilm tangles as shrinkage.

As an instance of the seriousness of leaks in castings that are required to be lead-tight, many foundries have been historically reluctant to cast aluminium manifolds and cylinder heads with sections less than 5 mm. This is because of the increased incidence of leaks that require the casting to be repaired or scrapped. The lack of pressure tightness relates directly to the presence of oxides whose size exceeds 5 mm (an interesting confirmation of the non-trivial size and widespread nature of these defects), and that can therefore bridge wall to wall across the mould cavity, connecting the surfaces by a leak path.

Leaks are often associated with bubble-damaged regions in castings. This is because all bubbles will have been originally connected to a surface as a necessary feature of their entrainment process. Some bubbles will have retained their bubble trail links to the outside world, whereas others will have broken away during the turmoil of filling. Bubble trails are particularly troublesome with respect to leak-tightness because they necessarily start at one casting surface and connect to the surface above, and as part of their structure, have a continuous pipe-like hollow centre. The inflated bubble trails characteristic of high-pressure die castings (Figure 2.39) make excellent leak paths. A core blow also leaves a serious defect in the form of a collapsed bubble trail (Figure 2.32). Despite its collapsed form, the thickness and residual rigidity of its oxide will ensure that the trail does not completely close, so that a leak path is almost guaranteed.

In general, the identity of a leakage defect in a casting can be made with certainty by sawing the casting to within a short distance of the defect, and then breaking it open and studying the fracture surface under the microscope. A new oxide film (probably from surface turbulence during pouring, or from a bubble trail) is easily identified from its folded and wrinkled appearance; an old oxide fragment (perhaps from the melting furnace or crucible) from its craggy form, like a piece of rock; and shrinkage porosity by its arrays of exposed dendrites. Fracture studies are a quick and valuable test and are recommended as one of the most powerful of diagnostic techniques. The reader is recommended to practice this often – despite its unpopularity with the production manager; the destruction of one casting will often save many.

Leak Detection

We turn now from the nature of leakage defects to methods of detection. Bubble testing has already been mentioned in which the inside of the casting is simply pressurised with air, the casting immersed in water and any stream of bubbles observed.

For castings which require a demonstration of leak-tightness against very high pressures they cannot be pressurised safely with a gas, but require to be pressurised with a liquid such as water. Thus the geometry of the usual bubble technique is reversed; leakage is detected by the emergence of a coloured dye in the water.

Even these time-honoured and apparently simple techniques are not to be underestimated because providing effective and rapid sealing of all the openings from the interior of the casting may not be easy in itself. It will almost certainly require careful planning to ensure that the correct amount of dressing or machining has been carried out to eliminate troublesome flash and gating systems etc. so that the sealing surfaces can be easily accessed and effectively sealed. Also, of course, the techniques are slow, not quantifiable, and both demand the constant attention of skilled personnel. After testing, the part often requires to be dried.

Hoffmann (2001) describes three basic methods of dry air leak testing suitable for production line applications: they measure (1) the rate of decay of gauge pressure, (2) the rate of decay of differential pressure and (3) leakage rate directly in terms of mass flow. For highly specialised applications, helium mass spectrometry offers testing capability beyond the limits attainable by dry air methods.

1. The first technique, the rate of decay of gauge pressure, is the simplest and lowest cost, and is generally suitable where pressures do not exceed 2 bar and volumes do not exceed 100 mL.
2. The differential pressure method pressurises a non-leaking reference volume along with the test part. A transducer reads any difference in pressure that occurs over time. The differential technique reduces errors from temperature changes, and is more accurate and faster than the direct pressure decay method. The technique is also well-suited to applications specifying higher test pressures, exceeding 10 bar, and where relatively small cavities must be tested to a very low leak rate.
3. The mass flow method pressurises the test cavity, then allows any leakage to be compensated by actively flowing air into the cavity. The in-flowing air is measured directly by a mass flow meter in terms of volume per second. The method involves a single measurement, usually less than 1 s. (It avoids the taking of two measurements over a time interval—during which temperature may change for instance—that is required for the first two techniques, thus halving errors and increasing speed of response.) The method can tackle a wider range of volumes, and is accurate down to 0.001 mLs^{-1}.

For castings that are required to be leak tight to even greater standards, helium mass spectrometry can measure down to rates that are 10,000 times lower. This is principally because the helium atom is much smaller than molecules of nitrogen and oxygen, and so can penetrate much smaller pores.

Krypton gas has been used for the detection of very fine leaks, because of its content of 5% radioactive Krypton 85 (Glatz, 1996). As before, the part to be tested is placed in an evacuated chamber to suck air out of the cavities. Krypton gas is then introduced to the chamber and allowed time to penetrate the surface pores. The Krypton is then pumped out, ready for re-use and air is admitted. The rate at which Kr is slowly released can be monitored to assess the volume of surface-connected internal pores. In addition, the spraying of the surface with a liquid emulsion of silver halide particles makes the surface sensitive to the low energy beta particles given off by the radioactive decay of Kr85. After the emulsion is developed by conventional photographic techniques, the part reveals the site and shapes of surface pores and cracks. The beta particles can penetrate approximately 1 mm of metal, revealing subsurface cracks (if connected to the surface elsewhere of course) and magnifying the width of pores and cracks that otherwise would be too small to see. The technique is more sensitive than dye penetrant testing because of the viscosity of gases is typically only 1/100 of that of liquids, making the test extremely searching.

Finally, it is worth emphasising that a good melt quality combined with a good filling system will usually eliminate most of the leaks found in castings (providing core blows can be avoided by careful design or venting of cores). This conclusion is confirmed by casting operations using intrinsically quiescent melt handling processes such as Cosworth Process. These foundries are so confident of the quality of their products that they do not even bother to test for leak tightness; none is ever found to leak.

9.12 SURFACE FINISH

There are two major aspects to the achievement of a good surface finish for castings; the first, applying to some metals, is surface tension of the liquid, and the second, important for many important alloys, the solid surface film on the liquid.

9.12.1 EFFECT OF SURFACE TENSION

It has been well understood for many years (Hoar, 1953) that when in contact with many non-metals, liquid metals enjoy the benefit of capillary repulsion; the resistance felt by the metal when attempting to enter a small hole or channel.

(In passing, we should note that if the liquid metal wetted the mould materials it would experience capillary attraction, effectively being sucked into the mould surface as water is sucked up a capillary tube. Mould materials are therefore selected however for their non-wettability. The founder goes to some lengths to avoid wetting conditions which cause penetration of metal into the mould.)

Assuming non-wetting conditions, when the pressure P in the liquid metal becomes sufficiently high, surface tension γ is no longer able to resist the penetration of the metal into the spaces between the sand grains of the mould. The size of

the holes between the sand grains can be roughly estimated assuming that the radius of the inter-granular spaces r is only approximately 15.4% of the radius of the sand grains.

The following arguments already presented in the development of Eqn 4.1, the resistance offered by surface tension is $P = 2\gamma/r$. If the pressure in the melt, density ρ, arises simply from its depth h, then $P = \rho gh$ where g is the acceleration due to gravity. From these equations the critical depth at which penetration first occurs can easily be estimated. For instance for liquid steel where $\gamma = 1.5$ N/m and $\rho = 7000$ kg/m^3, a grain size of 500 μm corresponding to a pore size of 75 μm and radius 37.5 μm indicates a critical depth at which penetration will occur as approximately 1.5 m.

This static estimate neglects the important dynamic problems created by a poor filling system in which the melt may violently impact the sand, this hammering effect by the liquid metal causing the mould to suffer additional transient penetration pressures.

The penetration of the mould in this way produces a 'furry' casting that may be quite unsaleable. The penetration may be only one grain deep, giving effectively an excessively rough surface. However penetrations of 20–50 mm are not uncommon in large castings. In a classical series of experiments, Hoar and Atterton (1950–1956) demonstrate that once the critical pressure difference to force the metal into the sand is exceeded, then penetration occurs rapidly, within a second or so. Figure 4.10 illustrates that once the surface grains are penetrated, the penetration is a run-away effect. Ultimately, the depth of penetration is controlled by the freezing of the leading edge of the advancing metal when it reaches the freezing isotherm in the sand. Clearly, this distance is greater for larger castings. The mix of solid metal and sand is difficult to remove from castings.

Attempts are made to resist such mould penetration by reducing the size of the pores by:

1. The use of finer sand for the mould or core. For cores, this approach is limited by the requirement to maintain the permeability of the core material so that core gases can escape during casting. Fine grain sand is, however, widely used for vacuum (V) process moulding, where the vacuum that is applied to maintain the rigidity of the mould assists in drawing the liquid metal into the pores between the sand grains. Thus, whereas normal sand castings have an average grain size in the range 250–500 μm, sands for the V process are approximately 50–150 μm. This can result in a dust nuisance when casting hotter metals such as iron, which is a pity because the vacuum moulding process is otherwise excellent in its environmental benefits. Newer plants are improving their designs to tackle this problem. Croning shell process benefits surface finish by its fine grains, usually less than 200 μm, and high percentage of binder, but permeability is maintained in this case by the thinness of the shell mould, usually never more than 10 mm.
2. The application of a mould wash—a ceramic slurry applied as a paint to fill the spaces between the sand grains. The pores in the dried coating are one or two orders of magnitude smaller than the pores between the grains, thus, in line with Eqn 2.2, enabling the mould surface to withstand 10–100 times greater pressures before metal penetration. Although the metal will often still succeed in penetrating the sand coating through cracks, the penetrated sand only adheres to the casting at the isolated points of failure of the coat, and so is relatively easy to remove. This action is generally used to counter metal penetration at the base of tall moulds, which can sometimes be more than a metre high.

The application of a core wash is only marginally successful, however, in resisting metal penetration with the use of sand cores in low-pressure die casting. This seems to be the result of the rather poor pressure control on most low-pressure machines, and the additive effect of the momentum of the metal, giving a pressure peak at the instant when the liquid hits the top of the mould (see Section 3.1.2). Sand cores are only rarely used, therefore, in low-pressure die casting. For similar reasons, sand cores have proved impractical for high-pressure die casting. In this case other solutions such as water-soluble salt, glass, or ceramic cores have sometimes achieved success. In general, only withdrawable steel cores continue to be used successfully.

Filling pressures are high in pressure die casting. This is widely alleged to be for the purpose of increasing surface finish and definition, i.e. the ability of the metal to fill small radii so as to reproduce fine detail. Pressure die-casting machines commonly operate at metal pressures of 1000 atm (100 MPa). Equation 2.1 indicates that such pressures

will force the liquid into radii of only 10 nm, approaching atomic dimensions! This is, of course, a vast overkill. The student should therefore be on his guard against such loose thinking. The high pressures are actually needed mainly to reduce the bubble defects produced by the turbulently entrained mould gases – the bubbles are simply squashed to acceptable dimensions. Consideration of Eqn 2.1 reveals that a mere 10 atm (1 MPa) would reproduce a radius of about 1 μm, which would be more than good enough for most engineering purposes.

Filling pressures are enhanced for the genuine purpose of reproducing detail in the centrifugal casting of jewellery. A casting travelling at 10 m/s on an arm of radius 1 m will experience an acceleration of 100 m/s^2. This is close to 10g. In the absence of mould gases, and replacing the acceleration g due to gravity with the total acceleration $(g + 10g) = 11g$ as the arm goes from the vertically up through the vertically down part of its stroke, Eqn 2.3 predicts that an improvement in the fineness of detail by a factor of 11 should be achievable. These predictions are likely to be all the more accurate for jewellery alloys based on noble metals such gold and platinum since, in principle, they will not be troubled by surface oxides (alloy components may assist to detract from this benefit of course).

In engineering, uses of centrifugal casting much higher accelerations are normally used, typically 50–100g. The high pressures in the liquid are, however, not normally needed for filling because the moulds are usually of simple shapes. The technique is valuable for totally unrelated reasons: (1) for pipes and cylinders and the like, because the centrifugal action avoids the requirement for a central cylindrical core to make a hollow shape; (2) for enhancing the pressure in the casting during freezing to reduce porosity; and (3) centrifuging the oxides and similar less dense inclusions into the centre of the bore, where, if necessary, they can be machined off.

As explained in more detail in Section 16.4, the production of shaped castings by this route involves pouring the liquid metal down a central down-runner, and accelerating it out along radial runners, to arrive in the mould at such a high speed that considerable damage is done to both mould and metal. The high centrifugal pressures are then needed to help to repair this damage constituted by entrained porosity and inclusions in the casting. Shaped castings would probably be cheaper and better if not centrifuged at all, but simply produced with a properly designed gravity-running system.

9.12.2 EFFECTS OF A SOLID SURFACE FILM

The previous considerations of the control of surface finish by surface tension do not apply to many metals and alloys that have strong, solid surface films, particularly if they are filled uphill by bottom gating of gravity poured castings, or by counter-gravity filling. The metal rises upwards, its surface oxide thickening during the time it moves across the top of the melt, arriving at the mould wall to become the skin of the casting (Figure 2.2). This leisurely formation and sideways sliding of the surface film allows it time to thicken. It seems possible that the quality of surface finish may be a function of the rate of rise of the liquid in the mould because this would be expected to be directly related to the thickness and rigidity of the surface film.

Having travelled across the meniscus and arrived at the wall of the casting, the metal effectively rolls out its solid skin like a track-laying vehicle against the mould surface (Figure 2.2). No liquid metal contacts the mould; the two are separated by a rigid, solid, plate-like film. The solid film has sufficient rigidity to bridge the gaps between grains of aggregate, thereby creating a smooth surface. The smoothness of the casting surface reflects the smoothness of the surface of the original liquid meniscus at the time the original surface film formed.

This mechanical process, allowing time for thickening and strengthening the oxide film on the liquid, can be supplemented by various chemical effects:

1. Aluminium alloys enjoy this benefit because of its strong alumina film. These include aluminium bronzes (Cu-10Al etc.) because the higher temperatures of these alloys give an even thicker and stronger alumina skin.
2. An Alcoa patent by DeYoung and Dunlay in 2002 describes how the addition of strontium (Sr) to aluminium alloys strengthens the surface oxide and consequently improves the surface of DC ingots.
3. Similarly, in 1989, Sare found that when melting the surface of cast irons by gas tungsten arc welding, grey iron produced a rough surface but ductile iron was smooth as a result of its small content of Mg that promoted a strong magnesia-rich surface film.

Perhaps the most impressive demonstration of the benefits of a strong skin is shown by cast iron in moulds that contain volatile carbonaceous additions such as coal dust or certain resin binders. The hydrocarbons chemically decompose ('crack') on the surface of the rising hot metal, releasing hydrogen which escapes somewhere (it would be interesting to know where it goes; whether into the metal or the mould atmosphere), but certainly depositing carbon on the surface of the liquid in the form of a strong film. This is known as lustrous carbon (Figures 6.33 and 6.34). Iron castings that are nicely bottom-gated can emerge from the mould with a black, glossy surface almost like a mirror. Such a good finish is the sign of a casting filled nicely.

For steel castings with poor filling systems, Puhakka (2011) reports a poor finish with generous amounts of so-called 'burn-on'. The poor finish almost certainly arises from impacting the mould surface with high momentum, with little or no time for the development of a useful thickness of protective film barrier. Conversely, the surface of his bottom-gated castings with good filling systems exhibit zero burn-on and an overall finish so smooth to the touch as to be almost strokable.

9.13 QUALITY INDICES

The confusion of the interplay of properties among yield strength, tensile strength and elongation, the strengths going up as the elongation reduces with different heat treatments and other factors, is solved by the concept of a quality index. This brilliant innovation introduces only a single value to indicate the quality of a cast material. So far, quality indices appear to be exclusively used in the Al alloy casting industry, and in particular for the widely used Al-7Si-Mg alloys.

The concept was invented by French researchers (Drouzy, Jacob and Richard, 1980) in the following form

$$Q_{DJR} = \sigma_{TS} + 150\text{Log E}$$

where the tensile strength σ_{TS} was in units of MPa and elongation E was in units of percent. The formulation as a single parameter is undoubtedly useful, and has become popular in the industry. Those castings achieving an index above 500 MPa were regarded as outstanding, but it is probably only a matter of time before techniques improve to yield values of 600 MPa or more.

Even though the single parameter quality index concept has been recognised as excellent, the Drouzy formulation of the parameter has been criticised by several subsequent researchers. In particular, the use of TS and elongation has elements of double counting and was not based on the really essential engineering design parameter, yield strength σ_Y (or near equivalent such as 0.2% proof stress). Finally, the incorporation of the log term was inconvenient and in fact hardly necessary. The author's laboratory (Din, Rashid and Campbell, 1996) came up with the simpler

$$Q_{DRC} = \sigma_Y + \text{kE}$$

where k is a constant determined from experiment to be 50 for both 356 and 357 alloys (respectively the low and high Mg versions of the Al-7Si alloys).

Both of these quality measures were based on empirical approaches which had no fundamental significance. In practice, a reader may wonder why there is even a specification on elongation because parts are designed to handle stresses well below the yield strength.

The answer on a legalistic level is put forward by the automotive companies who wish their components to bend rather than fracture in a crash, so that the component cannot be cited as a potential cause of the crash.

On a more general engineering level, it is clearly more desirable for a component to fail by plastic deformation than fracture because plastic deformation absorbs more energy. This statement points to the assessment of energy (or toughness) as described by the energy under the true stress–strain curve as a measure of quality. However, we all know that almost all component failures happen by fatigue fracture, although both fracture toughness and fatigue life are both strongly affected by defects. Therefore, quality indices giving a measure of the severity of defects would be expected to be useful in giving an indication of fatigue life.

Tiryakioglu (2009) initially suggested a more rational assessment based on the energy to fracture. This could be closely approximated to the average ($\sigma_{TS} + \sigma_Y$) multiplied by E (giving the area under the stress/strain curve). Because σ_Y is relatively fixed, and σ_{TS} is a function of σ_Y and E, it follows that E is a dominant factor in this proposed

assessment of quality. Finally, therefore, if E is measured at a known value of σ_Y, E alone can give an excellent measure of the quality of the material.

Tiryakioglu and colleagues (2009) proposed from fundamental grounds there should be an upper bound to the uniform elongation to fracture of Al alloys, because necking before fracture was generally never observed. Their theoretical predictions were revealed to be closely modelled by experimental data; the upper bound to elongation was revealed by plotting all the available data, mainly from aerospace alloy foundries. The results for the 356 and 357 alloys are shown in Figure 9.18(a) and the results for the Al-4.5Cu alloys A206 and A201 in Figure 9.18(b). A measure of quality at any value of yield strength and experimentally measured elongation E can now be defined immediately as

$$Q_T = E/E_m\%$$

The quality index now becomes the percentage of the maximum elongation E_m attainable at that level of yield strength (for instance as resulting from a particular heat treatment). This formulation of the quality concept by Tiryakioglu using Q_T is strongly recommended as giving a direct measure of the level of attainment of potential quality. The new index is applicable to all Al alloys and should be applicable to all cast alloys.

In fact, it is sobering to see the masses of mediocre or actually bad results in Figure 9.18 compared with the maximum elongation that is possible in the alloy at each particular yield strength. Clearly, a few results are close to $\sigma_T = 100\%$, but many achieve only 50% and a few only 5% or less of the potential value. There is plenty of scope for improvement in the industry.

9.14 BIFILM-FREE PROPERTIES

It is fascinating to look ahead, extrapolating a little from our current knowledge, to envisage the properties of metals if manufactured free from bifilms.

It is essential to realise that all the evidence currently available points strongly to the conclusion that metals would never fail by cracking (Campbell, 2011). This arresting prediction follows from a survey of molecular dynamics studies which investigate the atomic structures of metals by computer simulation. When the atomic lattices of various metals are subjected to tensile stress, the metals are seen to stretch, but are never observed to crack until the stress reaches the ultimate tensile strength of the metal, usually many tens of GPa. Thus failure mechanisms which were supposed to operated, such as a dislocation pile-up against a barrier such as an inclusion, leading to the formation of a crack, do not seem to occur in practice. This follows simply as a result of the enormous strength of the interatomic bonding; metal atoms are highly resistant to being pulled apart.

This profound conclusion is perfectly in line with the knowledge widely known for decades from the simple formula, $P = 2\gamma/r$, for the strength of liquid metals by the formation of an atomic sized bubble, which effectively cannot be solved at normally available stresses. Once again, tensile failure only occurs at stresses close to the ultimate failure strength measured in many GPa.

There appear therefore to be no intrinsic mechanisms which can trigger the failure of metals by cracking. This amazing conclusion reinforces the role of bifilms. These unsuspected and largely undetectable defects appear to be the only features capable of initiating cracks. They *are* the Griffith cracks required by all the theories of failure. This is an exciting discovery, and one which gives this book a significance I could not have dreamed of. Casting defects and their lingering existence in wrought metals constitute the only sources of failure by cracking. This massively important conclusion predicts that metals which cannot fail by cracking are possible by appropriate casting techniques. The processes to achieve this are easy, low-cost processes.

In the absence of failure by cracking, failure in tension would occur by plastic flow. Thus elongation to failure and RA would be expected to increase greatly achieving 100% for metals completely free from bifilms. Experimental evidence for the truth of this prediction is seen in Al alloy castings from aerospace foundries in Figure 9.18 in which results from 1% to 30% elongation are found even in those critical operations which would claim to have all casting parameters under control, whereas unfortunately overlooking the major parameter: the turbulence during pouring. Notice that these results are for elongation rather than RA; the elongation is sensitive to the rate of work hardening and is therefore not

straightforwardly predictable. Even so, the values of typically 50% for steels reflects their better freedom from bifilms compared with Al alloys as a result of the density difference which assists steels to reduce its bifilm content rapidly by flotation. For both steels and Al alloys, values of hundreds of percent can be achieved for conditions of superplasticity; such values would be expected to be more common as metal purities increased.

The benefits of directional solidification (DS) of castings in an upward direction are explainable for the first time. Such slow freezing conditions provide sufficient time to favour the flotation of bifilms, particularly in dense alloys such as Ni-base alloys and steels, and the pushing of bifilms ahead of the freezing front, so that the casting becomes reasonably free from bifilms. Polich and Flemings (1965) show for their DS steel castings (Figure 9.26) that tensile properties are independent of DAS compared with equiaxed casting which suffered from entrapped bifilms in which DAS is used as an indicator of tensile properties (see Section 9.4.3.2).

Ni-based single crystals are the ultimate example of bifilm-free behaviour, or possibly low bifilm content castings. Figure 17.1 illustrates how these products achieve a factor of 10 improvement in properties compared with equiaxed equivalents (in which their bifilm population would have no chance to escape, but would be trapped by rapid crystal growth from all directions).

Some steels, by virtue of their composition and high melting temperatures giving them the benefit of liquid surface films, display huge toughness. An excellent example is Hadfield Manganese steel containing approximately 13%Mn so that its surface oxide is rich in the low melting point MnO_2 (probably containing also SiO_2). Kim (2014) confirms the inclusions in this steel are beautifully spherical typically consisting of MnS patches in a glassy amorphous phase formed from a supercooled liquid, $MnO\text{-}Al_2O_3\text{-}SiO_2$. This steel is used for crossing points on rail track, and despite its severe service conditions, is highly resistant to failure by cracking.

The addition of boron to steels is widely known to increase toughness and hardenability of steels. These may be the result of the surface oxide on the liquid steel becoming a liquid boride, with a melting point of 1000°C or less, so that bifilms cannot form during pouring. Toughness is easily understood as the result of fewer crack-like defects. The benefits to hardenability might be the result of the reduction of bifilms leading to an increase in thermal conductivity, so that a quenching action will reach deeper into the steel because of the direct flow of heat rather than the tortuous flow around arrays of bifilms. Although the boride is certain to be liquid on the steel surface during casting, the liquid boride may not take into solution the stable oxides such as alumina and chromia which are also likely to be present, but will merely float on top of the solid film. If this occurs, the clearly beneficial action of the liquid boride may be the result of merely forming the centre of a liquid sandwich, bonding the stable bifilms together like a glue. Yu's investigation (2013) of a superalloy with added boron reports 'improved grain boundary adhesion' increased rupture life and eliminated notch sensitivity. All these observations would be expected from reduced bifilms or bonded bifilms at grain boundaries. Among the multitude of research which confirm the beneficial effect of B additions to steels, we can cite Mejia (2013) who finds improved hot ductility, Das (2013) who finds fewer ductile dimples on fracture surfaces (fewer inclusions on unbonded bifilms) and Song and Cooman (2013) who find the bainite formation at grain boundaries delayed by boron additions to a lean alloy steel. This latter observation seems associated with the ease of nucleation on a bifilm of those phases which are accompanied by a volume and/or shape change—this is easy into the 'air gap' at the centre of the bifilm. In the absence of a bifilm, the grain boundary will not constitute a favoured nucleation site for such transformations.

Turning finally to the effect of the absence of bifilms on corrosion: It cannot be claimed to be a piece of rigorous scientific evidence, but in the absence of any nicely researched information, I perhaps should report that I did once cast an aluminium alloy wheel with a good filling system. The wheel was subjected to the standard salt spray corrosion test used for wheels but was not found to corrode. This was a surprise at the time, but is now understandable from the viewpoint that bifilms are almost certainly the mechanism for pitting and other localised forms of corrosive attack as described in Section 9.10. Properly controlled experiments to demonstrate the role of bifilms in corrosion are, regrettably, not yet available but would be welcome.